Coordination Chemistry Reviews 416 (2020) 213340

Contents lists available at ScienceDirect

Coordination Chemistry Reviews

journal homepage: www.elsevier.com/locate/ccr

Review

Bacteriochlorins and their metal complexes as NIR-absorbing photosensitizers: properties, mechanisms, and applications

Barbara Pucelik [a,b], Adam Sułek [a], Janusz M. Dąbrowski [a,*]

[a] Faculty of Chemistry, Jagiellonian University, 30-387 Kraków, Poland
[b] Malopolska Centre of Biotechnology, Jagiellonian University, 30-387 Kraków, Poland

ARTICLE INFO

Article history:
Received 17 December 2019
Received in revised form 29 March 2020
Accepted 6 April 2020
Available online 5 May 2020

Keywords:
Bacteriochlorins
Bacteriochlorophylls
Chemical sensors
Light-harvesting antennas
Metal complexes
Metal-organic framework
Near-infrared
Photoacoustic tomography
Photocatalysis
Photodiagnosis
Photodynamic therapy
Photodynamic inactivation
Photosensitizer
Porphyrins
Reactive oxygen species
Singlet oxygen
Solar energy conversion
Dye-sensitized solar cells

ABSTRACT

Bacterichlorins possess a characteristic intense electronic absorption in the near-infrared part of the electromagnetic radiation (NIR) from 700 nm up to 900 nm, where endogenous chromophores do not absorb and which allows deep penetration through tissues. Although naturally-occurring metal complexes derived from bacteriochlorophylls are unstable and their use is limited, it is currently possible to obtain large-scale libraries of photostable synthetic compounds belonging to the bacteriochlorin family. This review presents an up-to-date overview of the most significant studies on the synthesis, spectroscopic, photochemical, and electrochemical characteristics as well as various potential applications of bacteriochlorins and their metal complexes. Particular emphasis has been given to the possibilities of their use in medicine, especially in photodynamic therapy of cancer (PDT), photodiagnosis (PD), and photodynamic inactivation (PDI) of bacteria, viruses, and fungi. The combination of (metallo)bacteriochlorins with polymeric micelles, lipoproteins, nanoparticles, and metal-organic frameworks in order to increase their efficacy is also discussed. Other potential applications of (metallo)bacteriochlorins discussed in this paper include their use as light-harvesting antennas, optical sensors, photocatalysts, and dye-sensitized solar cells for efficient solar energy conversion.
© 2020 The Authors. Published by Elsevier B.V. This is an open access article under the CC BY license (http://creativecommons.org/licenses/by/4.0/).

Contents

Abbreviations: ATP, adenosine triphosphate; BC, bacteriochlorin; BChl, bacteriochlorophyll; BPhe, bacteriopheophytin; BRC, bacterial reaction center; Chl, chlorophyll; DFT, density functional theory; 2DES, two-dimensional electronic spectroscopy; DLI, drug-to-light interval; DNA, deoxyribonucleic acid; DSSC, dye-sensitized solar cells; EBRT, external beam radiotherapy; EMA, European Medicine Agency; HOMO, highest occupied molecular orbital; HSA, human serum albumin; IC, internal conversion; IL-6, interleukin-6; ISC, intersystem crossing; KC, CXCL1 chemokine keratinocyte chemoattractant; LDI, light density index; LDL, low-density lipoprotein; LH3,4, light-harvesting complex 3,4; LPS, lipopolysaccharides; LUMO, lowest occupied molecular orbital; MDR, multi-drug resistance; MIP, macrophage inflammatory protein; MOF, metal-organic framework; MRI, magnetic resonance imaging; NADPH, nicotinamide adenine dinucleotide phosphate; NIR, near-infrared; OSC, organic solar cells; PA, photoacoustic tomography; PBR, peripheral benzodiazepine receptor; PCM, polarizable continuum model; PD, photodiagnosis; PDI, photodynamic inactivation; PDT, photodynamic therapy; Ph, phosphorescence; PS, photosensitizer; PSA, prostate-specific antigen; ROS, reactive oxygen species; TBAP, tetrabutylammonium perchlorate; TDDFT, time-dependent density functional theory; TNFα, tumor necrosis factor α; TTA-UC, triplet-triplet annihilation upconversion; UV, ultraviolet; VEGF, vascular endothelial growth factor; VR, vibrational relaxation.

* Corresponding author.
E-mail address: jdabrows@chemia.uj.edu.pl (J.M. Dąbrowski).

https://doi.org/10.1016/j.ccr.2020.213340
0010-8545/© 2020 The Authors. Published by Elsevier B.V.
This is an open access article under the CC BY license (http://creativecommons.org/licenses/by/4.0/).

1. Introduction

The interaction of light with biologically active compounds plays a key role in the living organisms' function. Light energy is a part of electromagnetic radiation that can lead to heating, mechanical effects, and chemical reactions. Thus, the transfer of energy through photon absorption results in a number of processes and reactions essential for biology, industry, and medicine. Moreover, numerous medical strategies employ light to visualize the interior of the body and are fundamental to its further application in a variety of more sophisticated, modern diagnostic and therapeutic tools [1,2]. Therefore, the study of the light-driven processes addresses issues of the most importance for both scientific research and the quality of health care. The light absorption in tissues is strongly dependent on the absorbed wavelength (λ_{max}). Ultraviolet (UV, 100–390 nm) absorbed by DNA, amino acids and proteins, is more energetic electromagnetic radiation than visible light (Vis, 390–720 nm) that, in turn, may be absorbed by endogenous pigments such as hemoglobin, vitamins and other biologically important molecules. Consequently, these forms of radiation do not pass through the body (UV) or do not penetrate deep enough into the tissues (Vis) [3]. On the other hand, near-infrared (NIR, 720–900 nm) is a low energy range of light where photons exhibit a maximum depth of penetration through tissues. It is also worth noting that the density of photon flux on the Earth's surface reaches a maximum at approximately 700 nm, and up to 40% of VIS + NIR photons reaching the Earth's surface are, in fact, NIR photons [4] (Fig. 1).

NIR photons are the most penetrating and least hazardous to human tissues and can, therefore, provide direct access to biological targets. The range of spectra between 650 and 850 nm, where light penetrates tissue up to 1–3 cm, has been termed as a phototherapeutic window (Fig. 1). It is a low energetic part of the spectrum, where the compounds present in living tissues do not absorb light, but it also corresponds to energies still sufficient for photochemical reactions (*e.g.*, generation of singlet oxygen through direct energy transfer). Recent reports have demonstrated the broad applications of NIR photons in photomedicine to facilitate biostimulation [5], imaging [6,7], diagnosis [8], and therapy of many diseases [9]. NIR photons are also extensively used in optical communication and could potentially be the most energy-effective in photocatalytic processes [4,10]. Unfortunately, their potential has not been fully exploited for many years due to the lack of chromophores, which by absorbing NIR radiation, would simultaneously be sufficiently (photo)stable. Thus, the synthesis of new photo- and thermally-stable chromophores characterized by intense absorption in the NIR is essential for their implementation in solar energy conversion, photomedicine, sensing, and photocatalysis.

Tetrapyrroles are a class of macrocyclic compounds that are commonly found in nature and, by performing various biochemical functions, are essential for the proper functioning of the majority of living organisms [11–13]. They are present in many enzymes and proteins whose functions include metabolism, transport of molecular oxygen, as well as electron transfer and energy conversion processes [11,13,14]. Moreover, they can be used as effective

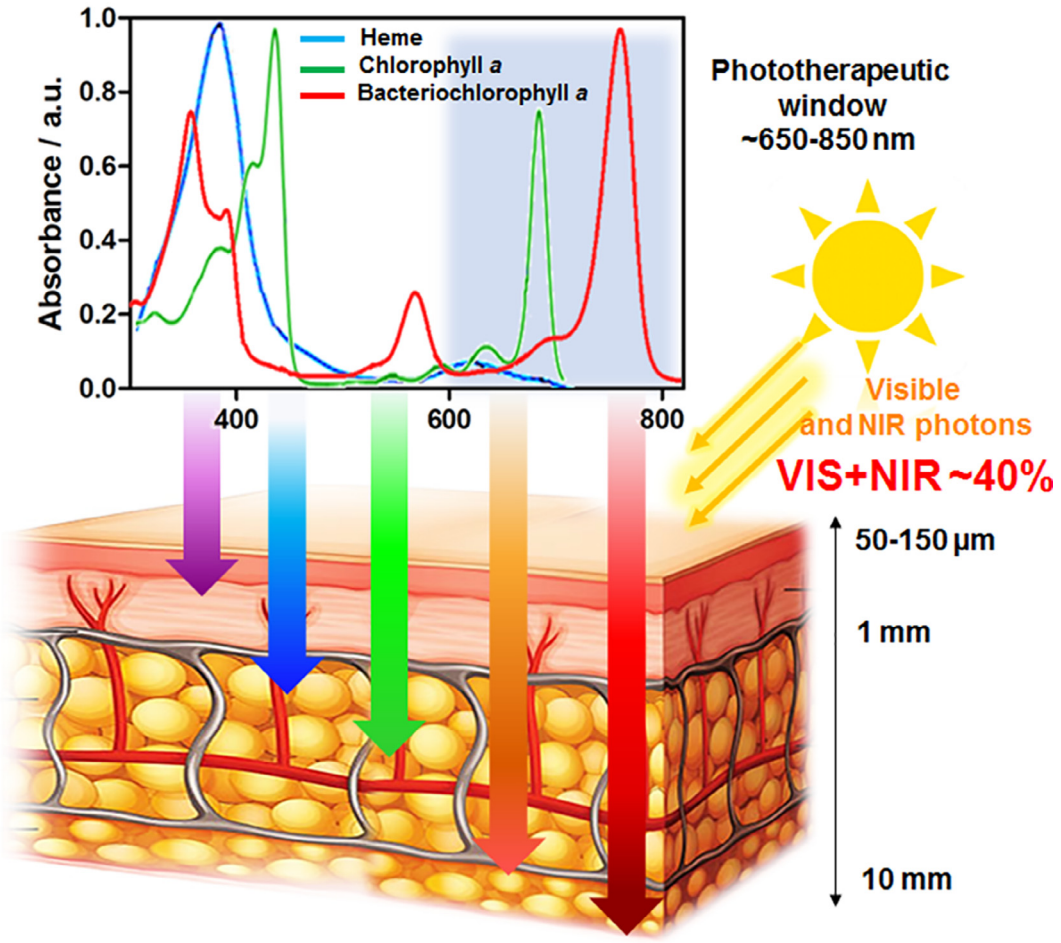

Fig. 1. Scheme presenting the electronic absorption spectra of naturally-occurring tetrapyrrolic chromophores along with the highlighted region of the "phototherapeutic window" and the interaction of light with human tissue.

catalysts for numerous chemical and photochemical reactions [15,16]. Tetrapyrroles are classified into three main classes: porphyrins, chlorins and bacteriochlorins. An example of a porphyrin-based biologically active compound is heme present in hemoglobin (Fig. 2, blue). The most studied chlorin-type molecule is chlorophyll *a* (Chl *a*) responsible for the green color of plants, algae, and cyanobacteria (Fig. 2, green). Whereas bacteriochlorophyll *a* (BChl *a*), involved in the photosynthesis in some bacteria, belongs to the family of bacteriochlorins (Fig. 2, red). Although at first glance, the difference between these macrocycles seems to be insignificant, their spectroscopic, photophysical and redox properties differ considerably, which will be discussed in detail in this review. Unlike porphyrins, which possess a full tetrapyrrolic system, chlorins have one reduced pyrrole, and bacteriochlorins have two reduced pyrroles on the opposite side of the macrocycle [17,18]. The chromophores presented in Fig. 2 are characterized by strong absorption of UV-A radiation, weak absorption in the green-orange region, and most notably, they possess an intense absorp-

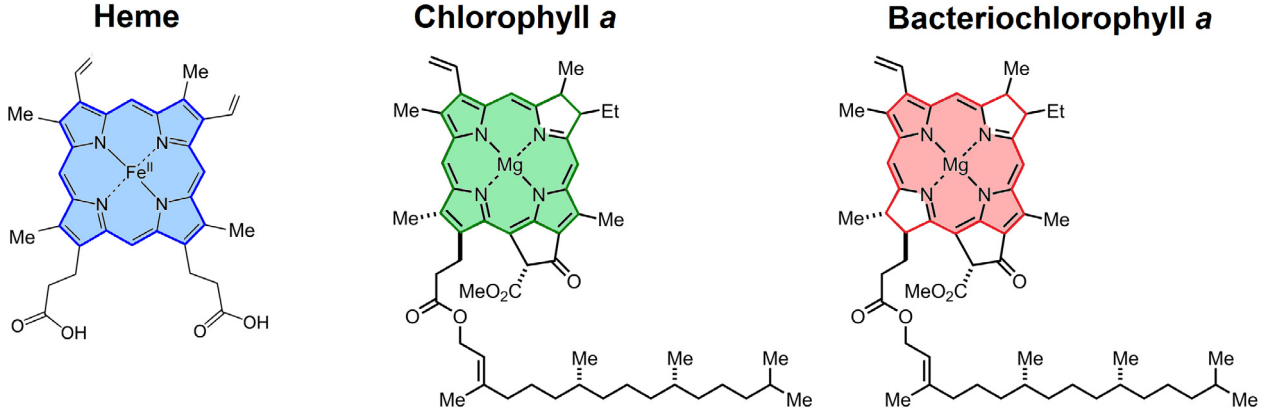

Fig. 2. Chemical structures of naturally-occurring chromophores: heme, chlorophyll *a* and bacteriochlorophyll *a*.

tion band in the red (typical for chlorins) or NIR (distinctive for bacteriochlorins) range of electromagnetic radiation [18]. While the results of research on the naturally-occurring macrocycles are undoubtedly valuable and inspiring, the easy access to a large amount of synthetic metallobacteriochlorins described in this review offers a number of new opportunities for the investigation of fundamental processes, fine-tuning of NIR optical properties, and the search for a range of photochemistry-based applications.

To gain access to stable and efficient bacteriochlorins, several *de novo* synthetic procedures have been recently developed [13,19]. Many of them afford bacteriochlorin with electron-withdrawing substituents. For example, geminal dimethyl groups lead to the stabilization of bacteriochlorin chromophore [20,21]. The other modifications that protect bacteriochlorins from oxidation include (i) insertion of appropriate metal ions into the macrocycle, (ii) presence of exocyclic rings in the macrocycle, and (iii) introduction of halogen atoms in the *meso*-tetraphenylbacteriochlorins [22]. The core structures of synthetic bacteriochlorins are shown in Fig. 3. Appropriate structural modifications enabled the synthesis of compounds containing very diverse substituents in different positions of the macrocyclic ring, which made it possible to obtain bacteriopyropheophorbides, bacteriopurpurinimides and tetraphenylbacteriochlorin derivatives, Fig. 3. There are also many N-fused porphyrins [23] or derivatives annulated with conjugated rings (*e.g.*, anthracene [24]) as well as phthalocyanines [25,26] that absorb in the far red or/and NIR spectral region [24,27]. Especially, the strong NIR absorption of (metallo)bacteriochlorins is crucial for light-harvesting and possible biomedical applications [28]. Many authors reported the use of (metallo)bacteriochlorins that are capable of mimicking bacteriochlorophylls, either as separate molecules or as components of natural protein complexes [20,29]. The other applications of bacteriochlorins include: (i) solar energy conversion [30,31]; (ii) chemical or biological sensing [32–34]; (iii) (photo)catalysis [35]; (iv) spectroscopic analysis and design of fluorescent probes [36]; (v) molecular imaging [37–39], (vi) optical communication [40,41] and last but not least (vii) photodiagnosis (PD) and (viii) photodynamic therapy (PDT) [42,43], Fig. 4.

2. Basic photophysical processes, photochemical mechanisms and reactive oxygen species (ROS) generation pathways

Redox reactions involving the electron transfer between donor and acceptor molecules are the key processes determining the effective course of photosynthesis. The reduction of molecular oxygen by the photosystem I (PSI) in the Mehler reaction is a coupled process that results in the creation of ATP without NADPH [44]. It is therefore not unusual that ROS produced during photosynthesis are redox and functioning signals as well as necessary regulators of energy and metabolic fluxes [44–46]. In general, a photoactive molecule (photosensitizer, PS), such as bacteriochlorophyll *a*, possesses a stable electronic configuration in the singlet ground state (S_0) with electrons having opposite spins located in the highest occupied molecular orbital (HOMO). Following photon absorption, an electron may be excited to the lowest unoccupied molecular orbital (LUMO), resulting in the formation of the PS singlet excited states ($^1PS^*$), Fig. 5.

Possible deactivation pathways of the PS excited states are illustrated in the modified Jabłoński diagram (Fig. 5). Higher PS vibrational states decay in a non-radiative way by releasing of heat. These fast processes ($\tau \sim 10^{-11}$–10^{-14} s), include both vibrational relaxation (VR) and internal conversion (IC). If the PS molecule appears at the lowest vibrational level of the excited singlet electronic state, a spontaneous emission may occur. It leads to the allowed transition to the singlet ground electronic state – S_0. The radiative process is called fluorescence and takes place in a nanosecond time regime. According to the Stokes rule, the maximum of the fluorescence (S_1-S_0 transition) band is shifted towards longer wavelengths with respect to the maximum of the absorption (S_0-S_1 transition) band. The transition of a PS molecule in the singlet excited state ($^1PS^*$) to a triplet excited state ($^3PS^*$) is not allowed due to the spin selection rule. However, it can be violated by spin-orbit coupling. If it happens, the spin reorientation occurs, and the molecule is transferred to the metastable triplet excited state (T_1) as a result of the process called intersystem crossing (ISC) [47]. Spin-orbit coupling usually occurs due to the so-called heavy atom effect caused by the presence of various metal ions, halogen and even oxygen atoms in the PS structure [48]. Consequently, these structural changes affect photophysical parameters such as the quantum yields of the intersystem crossing (Φ_{ISC}), fluorescence (Φ_F) and triplet state (Φ_T) as well as the triplet state lifetime (τ_T). $^3PS^*$ may either undergo phosphorescence (Ph) or, more preferably, can react with substrate molecule (*e.g.*, molecular oxygen) in accordance with two main mechanisms of oxygen-dependent photosensitization reactions. Type I photochemical reaction includes an electron or a hydrogen transfer from a photosensitizer in either singlet or triplet excited state to some substrate molecules, wherease type II photochemical reaction involves direct energy transfer from $^3PS^*$ to molecular oxygen in its triplet ground state ($^3O_2$) resulting in the generation of highly reactive singlet oxygen ($^1O_2$, $^1\Delta_g$). Apart from these two basic mechanisms, there are also some references to type III or even type IV mechanisms. Those photosensitized reactions are independent of the molecular oxygen concentration. Most generally, they involve activated PS molecules and components of biological structures whose oxidation leads to the formation of reactive organic radicals [18,49–51]. However, the most controversial issue still remains mechanism I. The process in which an electron transfer from the excited photosensitizer to dioxygen leads to the generation of superoxide radical ion ($O_2^{\cdot-}$). However, some authors suggest that the oxidized

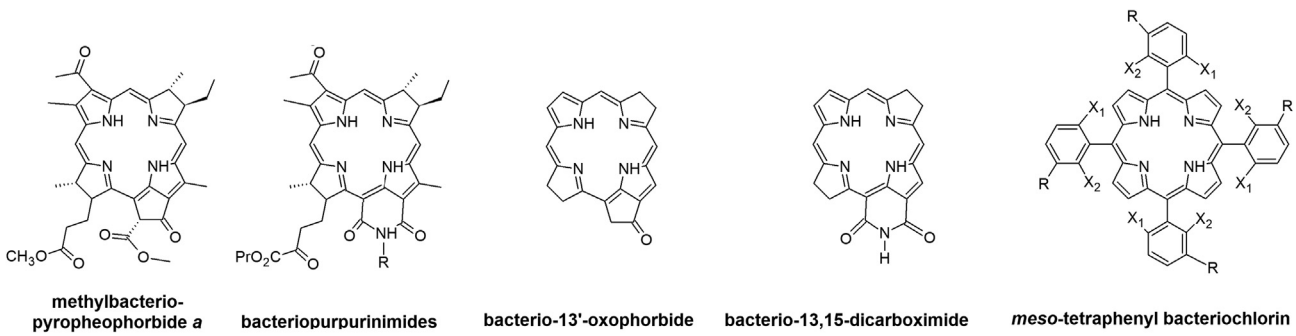

Fig. 3. Molecular templates of semisynthetic and synthetic bacteriochlorin derivatives.

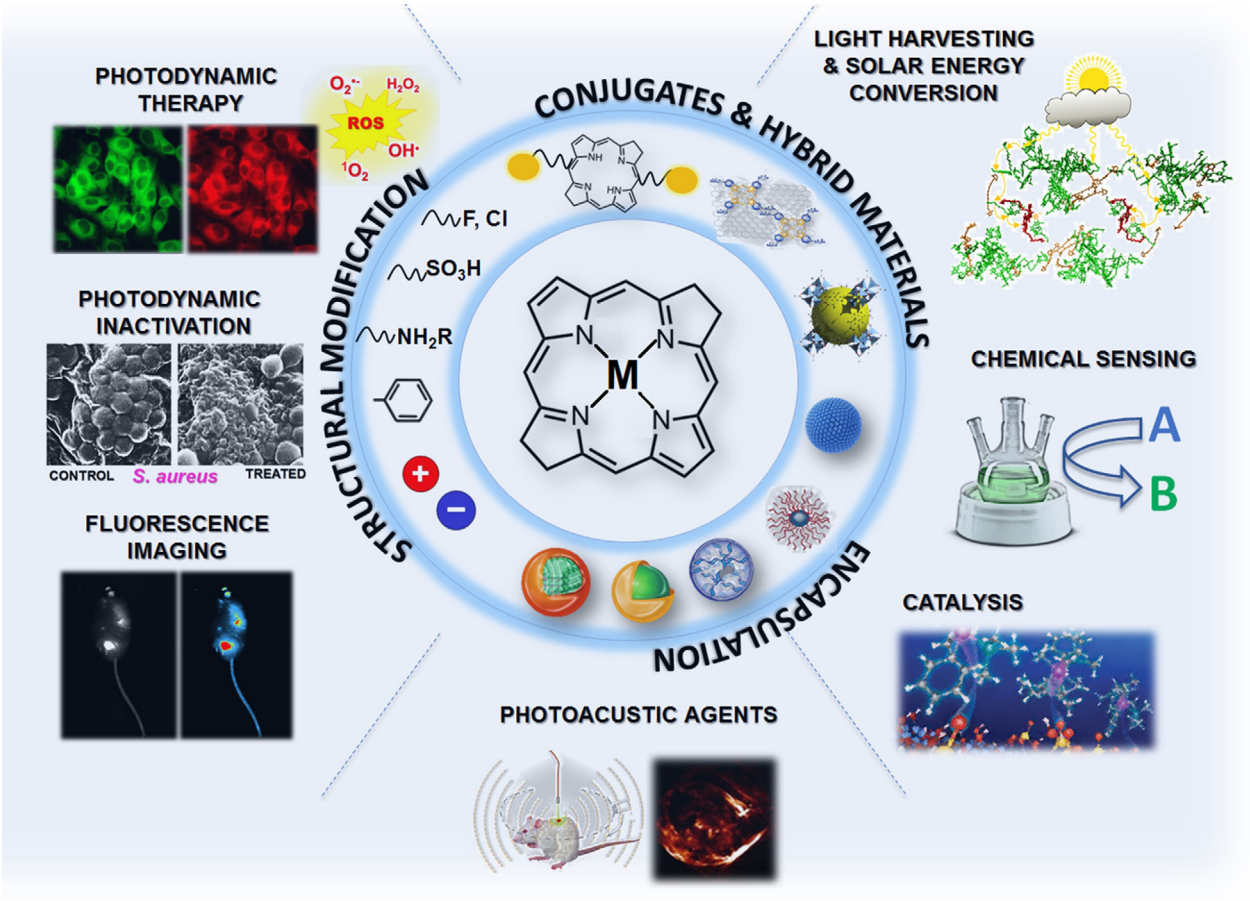

Fig. 4. Possible modification and functionalization pathways of the (metallo)bacteriochlorins and their potential applications.

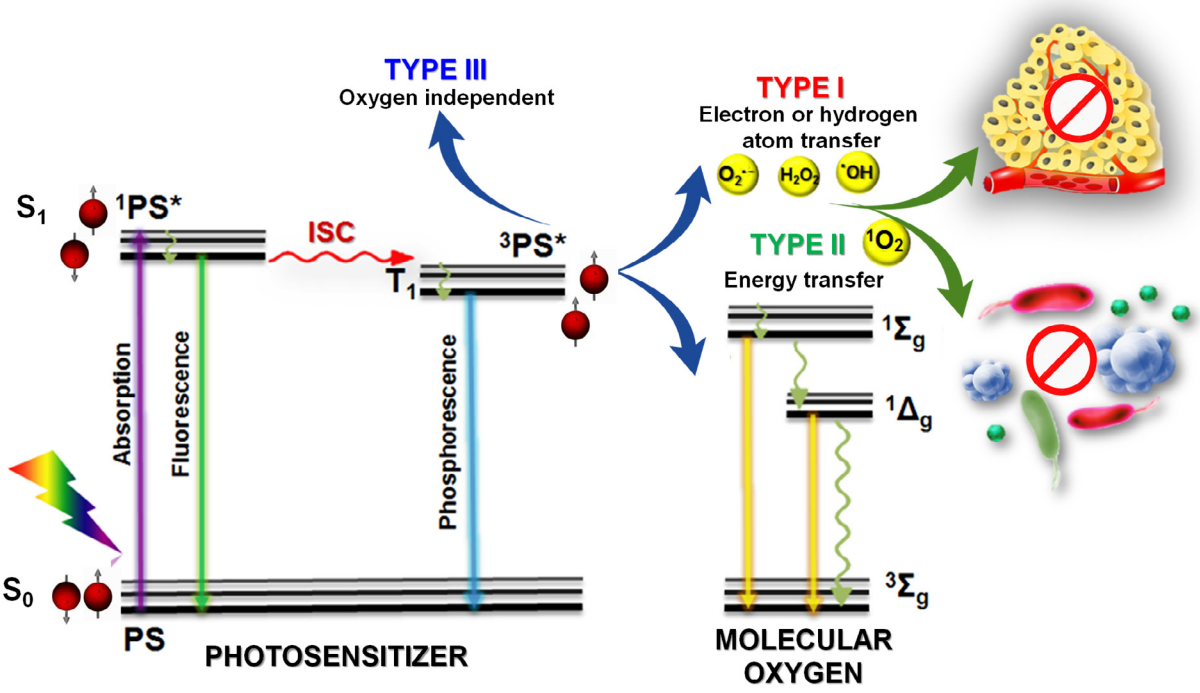

Fig. 5. Jabłoński diagram showing the possible photophysical processes, and photochemical mechanisms of ROS generation.

form of PS should also be considered as type II reaction [52]. These mechanisms have been described in detail by us [18,48,51,53–56] and by other authors [57–59], so they will be referred here only very briefly. Typically, a superoxide ion radical ($O_2^{\cdot-}$) is formed by a one-electron reduction of molecular oxygen. In the discussed photochemical processes, its formation is the result of the photoinduced electron transfer most likely from ^{3}PS*. Superoxide ion is quite a weak oxidizing agent in water. Nevertheless, in the subsequent step of oxygen reduction, hydrogen peroxide (H_2O_2) is formed, which in turn in the presence of transition metal ions, in particular Fe^{2+} and Cu^{2+}, undergoes a Fenton reaction resulted in hydroxyl radicals production [60]. Hydroxyl radical ($^{\cdot}$OH), due to its high standard reduction potential (2.31 V), is one of the most powerful oxidants capable of reacting unselectively with the adjacent chemical compounds, including organic pollutants, biomolecules (proteins, DNA, lipids), and with almost any constituent of cells [56]. Although the photosensitization under biological conditions usually leads to a combined effect of both: type I and type II processes, there are some factors more or less suitable for each of them. Most frequently, the contribution of each individual mechanism is affected by the type of PS, its concentration, type of solvent/environment in which the reaction takes place, and the amount of oxygen present in this environment. Low oxygen levels generally favor type I reactions, while type II usually occurs at higher oxygen concentrations [61].

The photophysical properties of naturally-occurring (bacterio)chlorophylls make them well adapted to support the energy transfer in photosynthesis. Unlike many endogenous pigments such as carotenoids, they do not undergo thermal relaxation [45], and thus, they can be maintained in the singlet excited state long enough for electron transfer as well as charge separation. However, these properties may create problems when light absorption exceeds photosynthetic light utilization. When excitation energy is not completely consumed during photosynthetic reactions, the lifetime of excited singlet state of bacteriochlorophyll (^{1}BChl*) increases in the light-harvesting antennae. This also enhances the probability of the ISC, resulting in the creation of a bacteriochlorophyll molecule in the triplet excited state (^{3}BChl*). It may cause a significant increase in the generation of described above reactive oxygen species: $^1O_2$, $O_2^{\cdot-}$, H_2O_2, and $^{\cdot}$OH. Therefore, the dissipation of thermal energy in bacteriochlorophyll systems can be understood as a protective mechanism responsible for preventing the formation of ROS instead of neutralizing them [45]. Nevertheless, it should also be noted that oxygen species generation is often associated with many beneficial effects. Moderate amounts of ROS are present in living organisms to guarantee normal metabolic functions and are involved in a number of signaling pathways in cells. A slight increase in ROS concentration enhances cell proliferation and increases the probability of cell survival. However, an excessive increase in their concentration can overcome the antioxidant capacity of cells and eventually lead to oxidative stress [62]. In normal cells, due to the presence of antioxidant enzymes, a small amount of exogenous ROS does not lead to any toxic effects. On the other hand, cancer cells, due to their dysfunctional metabolic activity, maintain ROS levels at the toxicity threshold, thus being in a permanent state of oxidative stress. An increase in ROS concentration in cancer cells triggered by drugs, radiation, photosensitizers, *etc.* may easily exceed their critical level, resulting in cell death. Thus, the fact that cancer cells are more sensitive to exogenous ROS has been used in numerous therapeutic strategies [63,64], including photodynamic therapy (PDT) and photodynamic inactivation of microorganisms (PDI) [53,65]. These two photochemistry-based modalities will be discussed in more detail later in this manuscript.

3. Photosensitizers based on the (metallo)bacteriochlorin framework: design and synthesis

3.1. Naturally-occurring bacteriochlorophylls

3.1.1. Physicochemical and spectroscopic properties of bacteriochlorophylls

The chlorophylls involved in plant photosynthesis and their synthetic analogs are the most studied pigments in terms of spectroscopic and photophysical properties [9,66,67]. Certainly less studied, probably due to their low stability, however essential for understanding fundamental processes and possible applications are bacteriochlorophylls (BChls) present in some photosynthetic bacteria [9,68–72]. Compared to chlorophylls (dihydroporphyrins), bacteriochlorophylls are tetrahydroporphyrins with two reduced pyrroles placed on opposite sides of the macrocycle. The structures of bacteriochlorophylls *a-e* are shown in Fig. 6 (bacteriochlorophylls *f-g* are misnamed) [9,73].

Both chlorophylls and bacteriochlorophylls contain Mg^{2+} as the central metal ion. It is known that the metal insertion into the tetrapyrrole ring changes its electronic structure and photophysical properties [75]. The progress in the reduction of pyrrole rings leads to intense absorption in the NIR. Whereas chlorophyll *a* absorbs at 662 nm and chlorophyll *b* at 644 nm, bacteriochlorophylls *a*, *b*, and *g* are characterized by strong absorption at 772 nm, 794 nm, and 762 nm, respectively [21]. Unfortunately, there are two major limitations concerning bacteriochlorophylls: (i) instability, including susceptibility toward adventitious dehydrogenation with the possible creation of the corresponding chlorin [72,76,77] and (ii) rigid and complete substitution of the macrocycle that reduces the possible semisynthetic transformations [21,42,78].

In order to overcome these limitations, a number of modifications are possible, including the peripheral substitutions of the macrocycle affecting their spectroscopic and photophysical properties. This modification results in a bathochromic shift of the low energy absorption band (Q band) towards NIR, while maintaining an appropriate energy level of excited states and lifetimes of these states long enough to allow sufficient photochemical reactions [79,80]. In that regard, synthetic chromophores have been also used for electron-transfer and energy-transfer processes. Thus, semisynthetic or synthetic bacteriochlorins can be an attractive alternative to bacteriochlorophylls. However, naturally-occurring bacteriochlorophylls still provide (Fig. 7) an excellent starting material for further modification [81].

Compounds obtained from bacteriochlorophylls were coordinated with several metal ions such as Zn^{2+}, Cu^{2+}, Pd^{2+}, Co^{2+}, Ni^{2+}, Mn^{2+}, Cd^{2+}, and Pt^{2+} [21,42,82,83] according to three main synthetic pathways [28]. The first one involves the coordination of a free macrocycle with Cd^{2+}, followed by transmetalation. The other modifications consist of the introduction of Mg^{2+} using a Grignard reagent and direct reaction with salts of appropriate metals. The insertion of metal ions into the macrocycles results in the significant change of their electronic structure and optical properties. These structural changes are particularly well described for porphyrins, for which an increase of symmetry from D_{2h} to D_{4h} is expected. This change leads to the degeneration of LUMO and a decrease in the number of Q bands in the electronic absorption spectra from four to two bands. In addition, one can observe a distinct batho- or hypsochromic shift of the Soret band, depending on the type of metal ion. Noteworthy, for Q bands, the introduction of metal ions always leads to their displacement towards shorter wavelengths [84–86]. For chlorins, however, no analogical changes in the electronic absorption spectra are observed. The coordination of metal ions does not influence the symmetry, but may cause a

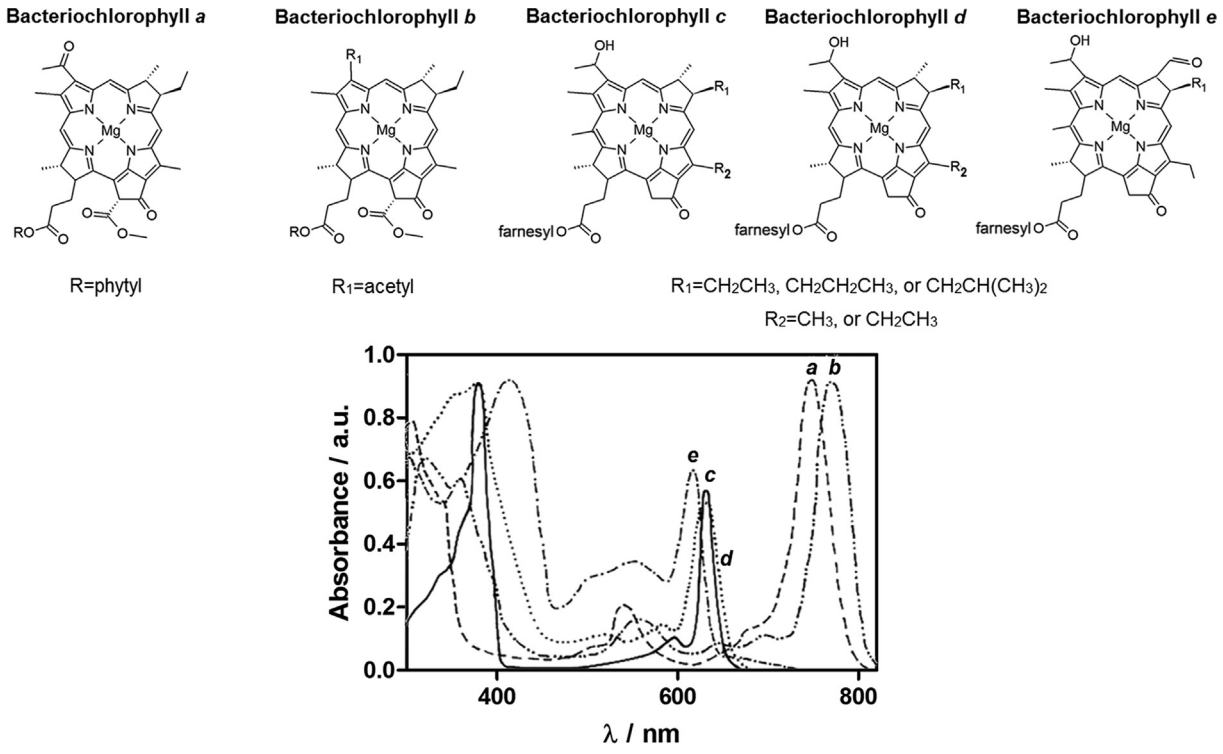

Fig. 6. Chemical structures and electronic absorption spectra of various bacteriochlorophylls derived from anoxygenic photosynthetic prokaryotes: BChl *a* of *Rhodobacter sphaeroides*; BChl *b* of *Blastochloris viridis*; BChl *c* of *Chloroflexus aurantiacus*; BChl *d* of *Prosthecochloris vibrioformis* and BChl *e* of *Chlorobium phaeovibrioides*. Adapted from [74].

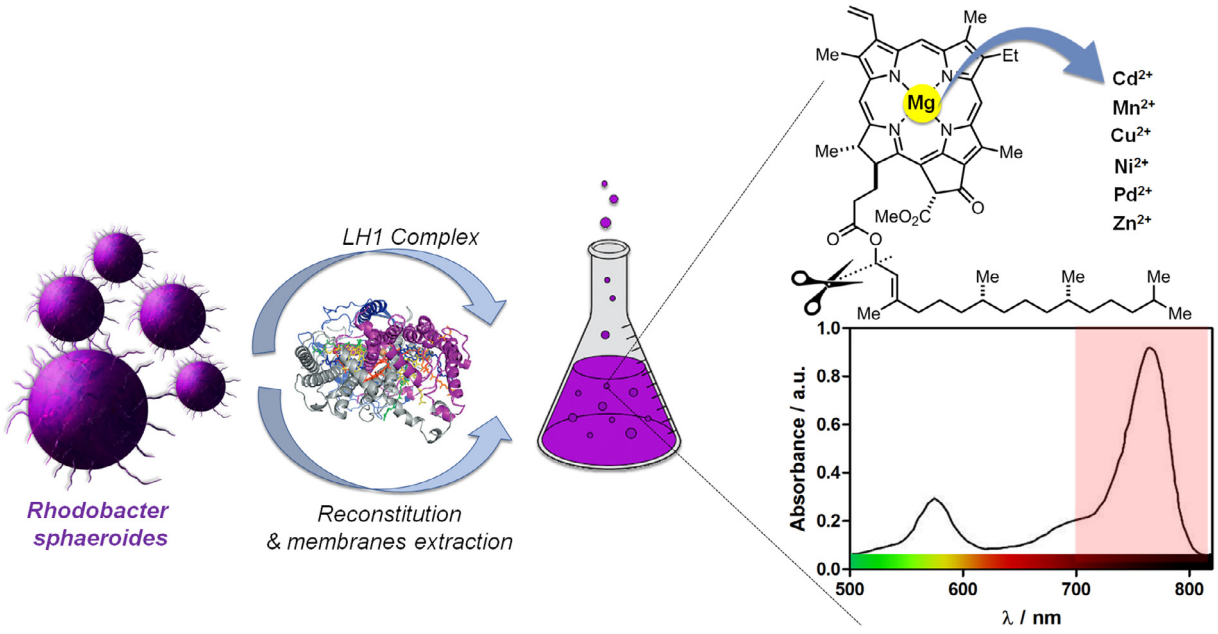

Fig. 7. Schematic illustration of the bacteriochlorophyll *a* preparation *via* extraction from *Rb. sphaeroides* along with its electronic absorption spectra and its possible ways of modification.

hypsochromic shift in the low energy absorption band assigned to the S_0-S_1 electronic transition. For example, chlorophyll *a* (Mg^{2+} chelated) possesses an absorption band at λ_{max} = 662 nm, whereas pheophytin *a* (free-base) absorbs at 667 nm in acetone [87]. Similarly, in the case of bacteriochlorins, the introduction of metal ions does not change the symmetry. Nevertheless, it leads to a bathochromic shift of the absorption band located in the red part of the spectra. Therefore, bacteriochlorophyll *a* (Bchl *a*) absorbs light at λ_{max} = 772 nm, whereas bacteriopheophytin *a* (BPhe *a*) at λ_{max} = 749 nm in diethyl ether [87]. More importantly, metal insertion significantly increases the molar absorption coefficient determined for long-wavelength Q bands [71].

A series of bacteriochlorophyll derivatives were also studied to determine the influence of the metal ions on the energy of electronic transitions and their redox properties [71]. Table 1 summarizes the spectroscopic (absorption and emission) and

Table 1
Spectroscopic and electrochemical properties of natural and transmetalated bacteriochlorophyll derivatives [71,88,90].

	Absorption λ_{max} [nm] (ε[10^3 M^{-1} cm^{-1}])				Fluorescence λ_{max} [nm]	Electrochemistry			
Compound	B_y	B_x	Q_x	Q_y		E^2_{ox}	E^1_{ox}	E^1_{red}	E^2_{red}
2H BPhe	362 (92.3)	389 (49.3)	532 (26.2)	754 (56.4)	759	0.57	0.29	−1.26	−1.66
Pd-BChl	334 (33.7)	388 (27.8)	535 (13.5)	763 (61.5)	764	0.52	0.23	−1.23	−1.66
Co-BChl	355 (40.6)	386 (27.5)	562 (10.2)	767 (56.3)	–				
Ni-BChl	366 (49.2)	391 (30.3)	598 (16.1)	771 (71.8)	–	0.29	0.08	−1.23	−1.65
Cu-BChl	358 (44.7)	395 (31.9)	573 (12.2)	780 (56.1)	–	0.36	0.08	−1.27	−1.65
Zn-BChl	364 (52.4)	390 (31.7)	579 (16.5)	773 (57.1)	782	0.35	0.00	−1.42	−1.76
Mg-BChl	374 (57.7)	–	612 (16.9)	781 (76.0)	788				
Cd-BChl	368 (65.6)	391 (44.1)	593 (19.4)	773 (69.6)	778	0.30	−0.01	−1.39	−1.75
Mn-BChl	373 (64.4)	–	601 (16.4)	780 (66.0)	–				

electrochemical properties of bacteriochlorophyll *a* and its metal complexes. As expected, the electronic absorption spectra of all studied compounds reveal four characteristic absorption bands (B_y, B_x, Q_x, and Q_y). All of the examined metal ions, but to a different extent, affect the energy of electron transitions. The most noticeable differences exsist in the energy corresponding to the Q_x and Q_y bands, while smaller differences are observed in the B_x and B_y bands. The most significant differences in the energy of S_0-S_1 transitions were indicated for the BPhe complexes with Cu^{2+}, Mg^{2+}, and Mn^{2+} metal ions. For these metal complexes, a large bathochromic shift (approximately 30 nm) of the Q_y bands is observed [71,72,88,89].

The presence of metal ions in the macrocycle is crucial for the proper functioning of many natural processes. In general, the differences in the type of metal ion in the bacteriopheophorbide may significantly change the photophysical and photochemical properties. Magnesium derivatives (five or six coordination number) usually indicates the fluorescence quantum yield equal to 0.1, quite long singlet excited state lifetime ($\tau_s \sim 10$ ns), and relatively good quantum yield of intersystem crossing determined in diethyl ether ($\Phi_{ISC} \sim 0.60$ for Chl *a* and $\Phi_{ISC} \sim 0.76$ for BChl *a*) [84,89]. Zinc complexes (four or five-coordinate) are characterized by much lower fluorescence quantum yield ($\Phi_F \sim 0.03$), a shorter singlet excited state lifetime ($\tau_s \sim 2$ ns), and a higher ISC quantum yield [84]. These differences can be attributed to the heavy-atom effect [91], which is even more pronounced for complexes with heavier metals. For instance, the Pt-chlorophyll *a* triplet state lifetime determined in deoxygenated organic solvents is ten times shorter than for free-base and Mg^{2+} and Zn^{2+} coordinated chlorophylls [90]. Palladium derivatives (four coordinate) are also characterized by negligible fluorescence, the highest possible ISC quantum yield ($\Phi_{ISC} \sim 1.00$), and short triplet excited state lifetimes [86].

Analyzing the influence of different metals on the photophysical properties of bacteriochlorophylls, it can be assumed that the choice of Mg^{2+} by nature and not Zn^{2+} (which more easily forms complexes with tetrapyrroles), was not only motivated by the greater bioavailability of magnesium, but also to protect the photosynthetic apparatus against the excessive generation of ROS. This effect is quite different and more sophisticated for paramagnetic metal complexes (*e.g.*, Fe^{2+}, Cu^{2+}, Ni^{2+} and Co^{2+}) with tetrapyrrolic ligands than for Mg-derivatives. For such compounds, fluorescence is not observed at all, and highly predominant internal conversion can be detected. For instance, copper complexes with coordination number 4 are characterized by very short singlet excited state lifetimes, do not possess fluorescent properties, and, unlike other derivatives, have other properties highly dependent on temperature [85]. Also, the choice of paramagnetic metal ions by nature is considered as a protective mechanism against photochemical reactions that can eventually lead to adverse effects. Nevertheless, despite the lack of photochemical activity, this kind of metalloporphyrins takes part in significant redox reactions and therefore participate in various biochemical processes [88].

3.1.2. Bacteriochlorophylls in the bacterial reaction center

The bacterial reaction center (BRC) with densely packed pigment molecules (*e.g.*, chlorins and bacteriochlorins) surrounding the protein matrix from photosynthetic purple bacteria is well characterized in terms of their structure and spectroscopic properties [92,93]. The conversion through a network of well-arrangement pigments into protein complexes is an ideal model system for investigation of the structure- and function- relationship due to the efficient energy transfer and charge separation. Two-dimensional electronic spectroscopy (2DES) has emerged as a powerful method appropriate for examination the electronic coupling between chromophores [93]. The measurement of well design sequences of three laser pulses with determined emission frequency (t_1, t_2, t_3) allows the capturing of dynamics with high time resolution inside the system. This high resolution, nonlinear optical spectroscopic method allows studying the chemical and biochemical processes as well as interactions and dynamics of complex molecular systems. For instance, the observation of the light-harvesting antenna of photosynthetic microorganisms shows strong pigment-pigment interactions by capturing energy flow on a 2D frequency map, Fig. 8 [94].

Zigmantas *et al.* have studied light-harvesting complex LH3 from photosynthetic purple bacteria with B800–B820 bacteriochlorins, which absorb in 800 nm and 820 nm, respectively [92]. By using the 2D electronic spectroscopy, it was possible to measure the different population times that reveal ultrafast molecular dynamics within the B820 ring. Moreover, the asymmetry of the 2D spectrum of highly symmetric structure LH3 with the couplings between BChls eliminates cross-peaks by forbidding selected electronic transitions. LH3 contains nine identical subunits with 27 bacteriochlorophyll molecules in the symmetric ring-like light-harvesting structure. Closely packed 18 BChls of B820 ring are strongly coupled, while nine rings of B800 are relatively large separated subunits with exhibit weak intramolecular coupling [92]. 2DES can be suitable for the molecules for which the high-resolution crystal structure cannot be obtained. For instance, Ginsberg *et al.* have studied the light-harvesting complex 4 (LH4) expressed by photosynthetic purple bacteria in the lack of light with 2DES [95].

Nonlinear polarization-dependent spectra combined with theoretical modeling confirm the LH4 structure that consist of 8 identical protein subunits in an annular structure with a total of 32 molecules [96]. The significant efficiency of photosynthetic charge separation involving bacteriochlorophylls has inspired many scientists to recognize these processes at the molecular level. Konar *et al.* have also examined the model of the bacterial reaction center isolated from *R. capsulatus* (mutant with lack of ubiquinone). In these studies, the strong interaction between pigments located

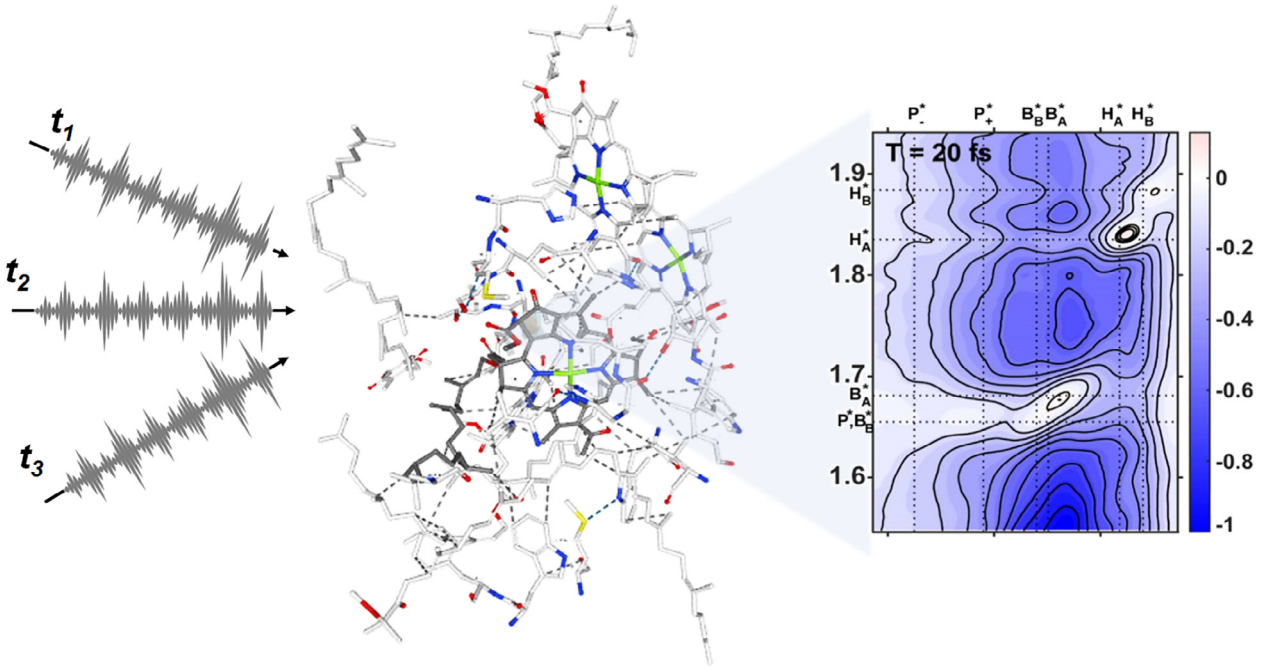

Fig. 8. 2D electronic spectroscopy (2DES) principle: 2DES records the signal which is emitted from a system (chromophores) after an interaction with a sequence of 3 laser pulses with noncollinear geometry carrying information about the properties of the sample. 2DES of the BRC (PDB: 1K6L) which undergoes charge separation, involving the energy-transfer and charge-separation processes with time and excitation frequency resolution. Measured 2D spectra are spread on so-called excitation and detection frequencies and show correlations between different optical transitions in the system under investigation. Representative 2DES spectra adapted from [94].

on two branches (named as A and B), each containing bacteriochlorophyll (BChl-A and BChl-2B), where an initially absorbed energy derives from bacteriopheophytin (HA and HB) and then is transferred to bacteriochlorophyll *a* (PA and PH) [94]. The energy of couplings has been reported from the range ~400–750 cm^{-1} for the special pair, to several cm^{-1} between H and P and HA and HB. Moreover, the excitation delocalization among the BRC is in accordance with the energy transfer and charge separation mechanisms. These data resolve Q_y/Q_x cross-peaks of most weakly-coupled BRC transitions with the two-color 2D spectroscopy [94]. The understanding of these naturally-occurring photosynthetic systems with efficient energy conversion influences the development of artificial light-harvesting devices.

3.1.3. Theoretical studies of bacteriochlorophylls properties

Parallel to experimental work, theoretical studies on the optical properties of bacteriochlorophylls containing divalent metal ions such as Co^{2+}, Ni^{2+}, Cu^{2+}, Zn^{2+}, Ru^{2+}, Rh^{2+}, Pd^{2+}, and Pt^{2+} were conducted. Particular emphasis was given to the derivatives containing metal ions, which have already been used in anticancer therapy (for instance, Ru^{2+} and Pt^{2+}). The main objective of these studies was to combine the cytotoxic effect of these metals with the spectroscopic properties of bacteriochlorophylls, enabling their application as PDT-photosensitizers. The theoretical calculations carried out using density functional theory (DFT) indicate that the geometries of the selected bacteriochlorophylls reveal many similarities [97]. The macrocycle is generally flat, and the introduced metal ions are placed in the plane of the ring, indicating the capability to insertion of metal ions with different sizes. Metal ions are most strongly bound to nitrogen atoms, which are derived from pyrrolic moiety. Based on the spectroscopic data present in the literature, the optical properties of the examined systems were also confirmed, Table 2 [97].

It was also concluded that all investigated complexes except Mg-BChl and Zn-BChl are stable in aqueous solvents, which enables their further investigation in biological systems. The message to be learned fom this study was that Ru-, Rh-, Pt- and Pd-bacteriochlorophylls can be interesting photosensitizing agents for future therapeutic purposes [97]. These predictions turned out to be quite accurate because such types of compounds have been successfully tested *in vitro*, *in vivo* and even clinically for many years as potent photosensitizers for photodynamic therapy (PDT), which will be discussed later.

Table 2
Theoretically calculated energies of HOMO/LUMO orbitals and energy gaps (eV) compared with the experimental values of maximum wavelength (λ_{max}) of the Q_X absorption band for (metallo)bacteriochlorins.

Compound	E_{HOMO}/eV	E_{LUMO}/eV	GAP/eV	Q_x λ_{max}/nm
Mg-BC	−4.83	−3.68	1.15	778
Co-BC	−4.86	−3.69	1.17	767
Ni-BC	−4.88	−3.70	1.17	779
Cu-BC	−4.89	−3.73	1.16	780
Zn-BC	−4.91	−3.72	1.18	773
Ru-BC	−4.92	−3.58	1.34	–
Rh-BC	−4.95	−3.63	1.32	–
Pd-BC	−4.92	−3.67	1.25	–
Pt-BC	−4.94	−3.65	1.29	763

3.2. Semisynthetic derivatives of bacteriochlorophylls

3.2.1. Bacteriopyropheophorbides and bacteriopurpurinimides

According to the procedure mentioned earlier, it is possible to convert the bacteriochlorophyll *a* extracted from *Rb. sphaeroides* into bacteriopurpurin-18. Bacteriopurpurin-18 in the next reaction steps is transformed into two types of bacteriochlorin derivatives: bacteriopurpurinimide and bacteriopurpurin *p6*, which are respectively equipped or not with a fused imide ring [98,99]. These types of long-wavelengths (metallo)macrocycles were developed by R.K. Pandey's group. For instance, the synthesis and characterization of a series of novel bacteriochlorins from 13^2-oxo-bacteriopyropheophorbide as a starting material were reported.

Fig. 9 illustrates the general procedure for the synthesis of bacteriopheophorbide derivatives from bacteriochlorophyll *a* [100]. The absorption spectra of these bacteriochlorins showed exceptionally large shifts of the Q_y absorption band towards near-infrared (λ_{max} from 816 nm to 850 nm). Moreover, the determined molar absorption coefficients for these low-energy bands also possessed remarkably high values, even up to 136 800 $M^{-1}cm^{-1}$. In the following studies, the biological activity of these compounds and some of the analogs was extensively investigated and their excellent PDT efficacy against various types of cancer cells and tumor models was proven [42,101].

In the same research group, a library of new compounds called bacterioverdins was developed (Fig. 10). These molecules contain a fused six-membered methoxy-substituted cyclohexenone (verdin) as an isomeric mixture [100]. The most significant properties of bacterioverdins include absorption at long wavelengths (865–890 nm) and the favorable redox potentials that ensure both stability and ROS generation ability, not necessarily through energy transfer reaction. The comprehensive electrochemical studies were conducted, which part of the results in the form of cyclic voltammograms registered for each compound is demonstrated in Fig. 11. The most interesting results of these studies include the observation that three of the studied compounds, those with fused cyclohexanone ring systems, show a remarkably smaller HOMO-LUMO energy gap, and thus more readily undergo oxidation/reduction, compared to the previously investigated by authors bacteriochlorins [102,103]. As already mentioned, the greatest advantage of these compounds is their extraordinary absorption in the NIR range, reaching wavelengths of nearly 900 nm. Hypothetically, such compounds could be used in PDT to treat large, subcutaneous tumor tissue, because photons in this range are able to penetrate very deeply through tissues. Nevertheless, it should be noted that absorption at such long wavelengths exceeds the range specified for a phototherapeutic window (630–850 nm). This is naturally related to the energy limitation in the generation of singlet oxygen by such photosensitizers. However, appropriate redox properties of this group of compounds may facilitate photoinduced electron transfer reactions leading to the formation of oxygen-centered radicals. Moreover, it seems that such compounds offer a completely different application potential, *e.g.*, for the construction of optical materials and information storage.

R.K. Pandey *et al.* have also reported the impact of the insertion of metal ions, *e.g.*, Zn^{2+}, Cu^{2+}, Sn^{2+}, In^{3+} on the photodynamic activity of examined complexes [104]. To investigate the effect of these metals on the photochemical properties, they prepared the corresponding complexes based on the pyropheophorbide framework (Fig. 12).

3.2.2. Pd-Bacteriopheophorbides

Compared to the corresponding free-based macrocycles, the Pt^{2+} and Pd^{2+}complexes are chemically more active and undergo more efficient ISC to achieve higher values of the triplet excited state quantum yields. Thus, combined with short excited-state lifetimes, they mainly act as type I photosensitizers generating oxygen-centered radicals in the biological environment [105]. The electronic absorption spectra of metallobacteriochlorins are similar to free-base analogues but slightly shifted either to shorter or more preferably longer wavelengths [106]. Most of the Pd-bacteriochlorins photochemical properties make them valuable for the application in PDT.

Palladium containing BChl *a* derivatives such as padoporfin (Tookad, WST09) and padeliporfin (Tookad Soluble, WST11) presented in Fig. 13 are particularly interesting photosensitizers when compared to their free-base analogues [107–110]. First of all, pal-

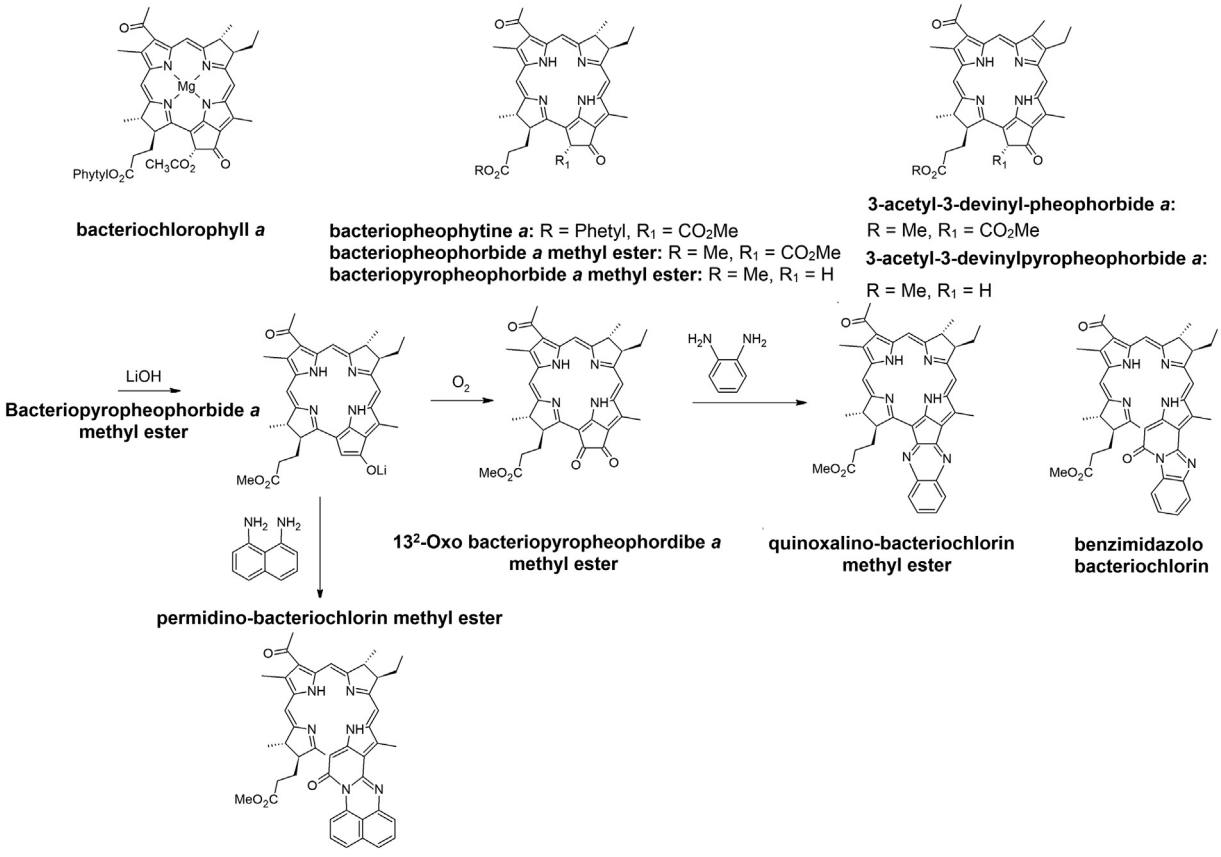

Fig. 9. Synthetic pathway for obtaining bacteriopheophorbide derivatives from bacteriochlorophyll *a* as a starting material.

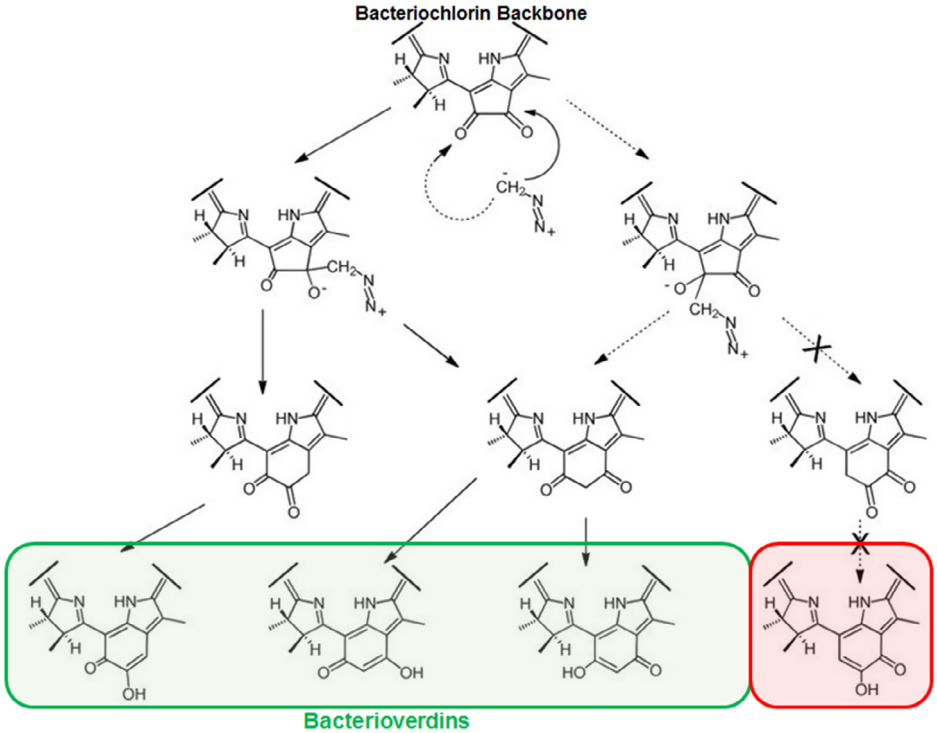

Fig. 10. The scheme to obtain bacterioverdins from 13^2- oxobacteriopyropheophorbide *a*; based on [100].

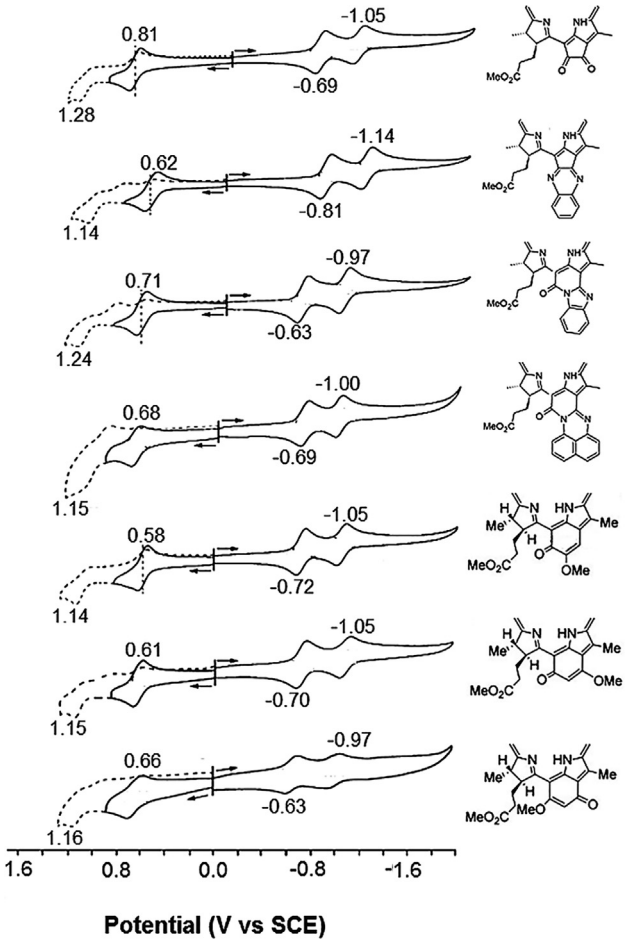

Fig. 11. Cyclic voltammograms of bacteriochlorin or bacterioverdin derivatives registered in CH_2Cl_2 containing 0.1 M TBAP at the scan rate of 0.1 $V{\cdot}s^{-1}$. Adapted from [76].

ladium bacteriochlorins, due to the heavy atom effect, are characterized by nearly unity quantum yield of ISC. Besides, as has already been demonstrated, bacteriochlorins coordinated with Pd^{2+} have the most batochromically shifted long-wavelength absorption band compared to other metal complexes. Pd^{2+} insertion into BChls results in the Φ_{ISC} approaching 1 and an increased phosphorescence quantum yield under anaerobic conditions. The high value of Φ_{ISC} is in line with the short lifetime of the singlet excited state. This brings the quantum yield of $^1O_2$ equal to unity (Φ_Δ = 1) in organic solvents [111]. Nevertheless, the relatively polar conditions (*e.g.*, micelle/water solution) enhance the probability of charge-transfer processes between Pd-BChl *a* triplet state and molecular oxygen [111]. Besides, the large NIR absorption, desired redox properties and high value of Φ_{ISC} determined for Pd-BChl derivative lead to a substantial formation of oxygen-centered radicals upon a short irradiation time [111]. Studies on the influence of human albumin (HSA) on the generation of ROS by WST11 have shown that the photogenerated ROS are $O_2^{\cdot-}$ and $OH^{\cdot}$ radicals rather than singlet oxygen. This suggests that WST11 photocatalyzed the electron transfer from PS associated with HSA to the colliding oxygen molecules through several cycles [105]. The obtained results may suggest that the resulting WST11-HSA complex can be considered as a single reaction center, which photocatalysis redox reactions required for the formation of ROS, which are the appropriate cytotoxic agents in PDT [105]. The following research focused on palladium derivatives of BChl *a* led to the development of photosensitizers possessing remarkable photodynamic efficiency.

3.2.3. Zn-derivatives of bacteriochlorophylls

Semisynthetic and synthetic zinc complexes of bacteriochlorophyll *a* can be easily prepared by the replacement of the central Mg^{2+} with Zn^{2+}. Among the bacteriochlorophyll derivatives containing metals other than Mg^{2+}, only Zn-chlorophylls have chemical features quite comparable to Mg-chlorophylls [112,113]. Nevertheless, Zn-derivatives are more stable than Mg-derivatives

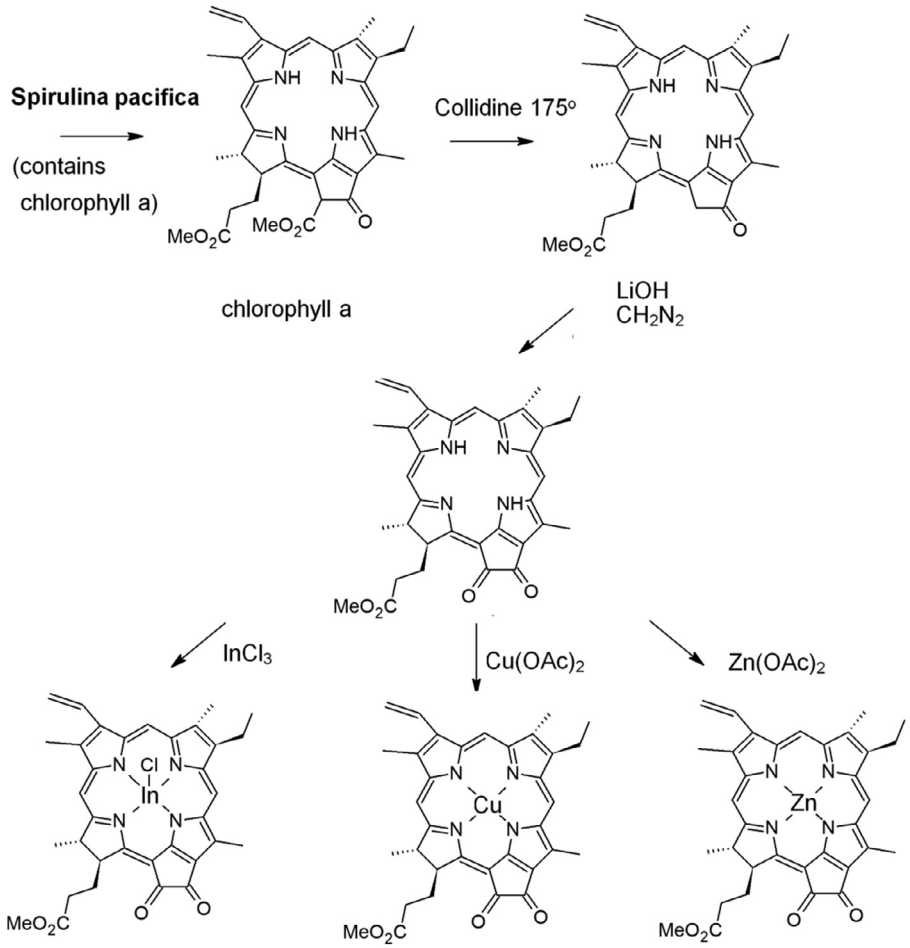

Fig. 12. Synthetic pathway for the synthesis of a series of (metallo)derivatives of methyl 132-oxo-pyropheophorbide *a*.

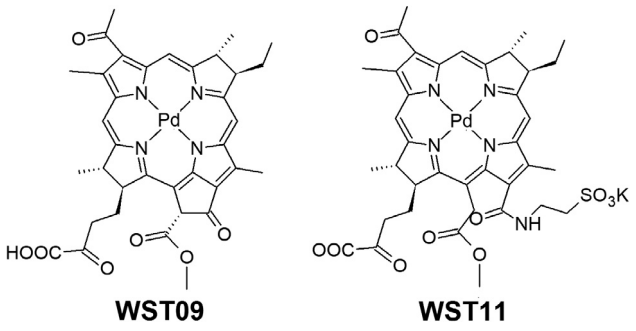

Fig. 13. Examples of Pd-bacteriochlorin derivatives: WST09 (padaporfin) and WST11 (padeliporfin).

and have been widely applied in artificial photosynthesis studies [114,115]. Zinc-bacteriopheophytins (Zn-(B)Pheo) are known to be good structural and functional models for naturally occurring bacteriochlorophylls [116,117]. It was found that Zn-BPhe may be used instead of BChl *a* in a special photosynthetic bacteria, *e.g.*, an *Addiphilium rubrum* [118]. Moreover, Zn-containing bacteriochlorophyll has been introduced artificially into the isolated antenna proteins as the replacement of light-harvesting Mg-BChl or accessory Mg-BChl in the reaction center complex [70,113].

Yang and coworkers have synthesized and characterized the series of zinc-bacteriochlorins with the different number of electron-withdrawing groups as peripheral substituents [29]. The authors reported that their optical properties are not that different from free-base bacteriochlorins and naturally-occurring bacteriochlorophyll derivatives [118,119]. However, Zn^{2+} insertion into macrocycle gives a lower fluorescence quantum yield ($\Phi_F \sim 0.03$), a shorter singlet excited state ($\tau \sim 2$ ns), and a higher quantum yields of ISC and triplet state when compared with metal-free compounds [29]. Despite the lack of significant changes in the electronic absorption spectra, it should be recognized that for the series of Zn-bacteriochlorin with the different number of electron-withdrawing substituents, the differences in the values of molar absorption coefficients are significant [21]. Moreover, the zinc complexes are quite fluorescent, with quantum yields ranging from 0.08 to 0.20 with an average value of $\Phi_F = 0.13$, which is comparable to free-base analogs ($\Phi_F \sim 0.15$). The fluorescence lifetimes are also similar to free-base analogs (3.3–4.4 ns) [29]. The quantum yield of intersystem crossing determined for the Zn-bacteriochlorins ($\Phi_{ISC} = 0.7$) is somewhat higher than the average value determined for free-base analogs ($\Phi_{ISC} = 0.5$). This increase is again attributed to the heavy atom effect [29,120]. In conclusion, the synthetic zinc bacteriochlorins are characterized by improved photostability and the photophysical properties desired not only for medical applications but also for solar-energy conversion, light-harvesting and catalysis [28,36–38,40]. Furthermore, they may also be applied in the development of conjugates and arrays designed with photosynthetic-like multipigment architectures [35,117,121–124].

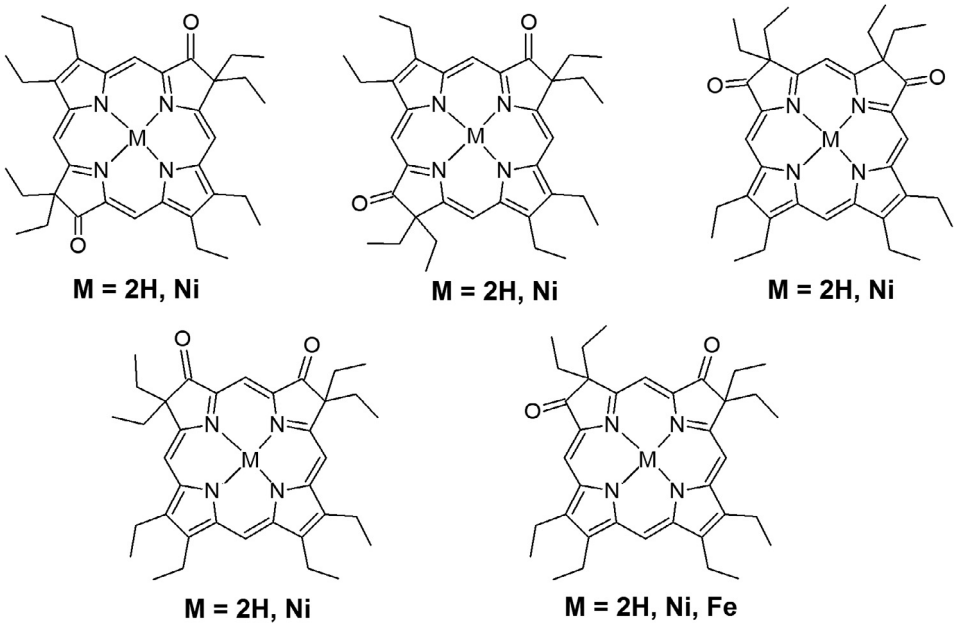

Fig. 14. Free-base and metal complexes of octaethyldioxoisobacteriochlorin.

3.2.4. Ni-derivatives of bacteriochlorophylls

By changing the centrally coordinated metal ion in the bacteriochlorophyll macrocycle, it is possible to modify various properties not only in its ground but also in the excited states. It has been shown that derivatives containing Ni^{2+} or Cu^{2+} ions undergo rapid, nonirradiated conversion to the ground state without any photochemical activity. The Stolzenberg group delineated the structural and reductive chemistry of Pd^{2+} and Ni^{2+} octa-substituted bacteriochlorin derivatives for biologically significant differences in analog metalloporphyrins [125–127]. The synthesis of the Ni-complexes (Fig. 14) was accomplished by isobacteriochlorin metalations.

In the following studies, Lahiri and Stolzenberg have described the possible mechanisms by which Ni^{+}-octaethylisobacteriochlorin anion can react with electrophiles [125]. They studied these processes in the context of the relevance of Ni^{+} form in cofactor F430, which is a Ni-containing prosthetic group of methyl coenzyme M reductase. This biologically-relevant enzyme catalyzes the reductive cleavage of the thioether-cofactor in the final step of methanogenesis. It also catalyzes the reductive dehalogenation of chlorinated hydrocarbons by methanoic bacteria [125]. Ni-substituted bacteriochlorophylls may also be applied in the context of the light-harvesting antenna. For instance, Fiedor and coworkers have reported that the replacement of the central Mg^{2+} in chlorophylls by Ni^{2+} results in an ultrafast (up to femtoseconds) internal conversion, while maintaining the fundamental optical properties in the ground state [128]. Another potential application of these Ni^{2+} complexes could be their use in the future as contrast agents for photoacoustic tomography.

4. Synthetic (metallo)bacteriochlorins

Despite the unquestionable success of palladium-bacteriopheoforbide, two main limitations of bacteriochlorophylls are related to (i) their relatively low stability and photostability, and (ii) the complete substitution pattern of the macrocycles, that reduces the possibility of semisynthetic transformations [29]. Synthetic bacteriochlorins offer an attractive alternative to semisynthetic derivatives of naturally occurring bacteriochlorophylls. The well-known synthetic methods of obtaining (metallo)bacteriochlorins include the hydrogenation and/or addition reactions (*e.g.*, vicinal dihydroxylation) of suitable porphyrin or chlorin [20,29]. Nevertheless, these methods, depending on the existing substitutes, could lead to the formation of regioisomers and leaves the bacteriochlorin more prone to aerobic dehydrogenation [29].

The synthesis of the family of β-alkyl-substituted stable (metallo)bacteriochlorins was recently described. This procedure implies the modification of the standard transmetalation procedure using a strong base to protonate centrally placed –NH groups and then adding the appropriate metal salt. The set of synthetic bacteriochlorins bearing the different number of carbonyl groups were testes under the following conditions: Zn^{2+} insertion to porphyrin ring and its further reaction in THF with a strong base upon the use of proper metal salt. In such a way several metal complexes can be obtained, namely: (i) derivatives with two aryl groups, M = Cu^{2+}, Zn^{2+}, Pd^{2+}, and InCl (but not Mg^{2+}, Al^{3+}, Ni^{2+}, Sn^{2+}, or Au^{+}); (ii) bacteriochlorins with two carboethoxy groups, M = Ni^{2+}, Cu^{2+}, Zn^{2+}, Pd^{2+}, Cd^{2+}, InCl, and Sn^{2+}; and (iii) bacteriochlorins with four carboethoxy groups coordinated with Mg^{2+} [21,29]. Compared to free-base counterparts, these complexes are characterized by a 20–30 nm bathochromic shift of the low energy absorption Q band. The theoretical calculations also indicated a decrease in the HOMO-LUMO gap upon metalation [29]. It was shown that metalation induced a slight distortion from the planarity and a shift in the electron density on the frontier orbitals, particularly in the LUMO level [29]. The fluorescence quantum yields (Φ_F ~ 0.01–0.03) and singlet state lifetime (τ_s ~ 270 ps) of the metal complexes were diminished by order of magnitude when compared to corresponding free-base compounds. They also displayed a triplet state quantum yield Φ_T ~ 0.9 and a triplet state lifetime τ_T ~ 30 μs [21,29]. The metal insertion also increases the heavy atom effect by increased spin-orbit coupling, especially for the In-bacteriochlorins presented in Fig. 15.

Another set of metallobacteriochlorins presented in Fig. 16 was synthesized and thoroughly characterized by electrochemical measurements and DFT calculations. Their most important spectroscopic, photophysical and redox properties, namely the

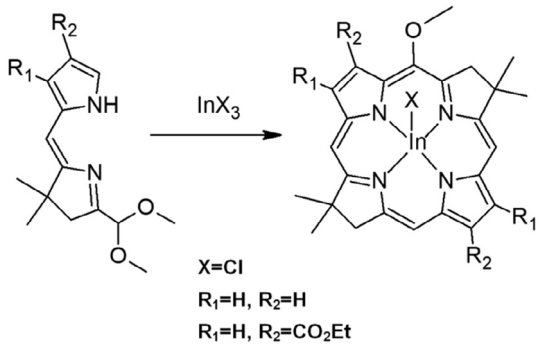

Fig. 15. Synthesis of Indium-bacteriochlorins during macrocycle formation.

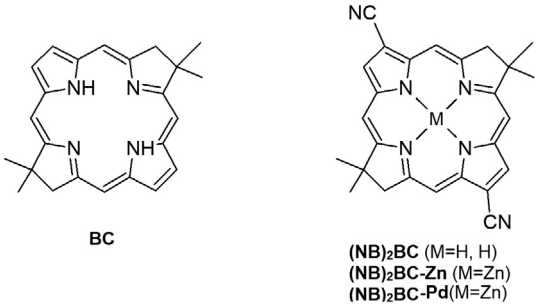

Fig. 17. The chemical structures of synthetic bacteriochlorin (BC) and its dicyano-(metallo)derivatives.

determined λ_{max}, the singlet and triplet state lifetimes, quantum yields of fluorescence and intersystem crossing (Φ_F and Φ_{ISC}) as well as HOMO and LUMO orbitals energies and oxidation potentials, are summarized in Table 3.

The impact of metal insertion into bacteriochlorin macrocycle was described in detail for dicyano Zn- and Pd-bacteriochlorins and compared with their free-base analogs ($(NC)_2$BC and BC, respectively), Fig. 17. Each bacteriochlorin indicats a typical electronic absorption spectra. Both modifications (metallation and introduction of cyano groups) lead to the noticeable shifts of the low-energy absorption Q_y bands. The absorption band registered for metal-free dicyano-bacteriochlorin $(NC)_2$BC in toluene is hypsochromically shifted (35 nm) compared to the non-substituted derivative [129]. The insertion of Pd^{2+} results in a slightly bathochromic shift to 751 nm, while the Zn^{2+} insertion causes an even more significant shift up to 761 nm, Table 4.

Moreover, in comparison to BC, metallobacteriochlorins are significantly less aggregated in water and are characterized by enhanced photostability due to the presence of metal ion and dicyano-substituents. BC, $(NC)_2$BC and Zn^{2+} complex indicate comparable singlet excited state lifetimes (τ_S = 3.9–4.1 ns) and fluorescence quantum yields (Φ_F = 0.14–0.15) determined in toluene and methanol. Nevertheless, the fluorescence lifetime and quantum yield of $(NC)_2$BC-Pd are remarkably reduced (τ_S = 23 ps, Φ_F = 0.0008). The parameters determined for these complexes are consistent with those determined for other Pd-bacteriochlorophyll derivatives [111] and imidazolium metalloporphyrins [129,130]. The intersystem crossing quantum yield determined for $(NC)_2$BC-Pd reached unity, in contrast to Φ_{ISC} = 0.63 determined for $(NC)_2$BC-Zn and 0.43 for $(NC)_2$BC. The values of Φ_{ISC} obtained for unsubstituted BC (Φ_{ISC} = 0.62) clearly demonstrate the influence of the cyano groups on the photophysical properties [129]. Consequently, the triplet state lifetimes in deoxygenated solutions are in the range from 80 μs to 170 μs for BC, $(NC)_2$BC,

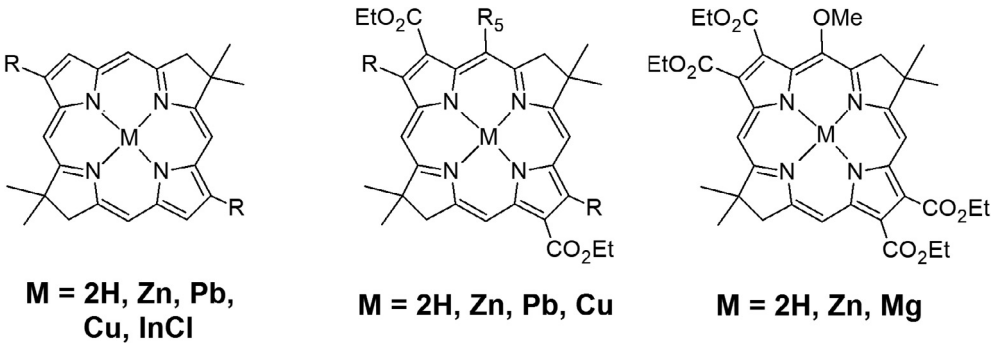

Fig. 16. Metallobacteriochlorins with a different number of electron-withdrawing groups.

Table 3
Photophysical, spectroscopic and electrochemical properties of metallobacteriochlorins with the different number of electron-withdrawing groups [20,21,29,129].

Metal	Number of with-drawing groups	Absorption λ(nm)				Fluorescence			Triplet state		Electrochemistry			
		B_y	B_x	Q_x	Q_y	λ (nm)	τ_S ns	Φ_F	Φ_{ISC}	τ_T μs	E_{ox}	E_{red}	HOMO	LUMO
	0	351	374	499	736	742	3.3	0.18	0.55	163	+0.21	−1.49	−4.40	−2.22
Free base	2	361	383	538	758	765	3.9	0.15	0.35	52	+0.38	−1.29	−4.65	−2.48
	4	361	368	550	759	763	4.3	0.16	0.24	46	+0.57	−1.05	−5.00	−2.95
	0	344	384	521	749	756	2.9	0.11	0.83	161	−0.04	−1.60	−4.26	−2.20
Zn	2	353	389	565	773	780	2.9	0.12	0.71	120	+0.45	−1.38	−4.55	−2.51
	4	354	385	581	774	782	4.4	0.13	0.80	38	+0.16	−1.10	−4.87	−2.92
Cu	0	337	383	512	755	–				0.5	−0.04	−1.53	−4.25	−2.25
	2	348	390	556	780	–				1.7	+0.18	−1.32	−4.53	−2.55
Pd	0	330	379	499	739	745	0.35	0.02	>0.99	12	+0.43	−1.14	−4.36	−2.26
	2	337	382	538	758	765	0.015	0.006	>0.99	5.8	+0.29	−1.29	−4.63	−2.54
InCl	0	350	388	539	763	769	0.21	0.016	0.9	44	+0.31	−1.25	−4.52	−2.52
Mg	4	360	380	599	776	780	5.4	0.16	0.60	90			−4.86	−2.94

Table 4
Spectroscopic, photophysical, and redox properties of selected bacteriochlorins [129].

PS	Absorption*; λ_{max}/nm				Fluorescence*			Triplet		Electrochemistry		
	By	Bx	Qy	Qx	λ_{max}/nm	Φ_F	τ_S/ns	Φ_T	τ_T/μs	E_{ox}	E_{red}	HOMO-LUMO
BC	340	365	489	713	716	0.14	4.0	0.62	169	+0.09	−1.67	2.25
$(NC)_2$BC	347	372	515	748	752	0.15	4.1	0.43	84	+0.60	−1.10	2.12
$(NC)_2$BC-Zn	343	380	546	761	763	0.15	3.9	0.63	121	+0.31	−1.14	2.01
$(NC)_2$BC-Pd	326	374	518	751	753	0.0008	0.023	0.99	7	+0.52	−1.03	2.05

*Determined in toluene.

and $(NC)_2$BC-Zn, but only 7 μs for $(NC)_2$BC-Pd. The triplet state properties influence the ROS generation ability by these photosensitizers. It is reported that the Pd-derivative produces a relatively high amount of ·OH. The other compounds generate a smaller amount of ·OH than $^1O_2$ and are, therefore, less susceptible to type I photoreactions. It is also demonstrated that the insertion of various metal ions influences the redox properties of studied photosensitizers. The first oxidation potential (E_{ox}) and higher reduction potential (E_{red}) of the four bacteriochlorins [BC, $(NC)_2$BC, $(NC)_2$BC-Zn, $(NC)_2$BC-Pd] are summarized in Table 4. In general, the introduction of the two cyano groups into bacteriochlorin core results in the fact that the obtained derivative ($(NC)_2$BC) is easier to reduce and more difficult to oxidize than the molecule without these substitutes (BC). Compared to free-base $(NC)_2$BC, the palladium derivative is slightly easier to oxidize and also slightly more difficult to reduce. In contrast, the Zn^{2+} complex is significantly easier to oxidize and, respectively, more difficult to reduce [129].

The importance of the redox potentials as factors influencing the balance between type I and type II photochemical mechanisms has been well established for dicyanibacteriochlorins and their porphyrin analogs [51,131]. As mentioned above, Pd^{2+} complexes of these tetrapyrroles are harder to oxidize and easier to reduce (in a ground singlet and triplet states) than their Zn^{2+} counterparts [129]. The redox properties of bacteriochlorins in the excited states affect not only their physicochemical (*e.g.*, photostability) but also play the crucial role in the generation of reactive oxygen species *via* either energy or electron transfer reactions. The photoactivity of photosensitizers mediated by type I photoreactions may be partially derived from the transient reduction of the macrocycle. Thus, it is expected to be higher when photosensitizer undergoes a reduction in its excited state. Nevertheless, photobleaching of photosensitizers [37,132] is mainly related to photooxidation (instead of photoreduction) and photoaggregation (due to the π-cation radical formation). Thus, the photosensitizer, which is the hardest to oxidize, is also the most stable compound [133]. The improved photostability of photoactive compounds may be realized by introducing electron-withdrawing groups or coordination the central metal ion (*e.g.,* Pd^{2+}) with high electronegativity into macrocycle [20,21,49,134]. This, in general, make photosensitizer harder to oxidize and easier to reduce. These statements may be supported by the redox potentials as well as energies of molecular orbitals determined theoretically in DFT calculation. Moreover, the molecular substitution pattern enables to control and tune the HOMO and LUMO energies, and redox potentials [20,135,136]. These relations were reported for the library of many synthetic photosensitizers, including chlorins, bacteriochlorins and their derivatives *i.e.* bacteriooxophorbines [38,111,137].

Recently, increased number of research reveals that type I photoreactions with the formation of hydroxyl radicals, superoxide and other oxygen-centered radical species play an important role in the photoactivity of photosensitizers. For instance, WST09 and WST11 are able to produce mainly superoxide anion and hydroxyl radicals [105]. The contribution of the type I mechanism was also determined for synthetic sulfonic and sulfonamide bacteriochlorins. It has been suggested that these bacteriochlorins may be expected to generate ROS *via* both mechanisms, whereas porphyrins undergo mainly energy transfer with the formation of singlet oxygen and they are in particular harder to oxidize than their reduced derivatives [129].

The pallet of metallobacteriochlorins described in this part (Fig. 18) [21,29] will be discussed in the following sections in the context of their applications such as photodynamic therapy and photodynamic inactivation. The analysis of Fig. 18 suggests that from the synthetic point of view: (i) the unsubstituted bacteriochlorins without any electron-withdrawing groups indicate a limited possibility to obtain the metal complexes through reaction with a strong base; (ii) similar strong-base conditions can be applied for a broader scope of metals using bacteriochlorin bearing two carboethoxy substituents; (iii) for bacteriochlorins bearing carboethoxy or imide 2–4 substituents, the Zn^{2+} can be inserted according to the standard porphyrin metalation procedure; (iv) for the derivatives bearing two carboethoxy substituents, reaction in the presence of strong bases allowed faster metalation process than the method involving the treatment with metal salt; (v) bacteriochlorin with 4 carboethoxy substituents gives the unstable Mg chelate under the strong base conditions; (vi) *ortho*-aryl substituents are known to significantly slow down the metalation of *meso*-tetraarylporphyrins [21].

4.1. Theoretical studies of synthetic bacteriochlorins with transition metal complexes

Parallel to experimental work, theoretical studies on the optical properties of bacteriochlorins and their metal complexes are also undertaken. L. Petit with collaborators performed theoretical calculations for a family of metallobacteriochlorins containing divalent transition metals including Mg^{2+}, Zn^{2+}, Mn^{2+}, Fe^{2+}, Co^{2+}, Ni^{2+}, and Cu^{2+}. DFT and TDDFT were applied to study electronic properties and structural changes. Fig. 19 presents the energies of orbitals for each metallobacteriochlorin and the corresponding orbitals for free-base bacteriochlorin (FBBC). Interestingly, although the energy of the HOMO-LUMO gap was lower than the energy estimated for the isolated ligand, no dramatic changes are observed in comparison to FBBC. The presence of metal ions has little effect on the relaxation of FBBC degeneration according to the interaction with the ligand [138]. Solvent effects included in these calculations by the implementation of the polarizable continuum model (PCM) clearly indicate that both water molecules are coordinated with the central metal ion. Unlike to evolution ion radius, the determined values are a bit reduced in the transition from Mn^{2+} to Ni^{2+}, and then they come back to Zn^{2+}. It may suggest that stronger adhesive interaction for metal than Fe^{2+} to Ni^{2+} concerning Mn^{2+}, Cu^{2+}, and Zn^{2+}. These calculations also revealed that Zn^{2+} is characterized by the lowest interaction with the ligand, while Ni^{2+} shows the greatest effect. The studies show the strongest ion interactions of the central metal with nitrogen for Fe^{2+}, Co^{2+}, and Ni^{2+}, whereas for atoms with half-filled (d^5 Mn) or filled (d^{10} Zn) orbitals, weaker

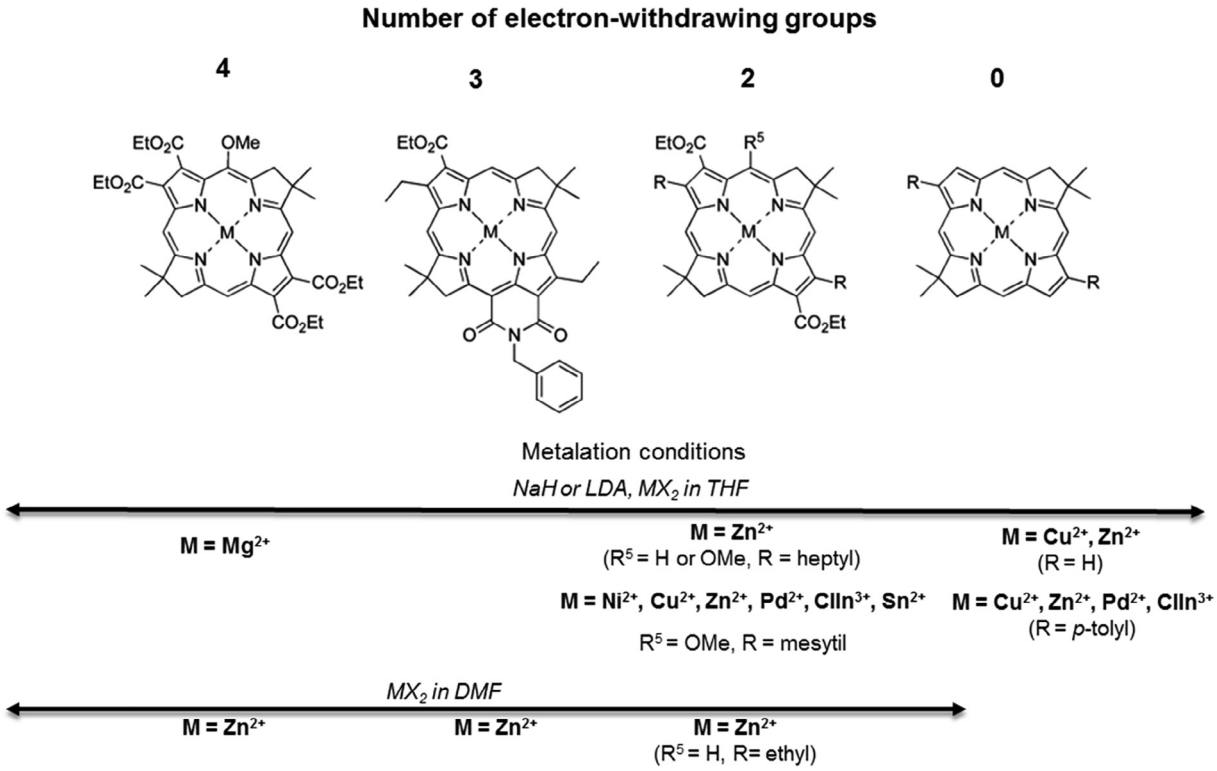

Fig. 18. The summary of the conditions for the metalation of synthetic bacteriochlorins. Adapted from [21].

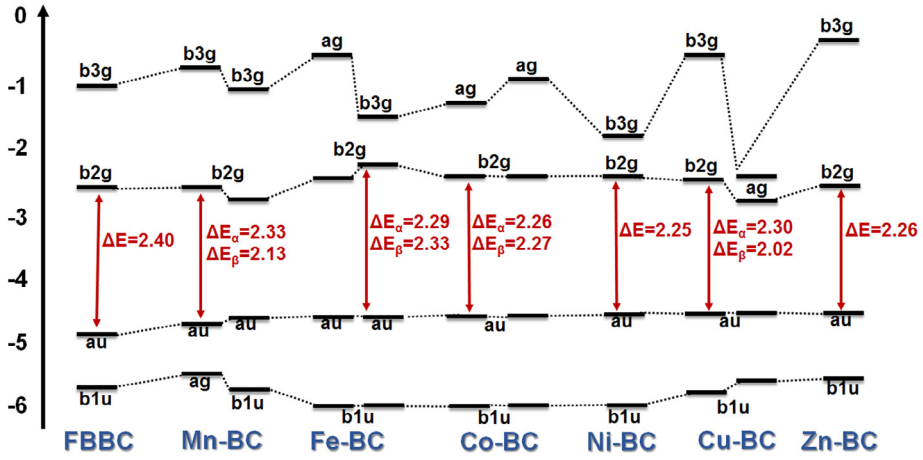

Fig. 19. Theoretical calculation of orbital energy levels for (metallo)bacteriochlorin derivatives. Adapted from [138].

interactions are observed. Special attention was paid to the less energetic part of the spectra, Table 5.

The result of these calculations clearly shows that the metalation causes red shift of Q_x and blue shift Q_y bands, while comparing to the free-base bacteriochlorin [139]. The intensity of electronic transitions indicates a slight increase in the molar absorption coefficients after the metalation of the free-base compound. All of these metal complexes except the Fe^{2+} complex possess an energy

Table 5
Calculated energies of electronic transitions (eV) along with oscillator strengths in parenthesis for FBBC bacteriochlorin and its metal complexes [138].

Compound	Q_x/eV	Q_y/eV	B_y/eV	B_x/eV
FBBC	2.10 (0.24)	2.57 (0.05)	3.81 (1.14)	4.10 (1.11)
Mn-BC	1.99 (0.25)	2.46 (0.05)	3.49 (0.51)	3.94 (0.49)
Fe-BC	2.05 (0.26)	2.62 (0.01)	3.09 (0.15)	3.93 (0.63)
Co-BC	2.04 (0.28)	2.66 (0.03)	3.72 (0.55)	3.83 (0.26)
Ni-BC	2.02 (0.26)	2.65 (0.03)	3.69 (0.61)	3.82 (0.10)
Cu-BC	2.05 (0.25)	2.58 (0.01)	3.57 (0.63)	3.77 (0.25)
Zn-BC	2.04 (0.27)	2.56 (0.04)	3.68 (0.18)	3.81 (0.88)

gap approximately 1 eV. This is most likely to be the case under biological conditions, so it can be presumed that these compounds fulfill one of the key requirements for their use as potent PDT photosensitizers.

4.2. Peripheral modification of synthetic bacteriochlorins

4.2.1. Halogenated sulfonated and sulfonamide derivatives

Recently, the library of *de novo* synthesized halogenated bacteriochlorins have been developed [140,141]. The preparation of these compounds consists of the following steps: (i) the synthesis of appropriate porphyrins by modified nitrobenzene method that involves the condensation of pyrrole with the appropriate aromatic aldehyde in the presence of nitrobenzene in acidic conditions; (ii) chlorosulfonation of the obtained porphyrins; (iii) either hydrolysis or reaction with amines to obtain respectively: hydrophilic (sulfonated) or amphiphilic (sulfonamide) halogenated porphyrins; (iv) diimide reduction of these porphyrins to bacteriochlorins; the metalation with the desired metal ion (as an example, the introduction of Mn^{2+} and Mn^{3+} is presented in the Section 4.2.2) [22,141–143]. The first attempt to the synthesis of the halogenated sulfonamide and sulfonated bacteriochlorins involved a modified Whitlock method, including the use of toluene as a solvent and catalyzed by a relevant organic base. In the following years, it was possible to develop an alternative synthetic procedure in accordance with the sustainable chemistry approach. This method is based on obtaining compounds under solid-solid conditions, without the use of any solvents. Its key advantages are: efficiency, simplicity, low environmental impact and the ability to provide a library of photostable NIR-absorbing dyes with various polarities and characterized by favorable physicochemical properties and enhanced biological performance [144]. The general scheme of the synthesis of halogenated bacteriochlorins and their metal complexes are presented in Fig. 20.

Fig. 21 shows the structure of selected compounds belonging to this family, together with their electronic absorption spectra [145]. Modifications within the tetrapyrrolic ring lead to the significant changes observed in their electronic structure. The typical free-base porphyrin with D_{2h} symmetry is distinguished by the presence of the intense absorption band in the blue part escribed as the Soret band and additional four Q bands in the range of larger wavelengths (500–700 nm) corresponding to transitions between vibrational levels of much lower intensity. The change in the symmetry of the system caused by the metal ion insertion results in a change in symmetry of the system to D_{4h}, which results in the reduction of the number of Q bands in the absorption spectra from

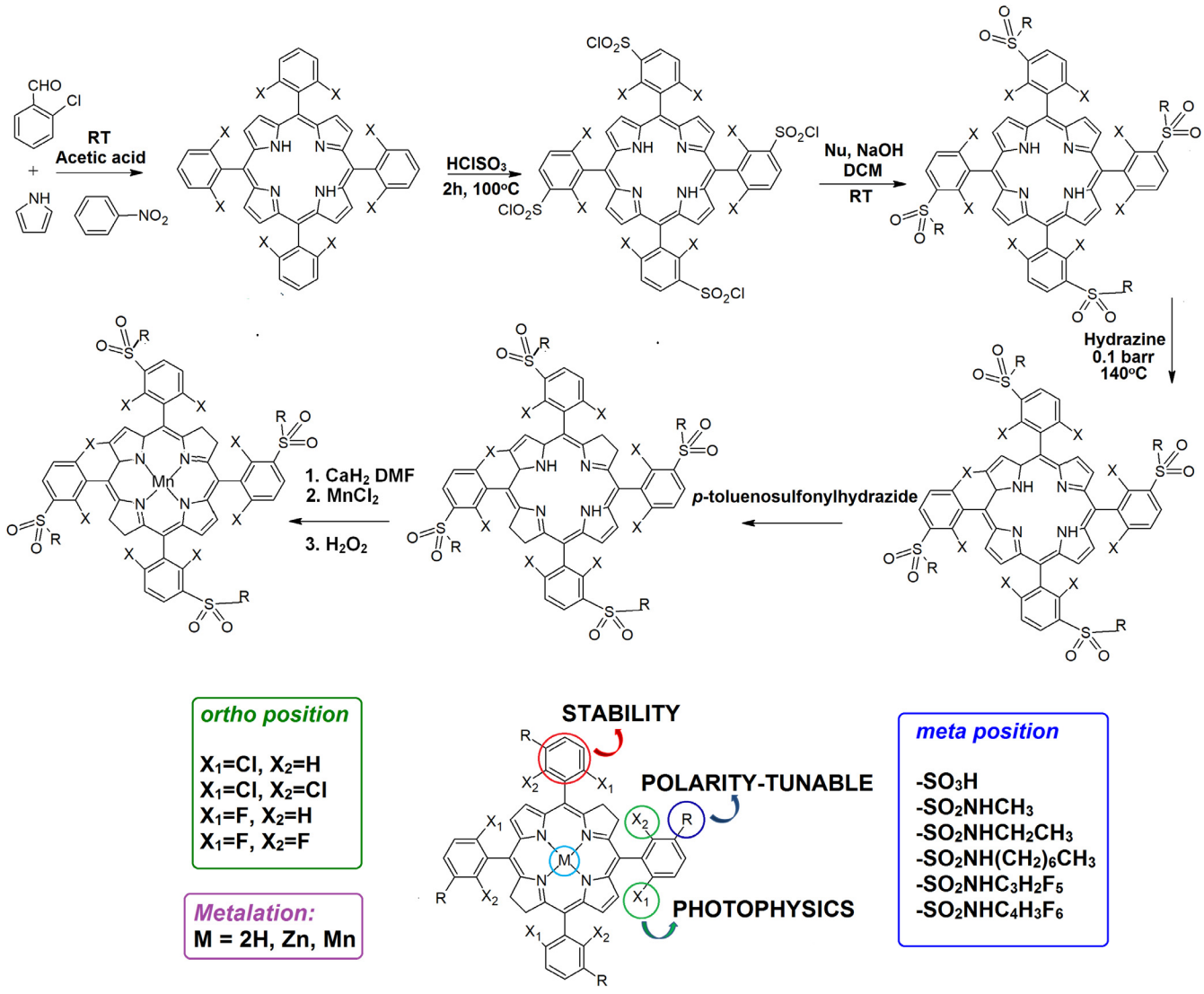

Fig. 20. Scheme of the synthesis of halogenated bacteriochlorin derivatives and the possible pathways of their modifications.

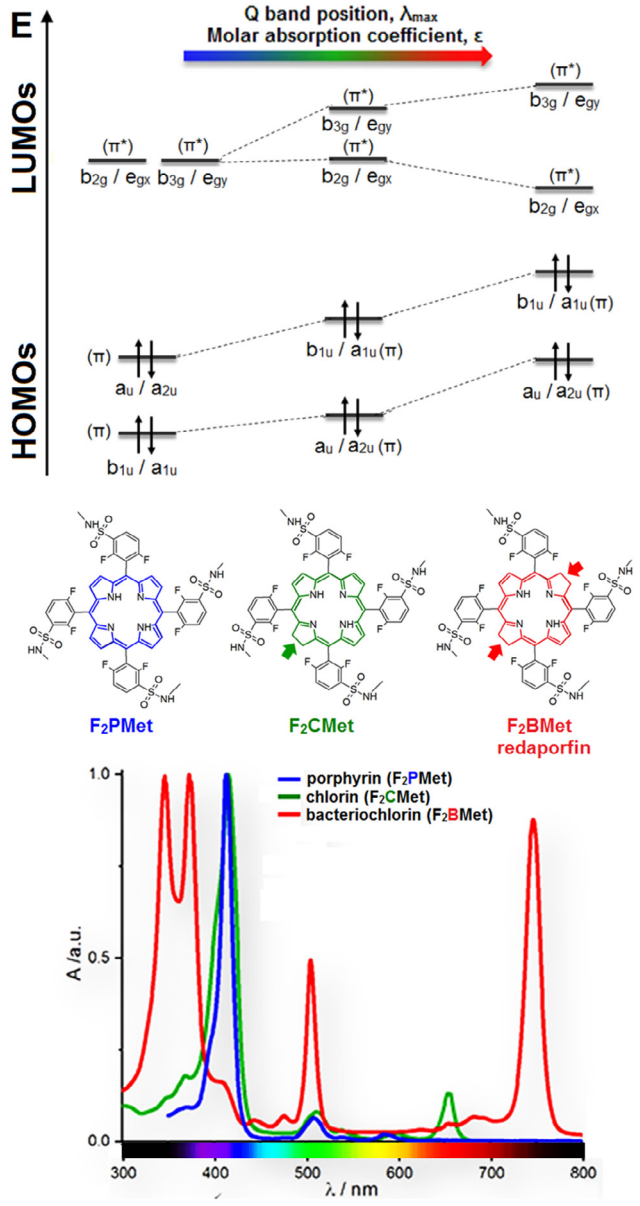

Fig. 21. Scheme illustarting the chemical structures of the studied fluorinated and sulfonamide porphyrin, chlorin and bacteriochlorin, together with their HOMO and LUMO energies and corresponding electronic absorption spectra.

four to two. These Q bands are formed as a result of the difference in dipole vectors between the HOMO-LUMO levels. The Soret band is most often observed as one absorption band due to the slight energy differences in the case of porphyrins. If the energy differences between the respective levels are significant, then the degeneration of the LUMO orbitals occurs, resulting in the splitting of the Soret band (Fig. 21) [146,147]. The reduction of subsequent pyrrole rings in the macrocycle results in the destabilization of the HOMO level and the LUMO orbitals. With the increasing degree of reduction of the pyrrole rings, the energy of transition between the occupied orbital $a_{1u}(\pi)$ and the unoccupied orbital $e_{gy}(\pi^*)$ increases, whereas between the orbital $a_{1u}(\pi)$ and the unoccupied orbital $e_{gx}(\pi^*)$ does not change. The effect of these modifications is manifested in the decrease in the energy of the HOMO-LUMO transitions following: porphyrins > chlorin > bacteriochlorins. The decreased HOMO-LUMO energy gap is also correlated with the redox properties of porphyrins, chlorins, and bacteriochlorins. Together with the degree of reduction, the HOMO level energy increases, so that the susceptibility to oxidation changes in the following series: porphyrin < chlorin < bacteriochlorin (lowering the oxidation potentials), without changing the reduction potential [148].

Despite the favorable optical properties of bacteriochlorins (λ_{max} = 740–780 nm), their significant limitation was low stability, susceptibility to oxidation, and, as a consequence, reduced possibilities of ROS photogeneration. Therefore, one of the objectives of the research discussed here was to apply desired modifications within the macrocycle, resulting in the pallet of photostable NIR-absorbing compounds, which through appropriate redox and photophysical properties shall generate a high amount of ROS according to both types of photochemical reactions (type I and type II mechanisms). The first possible modification consists of the introduction of phenyl rings into the tetrapyrrolic system in the *meso* positions, which act as steric hindrance, which ensures compounds with greater stability and more amphiphilic character. The introduction of halogen atoms (-F, -Cl) to the *ortho* position of the phenyl rings leads to spin-orbital coupling, increasing the yield of the intersystem crossing. Moreover, these electron-withdrawing groups stabilize the macrocycle against its oxidation. Achieving large values of the efficacy of the ISC process also creates the ability to control the mechanisms of photosensitization, and thus the efficacy and type of generated ROS. The parameter allowing to assess the effectiveness of the spin-forbidden transition is the spin-orbital coupling constant (ζ), which for the hydrogen atom is ζ = 0.24; in the case of chlorine: ζ = 586, and for fluorine ζ = 269 [149]. It appears that the presence of a chlorine atom allows achieving two times higher heavy atom effect. Nevertheless, the introduction of fluorine atoms into the structure of the tested compounds allowed to obtain optimal photophysical properties (improved photostability, generation of triplet states), while maintaining the fluorescence capabilities facilitating biological experiments being carried out (*e.g.*, subcellular localization, studies of pharmacokinetics and biodistribution [22,25,142,150–152]. The summary of properties determined for the library of halogenated bacteriochlorins is presented in Table 6.

In addition to the effect on the photophysical properties of the studied molecules, the introduction of fluorine atoms into the structure also plays an important role in pharmacological properties [153]. Fluorine exhibits high biocompatibility and is a widespread pharmacologically active compound [151]. The greater therapeutic efficacy of compounds containing fluorine atoms in the structure compared to non-fluorinated compounds has been described by other authors [150]. The next possible modification of the new synthetic bacteriochlorins involves their functionalization with sulfonic or sulfonamide groups as well as coordination with certain metal ions [154]. Substitution of sulfonic and sulfonamide groups allows to control the hydrophobicity of molecules and to increase their stability by the effect of steric protection [54,140,142,155]. The introduction of substituents with higher electron-receptor properties leads to increased hydrophobicity of photosensitizer, which affects its interaction with biological membranes [156,157]. Moreover, the presence of sulfonamides in the bacteriochlorin structure results in a remarkable increase in the selectivity towards cancer cells and tumors as well as photodynamic efficacy due to the higher lipophilicity of such photosensitizers [158].

4.2.2. Manganese complexes of halogenated bacteriochlorins

Manganese(III)-porphyrins are characterized by catalytic reactivity, the possibility of photoreduction to Mn^{2+} and suitability for the use as photoacoustic (PA) references [159,160]. Moreover, they may be used in the production of effective piezophotonic materials [161]. The described in the literature extraordinary spec-

Table 6
Photophysical, spectroscopic, and electrochemical properties of halogenated bacteriochlorins.

Compound	Absorption		Fluorescence			Triplet			Φ_Δ	Redox potentials		
	λ_{max} nm	$\varepsilon_{max}/10^3$ M^{-1} cm^{-1}	λ_{max} nm	Φ_F	τ_F ns	Φ_T	τ_T ns	$k_q/10^9$ M^{-1} s^{-1}		E^0_{red1} V	E^0_{ox} V	E^0_{ox1} V
FBMet	741	62	745	0.129	3.6		200	2.4	0.63			
F_2B	744	140	745	0.068	3.8	≈0.81	216	2.6	0.48	−0.95		0.65
F_2BOH	745	56	745	0.023			268		0.44	−0.93	0.55	0.70
F_2BMet	743	140	746	0.138	3.0	0.65	216	2.2	0.43	−0.74	0.80	
ClBOH	742	61	745	0.040			246	1.9	0.42			
Cl_2BOH	745	61	748	0.006			226	2.1	0.85			
Cl_2B	747	126	748	0.012		≈1	254	2.1	0.60			
ClBEt	743	76	746	0.038			228	2.1	0.61			
Cl_2BEt	745	110	747	0.013	0.39 0.54	≈1	265	1.8	0.66	−0.79	0.82	

troscopic and photochemical properties of Mn^{3+}-porphyrins have encouraged the synthesis of novel Mn^{3+} and Mn^{2+} coplexes of halogenated sulfonamide bacteriochlorins. The subsequent steps of the synthesis of these manganese complexes of halogenated tetraphenylbacteriochlorin are illustrated in Fig. 22 [162].

The properties of the electronic states of the Mn-based compounds are significantly different from free-base bacteriochlorins or their complexes with diamagnetic metals, Fig. 23. It was reported that the Mn^{3+} complexes reveal eight electronic transitions between various electronic states, including both: (i) π->π* transition, typical for bacteriochlorin and (ii) ligand-to-metal transitions. Among them, the transition corresponding to the strong absorption band at ~830 nm deserves particular attention. The lowest-energy transitions involve direct excitation from the singlet ground to triplet excited state (*e.g.*, $S_0(\pi,\pi^*) \rightarrow T_1(\pi,\pi^*)$ transitions). Nevertheless, the interaction of metal (d, d) orbitals and the orbitals of the macrocycle (π,π*) is not as significant as observed for manganese(III) porphyrins [163,164]. This smaller mixing of orbitals diminishes the intensity of the CT transitions and increases the triplet excited state lifetime. Interestingly, the bacteriochlorin abbreviated (Cl)$MnCl_2BMet_2$, as for a paramagnetic metalloporphyrin derivative, is characterized by the relatively long lifetime of the triplet excited state (τ_T ~ 570 ps) and a quite substantial quantum yield of the triplet state (Φ_T ~ 0.2). Hence, the applicabil-

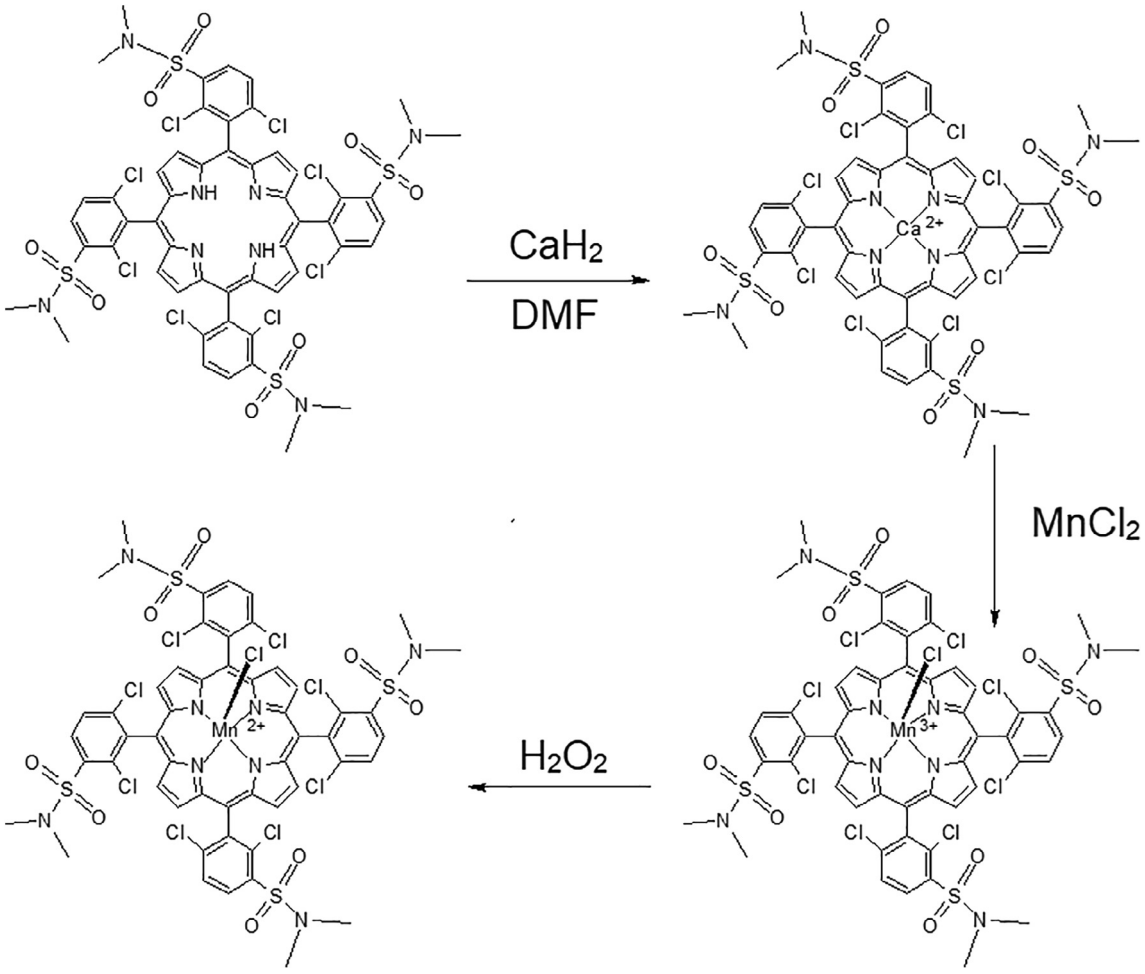

Fig. 22. The synthetic pathways leading to the preparation of Mn^{2+} and Mn^{3+} chlorinated sulfonamide bacteriochlorins.

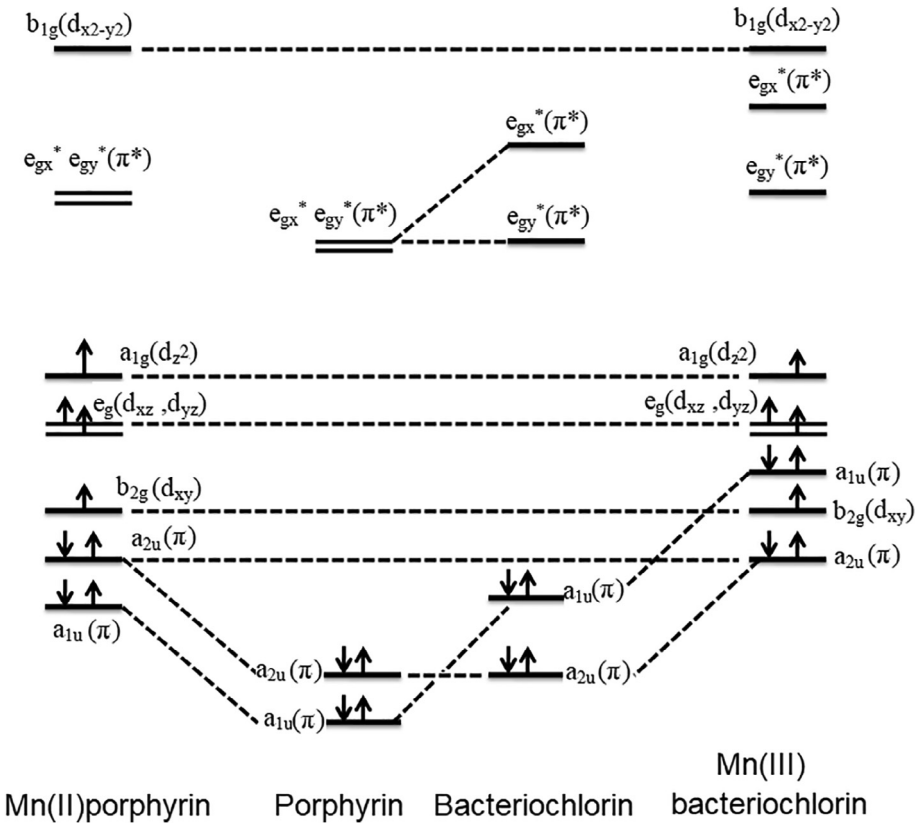

Fig. 23. Energy ordering of molecular orbitals (in D_{4h} symmetry) of tetraphenylporphyrins, bacteriochlorins and their manganese(III) complexes. Adapted and modified from [162].

ity of (Cl)$MnCl_2BMet_2$ in photocatalysis or photovoltaics may be considered. However, the efficient internal conversion in this manganese(III) bacteriochlorin and its quite intense absorption at λ_{max} = 829 nm ($\varepsilon \sim 50{,}000\ M^{-1}\cdot cm^{-1}$), where tissues are transparent indicate that this class of compounds can be suitable for biomedical applications such as photothermal therapy or even photoacoustic tomography [165].

4.2.3. Morpholino- and lactone-based bacteriochlorins

The conversion of pyrroline to morpholine moieties in near-planar *meso*-tetraarylbacteriochlorins results in ruffled mono- and bis-morpholinobacteriochlorins (Fig. 24) characterized by broadened and bathochromically shifted electronic absorption spectra. Observed changes in the optical properties have been assigned to a combination of two independent factors: (i) dihedral angle between morphine and pyrrole moiety and (ii) molecular planarity [139]. Conformational changes characterize bacteriochlorin derivatives containing one or two non-pyrrolic heterocycles with oxygen atom into the framework. Nonplanar conformations induced by peripheral substituents in porphyrin may cause red-shift of Q band even up to 50 nm [166]. The pyrrole reduction also distorted the planar macrocycle, especially in two-reduced bacteriochlorin, which increases ring flexibility. Insertion of oxygen in the reduced domain with sp^3 hybridization leads to even more remarkable conformation changes than in free-base bacteriochlorin. Nevertheless, the general trend between distortion and spectrum is red-shifted [167]. However, in some cases of structural changes, morpholino- bacteriochlorins indicate blue-shifted Q band caused by space-through interaction of electron-donating oxygen with aryl groups.

Mazzone and co-authors have also provide computational studies on the morpholino-bacteriochlorins, which entails a distortion

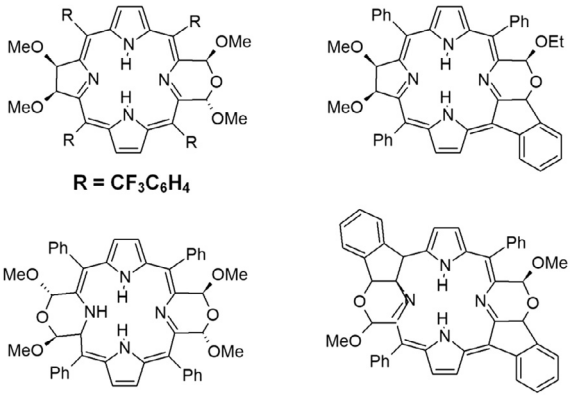

Fig. 24. The chemical structures of morpholino- derivatives of bacteriochlorins with one and two oxygen atoms in macrocycle.

of the entire macrocycle derived from the insertion of the oxygen atom between the two pyrrolidone carbons [168]. Computational studies of the morpholino-derivatives with the introduction of a different number of the phenyl group in the *meso* position also show a notable effect on the conformation. Compared to dihydroxy-dimethoxy bacteriochlorin, a bathochromic shift of 50 nm is observed for the morpholino-bacteriochlorin, which is in line with spectroscopic experiments performed in solutions. The crucial requirement for ideal photosensitizer is the energy gap between the ground singlet and triplet excited state higher than 0.98 eV adequate to the energy gap between triplet and singlet oxygen. Considering the optical properties of these compounds, including the HOMO-LUMO gap (Q band), as well as the energy gap between the singlet-triplet excited state, the expanded

bacteriochlorins bearing morpholino groups can be proposed as photosensitizers act *via* type II photochemical mechanism with the singlet oxygen formation [168].

Nevertheless, the extension of the π-conjugation system may cause undesirable changes in solubility (*via* π-π stacking), stability and aggregation. Thus, the modulation of aromaticity in the tetrapyrrolic ring is a significant challenge, especially in reduced porphyrinoids. Another group of extended bacteriochlorin-like compounds with a long-wavelength absorption in the NIR is represented by porpholactones. The introduction of an oxygen atom into the macrocycle ring in β-peripheral position may extend π-system without causing disadvantages mentioned above. Additionally, the isomerization of β-oxazolone may tune the electronic ground states, singlet and triplet excited states as well as the redox potentials. The porpholactone derivatives are characterized by strong absorption in the NIR, shifted similarly to naturally-occurring hydroporphyrins. The introduction of the oxazolone group in the macrocycle leads to, besides the π-system extension, lower symmetry (C_s) and stabilization of the HOMO and LUMO levels. The isomerization may also significantly influence the photophysical and photochemical properties of porpholactones. In this case, similarly to naturally-occurring (bacterio)chlorophylls, cis/trans isomers indicated the changes in the absorption spectra. Moreover, it provides high efficiency in energy storage in photochemical processes, *e.g.*, mediated by *cis*-isomer of chlorophyll *d* derived from cyanobacteria, which possess lower molar absorption coefficient than chlorophyll *a* (non-isomeric). Moreover, compared to the Q_y absorption of chlorophyll *d* (*cis*-isomer), its *trans*-isomeric form (chlorophyll *f*) indicates the stronger red-shift in the NIR (*ca.* 18 nm), Fig. 25 [169].

Zhang and coauthors have developed the novel synthesis method of the porpholactone using desired ruthenium salt and oxone. The oxidation of tetrapentafluorophenylporphyrin results in porpholactone (F_{20}TPPL, 85%) and porphodilactone (F_{20}TPPDL, 15 %) derivatives with both trans- and cis- isomers [169]. It was also demonstrated that regioisomeric bacteriodilactone-based derivatives with non-bonding electrons are more aromatic than their typical bacteriochlorin analogs [96,171], with red-shifted of Q_y band (19 nm) and increased absorption comparable with chlorophyll *f* and chlorophyll *d* [172]. Although porpholactones indicate the similar optical properties to chlorophylls, their coordination capabilities are comparable with porphyrin derivatives. In this respect, porpholactones and their metal complexes (Zn^{2+}, Pd^{2+}, Pt^{2+}, Fig. 26) [172] play an important role as a molecule for many applications including photodynamic therapy, optical imaging, and well as a novel sensing materials (see chapter 6). Moreover, they might be applied in catalysis, photocatalysis and even electrocatalysis.

The regioisomerisation of metal complexes of porphodilactones may also cause changes not only on absorption spectra but may also alter the triplet excited states. For instance, *trans*-isomers of Pd^{2+} and Pt^{2+} complexes showed red-shifted and longer-lived phosphorescence than *cis*-analogs (Table 7) [170]. The discussed porpholactones and their metal complexes might be applied as small molecule activation catalysts and photo- or electrocatalysts. Computational study of the ground and excited states for lactone-based bacteriochlorin demonstrated the change of their stability as well as has an impact on the absorption spectra [96]. The stabilities and strong electronic influence of series regioisomeric porphodilactone (Fig. 26) due to the charge delocalization, was also reported.

5. Application of (metallo)bacteriochlorins in photodynamic therapy (PDT)

5.1. Basic principles of PDT

Photodynamic Therapy (PDT) is a photochemistry-based medical strategy, dedicated mainly for cancer treatment, but recently also widely used in the inactivation of localized bacterial infections

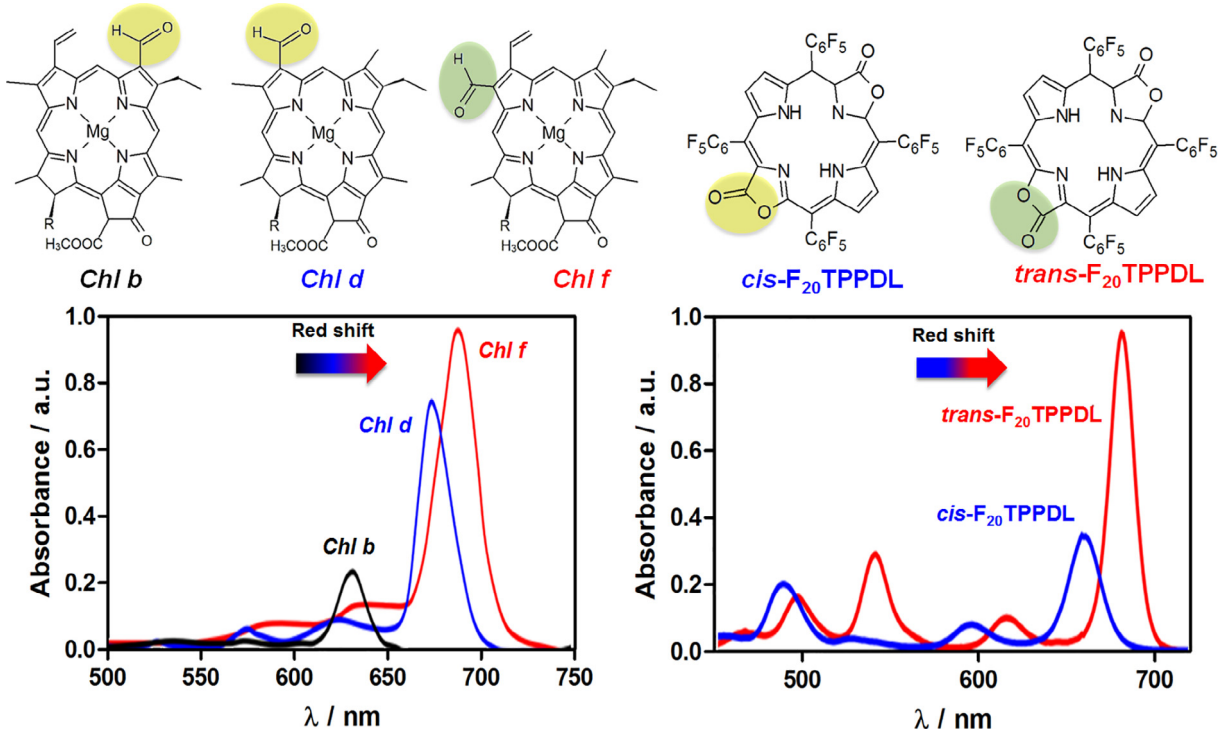

Fig. 25. The influence of the orientation of β-substituents on NIR absorption of naturally-occurring chlorophylls (Chl *b*, *d*, *f*) and porpholactones (cis- and trans-F_{20}TPPDL). Adapted and modified from [170].

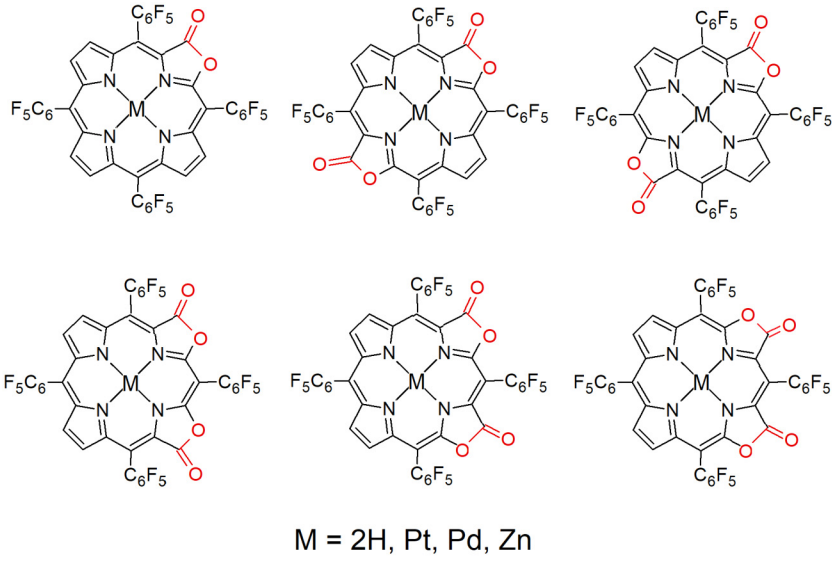

Fig. 26. The structure of *meso*-C_6F_5-porpholactonebacteriochlorin (metallo)derivative and its possible regioisomers [96].

Table 7
Photophysical and electrochemical properties of the cis/trans porphyrinoids and their metal complexes [171,173].

PS	isomer	Absorption		Emission				E_{ox}	E_{red}		ΔHOMO-LUMO	
		B/nm	Q/nm	F/nm	Ph/nm	τ_{Ph}/μs	Φ_{Ph}	1st	1st	2nd	exp	calc
2H	cis	408	505, 600, 657	662, 711				+1.66	−0.44	−0.85	2.10	2.45
	trans	410	512, 551, 676	678, 755				+1.61	−0.37	−0.87	1.98	2.34
Pt	cis	391	550, 562, 607		836	935	0.04	+1.60	−0.54	−0.92	2.14	2.49
	trans	402	488, 525, 574, 623		866	1000	0.06	+1.59	−0.45	−0.99	2.04	2.41
Pd	cis	411	514, 555, 568, 617		859	969	0.01	+1.58	−0.50	−0.94	2.08	2.45
	trans	411	505, 543, 585, 638		916	1058	0.01	+1.56	−0.41	−0.94	1.97	2.34
Zn	cis	423	532, 579, 634	640				+1.31	−0.86	−1.06	2.17	2.41
	trans	422	536, 606, 662	670				+1.25	−0.75	−1.28	2.00	2.24

[53,174]. Three nontoxic components are needed to initiate photochemical reactions: a photosensitizer (PS), a visible/near-infrared light and molecular oxygen commonly present in the cells or tissues. These components together result in the generation of highly cytotoxic reactive oxygen species. Fig. 27 shows the subsequent steps of the PDT procedure. The administered photosensitizer is activated, and then undergoes several photophysical processes and photochemical reactions. As discussed in Chapter 2, PS in the triplet excited state is able to transfer an electron/hydrogen atom or energy to another molecule, *e.g.*, O_2 to generate ROS. These species are involved in the destruction of biological structures, leading to oxidative stress within the tumor according to three related anti-cancer mechanisms: (i) direct cytotoxic effect resulting in apoptosis, necrosis and/or autophagy (cell self-healing process), (ii) the indirect closure of tumor blood vessels, and (iii) stimulation of the immune system to local and systemic responses, and induction of pro-inflammatory processes eventually leading to the development of antitumor immunity [49].

The contribution of each mechanism depends on the applied light dose, drug dose, drug-to-light interval (DLI), oxygen concentration in the tumor tissue and applied irradiation margin [18]. The immune response against cancer cells is probably the most important aspect of PDT because it creates the possibility of not only destroying the primary tumor but also preventing the occurrence of metastases and finally taking a big part in the complete cure of the disease [175,176]. On the other hand, the critical step in the PDT studies is to develop a photosensitizer (PS) characterized by desired chemical and biological properties [132,177]. For instance, it should indicate a strong absorption in the phototherapeutic window, high values of Φ_{ISC} and Φ_T, as well as long triplet state lifetime [18].

Photogenerated ROS causes damage to biological structures at the site of the PS localization, which consequently leads to tumor destruction. An important issue is the determination of whether and how the metal insertion or other substituents introduced into the macrocyclic ring affect the ability to control photoinduced electron and energy transfer reactions [55,154,157,178,179]. These studies are focused on the idea of how modifications influence the ROS generation in cancer cells [18,55,153,157,179,180], and improve their selectivity towards diseased areas [178,181–184]. The most frequently studied PDT-photosensitizers are tetrapyrrolic macrocycles, including bacteriochlorins and metallobacteriochlorins [58]. Clinically used photosensitizers, depending on their polarity, may either bind to the plasma proteins (hydrophilic compounds) or accumulate in different cellular compartments (compounds with higher lipophilicity) [58,174,185]. In most cases, the cell nucleus is not the primary target for photosensitizers, whereby PDT does not induce genotoxic effects compared to classical chemotherapy and radiotherapy [186,187].

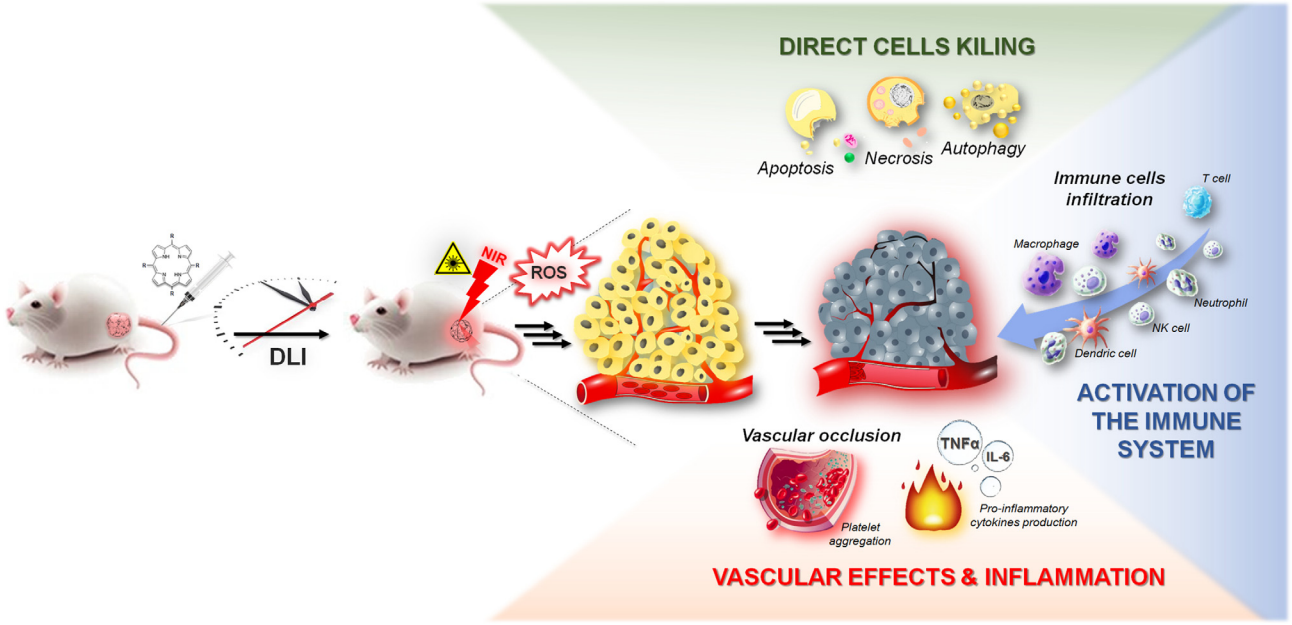

Fig. 27. Principles of photodynamic therapy (PDT): photosensitizer (PS) is administered, and after a given drug-to-light interval (DLI), it is activated by visible or NIR light leading to ROS generation that is responsible for various biological mechanisms and PDT activity.

The ability of PS to accumulate in cells and their intracellular localization not only determines the appropriate choice of formulation and incubation time but also allows to indicate the primary site of photodamage [188]. For many years, singlet oxygen has been considered the most important toxic agent responsible for photoinduced cellular damage in PDT. Despite a relatively short half-life, it is characterized by quite a large interaction range (its activity reaches the radius of 20–550 nm) [189,190]. For comparison, hydroxyl radicals generated according to type I mechanism possess a radius of only 1 nm, but are more reactive than singlet oxygen, which in turns is more selective oxidant. In the development of new photosensitizers, besides the determination of physicochemical and photochemical properties, pharmacokinetic studies *in vivo* are essential to evaluate absorption, distribution, metabolism, and excretion of potential drug candidates. The selectivity of photosensitizers can be determined using tumor-to-skin (T/S) and tumor-to-muscle (T/M) ratios. However, many features can affect the tissue distribution and pharmacokinetic profile after intravenous PS administration. The most critical of these are PS charge, formulation and parameters of applied therapeutic protocol including drug dose, tumor model, drug-to-light interval (DLI), administration route, light dose and type of the light source. Thus, the direct comparison of the results obtained from different laboratories is difficult and should be untertaken with coution [191]. The pharmacokinetics and biodistribution largely determine the choice of DLI [158,180,184]. The current state of knowledge allows to distinguish three basic variants of protocols. The first one is characterized by short DLI from 5 to 15 minutes and is named vascular-targeted photodynamic therapy (V-PDT). The second one (cellular-targeted photodynamic therapy, C-PDT) involves the selective delivery of PS to cancer cells. For this protocol DLI reaches >12 h, but usually involves 24 h, 72 h, or even 96 h from PS administration to tumor irradiation. The last protocol is focused on the targeting endothelial cells (endothelial cells-targeted photodynamic therapy, E-PDT). It is characterized by an intermediate DLI (usually 3 h) when the photosensitizer is found mainly in the blood and endothelial cells with simultaneous accumulation in tumor cells [153,180,192].

5.2. Bacteriochlorin-based photosensitizers for PDT

5.2.1. Bacteriochlorophyll derivatives as naturally-occurring and semisynthetic photosensitizers

Bacteriochlorophylls are characterized by stronger absorption in the NIR than chlorophylls, which makes them theoretically more suitable candidates for anticancer PDT [193]. However, naturally-occurring Chls and BChls are not relevant for photomedicine because they are not enough photostable. Moreover, they contain a hydrophobic chain in the structure (phytyl), which hinders their safe application and further localization in cancer cells. Nevertheless, through the use of structural modifications within the macrocyclic ring discussed in the Chapter 3, it is possible to increase their application potential.

5.2.1.1. Bacteriochlorophylls as PDT sensitizers. Many bacteriochlorophyll derivatives were tested both in *in vitro* and *in vivo* conditions. The photoactivity of BChlide *a* and BChl-Ser was evaluated in M2R mouse melanoma cells [194]. It was also reported that BChl derivatives could be active even under hypoxic conditions, acting mainly *via* type I photoreactions with hydroxyl radicals formation [195]. Moreover, replacement of the Mg^{2+} with Pd^{2+} in BChl structure significantly increased the photodynamic effect in various cells, decreasing the LD50 value by order of magnitude without any change in the dark toxicity [196]. BChl-Ser was applied as PS against M2R melanoma and showed quite short elimination time from the body (16 h), which prevents skin photosensitivity [194]. The optimized PDT protocol involved drug dose of 20 mg/kg BW, light dose of 108 J/cm^2, and tumor irradiation immediately after PS administration. [197,198]. The described protocol, focused mainly on the tumor vasculature disruption and blood flow stasis, was characterized by significant efficacy, reaching over 80% cures of mice [197]. The PDT activity was confirmed in other tumor models, for instance in SD sarcoma-bearing rats [199,200]. BChl-Ser-mediated photodynamic efficacy was also tested in combination with hyperthermia [199,200]. The tumor response to PDT with BChl-Ser as photosensitizer was further controlled with a specific intertissued oxygen microsensor. The rapid reduction of tumor

oxygen concentration was observed due to the efficient ROS production during irradiation [201].

The first BChl-based compound, which was entered into the clinical trials, was Pd-bacteriopheophorbide (padoporfin, Tookad, WST09, see Fig. 13 and chapter 3.2.2) [202]. Vascular-targeted PDT (V-PDT) with Tookad led to a significant therapeutic efficacy against human prostate cancer as well as bone metastases. In the discussed PDT protocol, NIR laser irradiation (λ = 770 nm) with a light dose of 90 J/cm^2 was carried out immediately after intravenous PS administration at a dose of 4 mg/kg BW [109]. The therapeutic efficacy of Tookad was also verified towards prostate cancer in dogs with the therapeutic regimen including NIR light irradiation (λ_{max} = 763 nm), light dose of 200 J/cm^2 and a quite high drug dose of 5 mg/kg BW [81]. Tookad-V-PDT was also effective in the treatment of HT29 colon carcinoma (multidrug-resistant and wild types) as well as C6 glioma tumors growing in mice [203–206]. WST09 (padoporfin) has proven to be a promising photosensitizer first in preclinical [207], then in early clinical trials for PDT of prostate cancer [208,209] and was finally applied in clinics in 2004.

The data obtained from patients recruited to phase I suggested that the skin photosensitivity related to V-PDT is negligible under clinical protocol involving PS dose of 0.1–2 mg/kg and irradiation (λ = 763 nm) at ligh doses from 10 to 360 J/cm^2 [210]. The drug and light doses escalation studies were also performed in patients with locally recurrent prostate tumors receiving external beam radiotherapy (EBRT) and the tumor response were monitored with Gd-enhanced MRI [208]. The phase I/II clinical trial conducted by Gertner *et al.* indicated the safety as well as overall efficacy and pharmacokinetic data of padoporfin-V-PDT [211]. The parallel trials conducted by Arumainayagam *et al.* also involved the drug and light dose escalating studies. The patients (Gleason score $\leq$7 and PSA <20 μg/L) were subjected to V-PDT with 2 mg/kg padoporfin administered in a 20 min *i.v.* infusion and irradiation with 763 nm diode laser (100–300 J/cm^2). The optimal light dose able to efficient tumor destruction was indicated as 200 J/cm^2. Moreover, the short-term side effects that appeared on the urinary tract were insignificant. Nevertheless, in one case, the cardiovascular event and stroke were noted as an adverse result of hypotension. It was supposed that these consequences are related to the padoporfin formulation containing Cremophor EL (CrEL), and thus the clinical trial has been canceled [212].

Nevertheless, due to the high efficacy in PDT protocols directed against tumor vasculature and positive results of phase I and II clinical trials, padoporfin was replaced by the derivative with higher hydrophilicity (padeliporfin, Tookad Soluble, WST11, see Fig. 13) [105,110]. WST11 has a hydrophilic character that originated from the presence of negatively-charged -SO_3H groups [78,108,213]. The introduced modification ensures that this derivative does not require the use of any special delivery vehicles for its intravenous administration. Tookad Soluble is capable of forming the non-covalent complex with human serum albumin (HSA) after intravenous administration. Thus, after injection, it can exist in two forms (free-unbound and bound with HSA) and remain in the circulation system, which can reduce the photodynamic treatment directed to the tumor vasculature [105,214]. Nevertheless, WST11 indicated the highest concentration in blood immediately after *i.v* injection. During the time (up to 1 h) this concentration increase in other tissue and finally the PS is eliminated from the body [110]. Moreover, WST11 does not induce systemic toxicity and its short life-time guarantees the rapid removal from the body that also reduces the possibility of phototoxic side effects. In contrast to WST09, WST11 does not accumulate in endothelial cells, and its photodynamic action is directed only toward blood vessels [110]. The structural changes between WST09 and WST11, as well as in their formulations, result in differences in their pharmacokinetic profiles and tissue distribution. WST09 indicated the high activity in V-PDT due to maximal concentration in plasma achieved after ca. 5 min and was eliminated from the body already after 3 h. The effective concentration of WST09 in other organs, *i.e.*, in the liver and kidneys was initially high and then decreased over time. These trends in tissue distribution, as well as body clearance, suggest the undesirable binding to the RES system, which is characteristic for hydrophobic drugs [215]. In consequence of short circulation time in the body, PDT with Tookad Soluble requires very short DLI. It should be highlighted, that both photosensitizers (WST09, WST11) indicated no capacity to accumulation in tumor and surrounding healthy tissue (skin or muscle). This effect provides their high selectivity towards tumor vasculature and tumor microenvironment (extracellular milieu) [214,215].

The phase I/II clinical trials with water-soluble padeliporfin also revealed its safety and tolerability in patients with prostate cancer [216]. Azzouzi and coworkers have performed a comprehensive analysis of data obtained in phase I/II (NCT00946881) and phase II trials (NCT00707356, NCT00975429) from the patients (Gleason score $\leq$7, PSA <10 μg/L) after V-PDT (4 mg/kg, 10 min *i.v.* infusion, 753 nm, 200 J/cm^2) [217]. The primary outcome was long-term negative biopsies determined in 68.4% of examined population (>100) and 80.6% of patients received the hemiablation with light density index (LDI, the parameter characterized the ratio of the length of applied fiber optics in cm to the volume of treated area expressed in mL) higher or equal to 1. Based on these results, it was also indicated that in both groups, the prostate necrosis was relatively high and PSA concentration decreased significantly [203]. In phase II studies, the hemiablation in patients was also observed during V-PDT with transperineally delivered radiation [218]. In other studies, the necrotic area in *ca.* 90% of the treated prostate tumors was detected using MRI. Moreover, V-PDT with padeliporfin was presented as a highly tolerable and safe procedure and the related adverse effects like prostatitis and other urinary tract problems (*e.g.*, haematuria) were reported only in single cases [217]. During phase II investigation, the optimization of V-PDT protocol was performed. For this reason, the men with PSA <10 μg/L were subjected to the treatment and the most prominent therapeutic outcome within the negative biopsy was observed in 83 % of patients. Moreover, from the statistical point of view, the average scores of the International Prostate Symptom Score (IPSS), as well as the quality of patients' life, indicated a significant improvement with no further changes in the International Index of Erectile Function score (IIEF-5). Moreover, it was demonstrated that the patients treated with lower dose of padeliporfin (2 mg/kg) revealed no significant therapeutic effect, while patients subjected to a higher dose of PS (6 mg/kg) were characterized by necrotic areas in surrounding organs [219]. Moreover, the histological changes and long-term consequences examined 6 months after V-PDT revealed relatively low adverse effects [220].

In the next step, Steba Biotech [221], as well as Azzouzi *et al.* [223] have undertaken a multicenter phase II clinical trial to select the optimal PDT conditions and estimate the safety and health-related quality of life [222]. During II and III phases of clinical trials, the standardized procedure of V-PDT mediated with padeliporfin against prostate cancer was drawn up [204,217,223]. The efficacy and feasibility of salvage radical prostatectomy (RP) after padeliporfin-V-PDT was assessed based on the data from: NCT00707356, NCT00975429 and NCT01310894, respectively. For further evaluation of V-PDT against prostate cancer, the interventional III phase of trials has been developed in the group of patients recruited from Mexico, Panama and Peru. In the follow-up investigation, the multicentre, randomized controlled and open-label

Table 8
The summary of clinical trials with padoporfin and padeliporfin in V-PDT against prostate cancer. Adapted and modified from [226].

Phase	Patients	PS	PS dose [mg/kg]	Irradiation	Ref.
I	10	Padoporfin	0.1–2	763 nm, 100–360 J/cm^2	[210]
I	24	Padoporfin	0.1–2	763 nm, 100, 230 and 360 J/cm^2	[208]
I/II	15	Padoporfin	0.1–2	763 nm, 100 J/cm^2	[211]
I/II	34	Padoporfin	2	763 nm, 100–300 J/cm^2	[212]
I/II	30	Padeliporfin	2, 4, 6	753 nm, 100–200 J/cm^2	[219]
II	28	Padoporfin	2	763 nm, 0.1–1000 J/cm^2	[209]
II	40	Padeliporfin	2, 4, 6	753 nm, 200 J/cm^2	[218]
II	40	Padeliporfin	2–6	753 nm, 200 J/cm^2	[219]
II	85	Padeliporfin	4	753 nm, 200 J/cm^2	[217]
II	56	Padeliporfin	4	753 nm, 200 J/cm^2	[220]
II	86	Padeliporfin	4, 6	753 nm, 200 and 300 J/cm^2	[224] NCT00975429
II	117	Padeliporfin	4	753 nm, 200 J/cm^2	[203]
II	40	Padeliporfin	2, 4, 6	753 nm, 200 J/cm^2	[222]
II	40	Padeliporfin	2, 4, 6	753 nm, 200 and 300 J/cm^2	[224] NCT00707356
II/III	86	Padeliporfin	4	753 nm, 200 J/cm^2	[227]
II/III	16	Padoporfin	2	763 nm, no information about radiation fluence	[224] NCT00312442
II/III	1	Padeliporfin	4	753 nm, 200 J/cm^2	[204]
II/III	19	Padeliporfin	4, 6	753 nm, 200 and 300 J/cm^2	[228]
III	81	Padeliporfin	4	753 nm, 200 J/cm^2	[224] NCT01875393
III	400	Padeliporfin	4	753 nm, 200 J/cm^2	[224] NCT01310894

phase III (*ca.* 400 patients) was realized to compare the results of padeliporfin-V-PDT with active surveillance in the prostate cancer treatment [221,224,225]. The main characteristics of the described clinical trials are summarized in Table 8.

Padeliporfin received EMA approval in 2017, is marketed in Mexico and is under consideration by FDA. Finally, in November 2017, it was successfully approved for clinical practice in Mexico, Israel, as well in the European Union (in 31 countries) and the European Economic Area (EEA) [230]. Furthermore, besides early-stage localized prostate cancer, padeliporfin is also being developed against other various types of tumors. In 2018 phase I clinical trials in urogenital cancer (recurrent, second-line therapy or greater, inoperable/unresectable) in the USA were started (NCT03617003) and were launched for prostate cancer in the United Kingdom. Moreover, at the beginning of 2020, Steba Biotech informed about planning a phase III clinical trial in prostate cancer in USA (NCT04225299) [229].

Recently, V-PDT with WST11 is applied with the combination of neoadjuvant or other treatment modalities. For instance, the possibility of potentiation of antitumor response by V-PDT with PD-1/PD-L1 immune checkpoint inhibition against melanoma was described [230]. V-PDT was also combined with androgen deprivation therapy (ADT), which is the most effective strategy for metastases [231]. Moreover, it may be a promising strategy because transcriptome profiling provided an upregulated androgen response pathway following WST11-V-PDT [231]. Thus, it can be hypothesized that targeting this pathway by a combination of ADT with V-PDT should be more effective compared to PDT or ADT monotherapies [231].

5.2.1.2. 13^1-oxo-bacteriopyropheophorbide a derivatives. As mentioned in chapter 2.2.1., the modification of bacteriochlorophyll *a* leads to bacteriopurpurins with increased stability. Pandey *et al.* reported synthesis and characteristics of the series of alkyl ether derivatives of bacteriopurpurin-18-N-alkylimides. Their photodynamic efficacy was investigated *in vitro* and *in vivo* against the radiation-induced fibrosarcoma (RIF) tumor model. The phototherapeutic protocol consists of DLI = 24 h, drug dose of 0.2 μmol/kg, intravenous administration of PS and irradiation with NIR light (785 nm) with a total light dose of 135 J/cm^2. It appeared that the heptyl ether substituents with relatively high lipophilic characters are the most potent PDT photosensitizers resulting in 80% cures of treated mice. All of the described data lead to the conclusion that photosensitizers with longer alkyl ether carbon chain indicate the highest PDT efficacy [98].

In other studies, 13^1-(4-aminobutylcarbamoyl)bacteriochlorin methyl ether derivatives with different-length of aliphatic chains were synthesized and characterized. These photosensitizers were photodynamically active even at nanomolar concentrations against various types of epithelial cells. Moreover, the *in vivo* studies performed on S37 sarcoma tumor-bearing mice confirmed their potential as PDT agents. The most significant therapeutic effect was achieved after the application of 2.5 and 5 mg/kg BW drug doses. After the application of the optimized PDT regimen, the

100% of tumor growth inhibition, as well as long-term cures of animals followed up to *ca.* 4-months post-PDT was observed [213].

5.2.2. Synthetic bacteriochlorins as PDT photosensitizers

In contrast to naturally-occurring bacteriochlorophyll derivatives, many PDT photosensitizers used in clinical practice are hydrophilic or amphiphilic. A characteristic feature of hydrophilic photosensitizers (>2 negative charges) is the lack of the ability to penetrate biological membranes. They can accumulate in the cells mainly *via* endocytosis or by photochemical internalization (PCI) [232,233]. In many studies, it has also been shown that hydrophilic photosensitizers (*e.g.,* padeliporfin) [234,235] can accumulate in lysosomes. Hydrophilic photosensitizers are easier to prepare in aqueous solutions for their *in vivo* administration [177]. After intravenous injection, they interact with plasma proteins, accumulate mainly in the tumor microenvironment and lead to significant vascular effects.

5.2.2.1. Stable synthetic (metallo)bacteriochlorins. Lindsey and coworkers described the library of synthetic, polarity-tunable bacteriochlorins containing positively-charged substituents. The biological activity of some of these photosensitizers (Fig. 28, left) was tested *in vitro* against, *i.e.*, murine pigmented melanoma (B16 cells) [236] and human cervical cancer cells (HeLa). Many of them have demonstarted remarkable PDT efficacy at the low drug dose (LD_{50} < 100 nM) [236–238].

The significant photodynamic activity of selected bacteriochlorins may be related to their molecular design and substitution pattern. The lipophilic character of these photosensitizers provides their specific accumulation in critical organelles such as endoplasmatic reticulum (ER) and mitochondria. Moreover, their spectroscopic and photophysical properties (discussed in detail in chapter 4), *e.g.*, high molar absorption coefficient (~120,000 $M^{-1}{\cdot}cm^{-1}$), determined for the NIR absorption band and the high triplet state quantum yield make them very efficient against resistant cancers including pigmented melanoma [236,237].

In the following studies, selected synthetic metallobacteriochlorins including free-base unsubstituted bacteriochlorin (BC), its dicyano-derivative $(NC)_2BC$, as well as corresponding zinc $(NC)_2BC$–Zn and palladium $(NC)_2BC$–Pd complexes were also investigated *in vitro* against HeLa cells (see Fig. 17) [212]. The photophysical and photochemical properties of these compounds were described in chapter 4. The effect of dicyano peripheral substituents, central metal ion (Zn^{2+}, Pd^{2+}) and CrEL formulation on the photodynamic activity was examined in biological conditions. Their efficacy (DLI = 24 h, light dose = 10 J/cm^2) may be arranged in the following order: $(NC)_2BC$-Pd > $(NC)_2BC$ > $(NC)_2BC$–Zn ≈ BC.

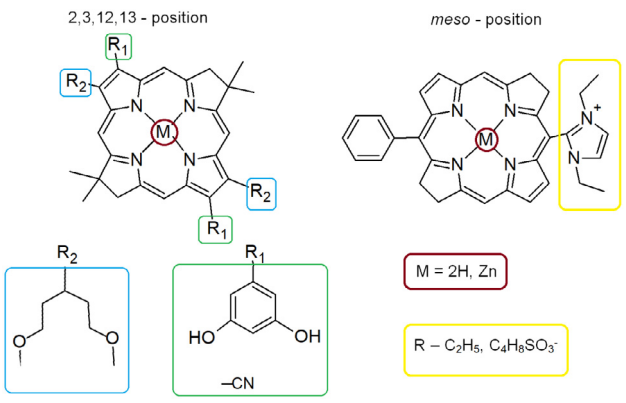

Fig. 28. Synthetic (metallo)bacteriochlorin-based photosensitizers with modification in 2, 3, 12, 13 position (left) and in *meso* position (right).

Moreover, these bacteriochlorins indicate different subcellular accumulation in organelles such as mitochondria, lysosomes and ER. Noteworthily, the best efficacy of Pd^{2+} complex is most likely related to damages of mitochondria and lysosomes caused mainly by photogenerated hydroxyl radicals. These results confirm that structural modification of bacteriochlorin-backbone *via* metal insertion and introduction of electron-withdrawing substituents (such as cyano moieties) provide a promising template for the development of more active NIR-absorbing photosensitizers [239].

5.2.2.2. Halogenated sulfonic and sulfonamide bacteriochlorins. Probably the most versatile photosensitizers are amphiphilic compounds – containing both hydrophilic and hydrophobic substituents in their molecular structure [186,187]. They accumulate both in individual cell organelles, as well as membrane structures and intracellular space. Thus, they can be used either in protocols targeting peritumoral vessels (V-PDT) or directed to cancer cells (C-PDT) [57,240,241]. Bacteriochlorins possessing halogen atoms in the structure (chapter 3.2.1.) exhibit a low tendency to aggregation, strong absorption in the phototherapeutic window, enhanced stability and efficient formation of long-lived triplet states. Furthermore, sulfonic/sulfonamide substituents allow the control of the hydrophilicity/hydrophobicity balance and provide additional protection against oxidation [22,54,142]. Halogenated and sulfonamide bacteriochlorins have been successfully tested against various types of cancer cells [154,157,180–182,184,242]. They have proven to be non-toxic in a wide concentration range (0.001–50 μM), which make them potentially suitable for biomedical applications. It has also been shown that studied photosensitizers efficiently accumulate in cancer cells depending on the molecular structure of PS, incubation time as well as cellular phenotype [54,178,243]. The time-dependent cellular uptake of chlorinated sulfonamide derivatives increased steadily over time and reached a maximum after 18–20 h of incubation [158]. Similar results were obtained for fluorinated sulfonamide bacteriochlorins, while the more polar, negatively-charged sulfonated bacteriochlorin (ClBOH) indicates a relatively low ability to accumulation in cancer cells [243]. The cellular uptake of the studied compounds seems to be facilitated by their well-balanced amphiphilic character. Sulfonamide bacteriochlorins are uptaken by cancer cells in amounts ten times higher than their sulfonated analogs [155]. Moreover, amphiphilic (sulfonamide) photosensitizers revealed a high degree of localization in critical cellular targets such as ER and mitochondria, whereas hydrophilic (sulfonated) compounds were found mostly in the lysosomes. The photodynamic effect mediated by these bacteriochlorins led to pronounced morphological changes in cells integrity. Most of them can be related to the hallmarks of apoptotic cell death, *i.e.*, cells shrinkage and pyknosis were visible by light microscopy [186,187,244]. Furthermore, it was reported that fluorinated sulfonamide bacteriochlorin is able to induce autophagy [245] and immunogenic cell death *in vitro* [246,247]. Following photodynamic action with appropriate light doses and in the presence of photosensitizers, complete inhibition of cell proliferation can be assessed. For instance, the irradiation of cancer cells with low-powered halogen lamp performed after 18–20 h of incubation with sulfonamide bacteriochlorins leads to significant inhibition of proliferation in all tested cell lines. For better understanding the photodynamic activity and evaluating the effect of the light fluence on cells viability (PS concentration with no toxicity in the absence of light), the S91/I3 and A549 cells were incubated with photosensitizer at the desired concentration and then irradiated with different light doses at 0.06; 0.16; 0.32 J/cm^2. Furthermore, the wide range of PS concentrations (1–10 μM) was applied to evaluate the effect of the PS concentration on cells viability. The representative results of these experimental conditions examined for four tested bacteriochlorins are presented in

Fig. 29. It is clearly demonstrated that with regards to their substitution pattern – the most effective photosensitizer is difluorinated sulfonamide bacteriochlorin (F_2BMet), in contrast to monochlorinated sulfonamide one, which exhibit the lowest efficiency (ClBEt). In addition, there is no correlation between observed photodynamic efficacy and, determined for each photosensitizer, singlet oxygen quantum yields, but it is closely related with their ability to generated oxygen-centered radicals.

The *in vivo* results obtained for the library of synthetic halogenated bacteriochlorins indicate that they are nontoxic even at high drug doses (up to 100 mg/kg BW) and preferentially accumulate in organs such as the spleen, liver and tumor. It was established that the maximum concentration of halogenated bacteriochlorins accumulated in murine melanoma tumors is observed after 24 h post-PS administration [180,181]. For the photodynamic therapy *in vivo*, the tumors with a diameter of approx. 0.5 cm were selected [154]. After 24 h post-PS or *i.v.* injection of photosensitizer, tumors were irradiated with laser light (650 or 750 nm) with a power ranged from 50 to 100 mW/cm^2. It has been shown that excitation of the sulfonated bacteriochlorin with laser light from the near-infrared range results in significant inhibition of tumor growth after photodynamic therapy in all tested experimental groups of animals [154,155,178,180,242]. Moreover, after photodynamic treatment with analogs sulfonated chlorin, the complete curative effect can also be observed. Noteworthy is that chlorin derivative was found to be more effective *in vivo*, despite the much inferior photodynamic effect determined *in vitro* and less favorable spectroscopic properties [181,183]. This effect was explained by relatively higher redox potentials examined for this chlorin derivative, and in consequence, its higher photostability (the quantum yield of photobleaching for this compound was lower by one order of magnitude when compared with bacteriochlorin analog). The higher stability of chlorin derivative also influences its pharmacokinetics and interactions in biological environment after administration *in vivo*. This photosensitizer indicates to be more biocompatible and shows improved pharmacokinetic properties characterized by longer circulation time in the body and thus, higher ability of accumulation in the tumor tissue [158,181,184]. The photoactive drug designed for cellular tageting should lead to high T/S and T/M ratios and be characterized by high bioavailability. Both requirements are revealed for chlorin derivative; thus, it can be suggested that investigated chlorin derivative as photosensitizer allows achieving acceptable profiles of tolerability, safety and high therapeutic efficacy in photodynamic therapy of murine tumors [183]. Despite such therapeutic success, in further studies, even more effective photosensitizers were sulfonamide derivatives [155,158]. In all PDT-treated mice with a bacteriochlorin-based photosensitizer, complete tumor regression was observed with no normal tissue damage in the immediate vicinity of the tumor. The explanation of this therapeutic outcome may be related to higher photostability of sulfonamide derivatives and more favorable spectroscopic properties [54,142]. The lead compound from this library is difluorinated sulfonamide bacteriochlorin (F_2BMet, redaporfin). The high phototherapeutic efficacy of redaporfin was confirmed in various tumor models (*e.g.*, CT26, A549, LLC, B16F10) [54,155,156,180,184,192]. The dose-escalation and toxicological studies demonstrated the low toxicity of redaporfin and its CrEL-based formulation after application with optimized PDT protocol (DLI = 15 min; drug dose = 1.5 mg/kg; light dose = 74 J/cm^2; laser power = 130 mW; margin Ø = 13 mm). For instance, redaporfin-PDT of a CT26 tumor-bearing BALB/c mice provided a significant long-term antitumor effect with a high cure rate of 83% [154,242]. The mechanisms of photodynamic activity of redaporfin were studied in detail and this photosensitizer reached clinical trials in the treatment of head and neck cancers (NCT02070432) [248,249]. Parallel to the clinical trials, there are ongoing studies on the use of redaporfin for PDT treatment of multidrug resistanct (MDR) tumors [250] and in the combined therapy with immune checkpoints inhibitors.

5.3. Vascular effects of redaporfin-based PDT

Based on the results of the comprehensive research described above, redaporfin has been chosen for the evaluation of vascular effect in PDT. Studies carried out on S91/I3 tumors growing in DBA/2 mice indicated that treated tumors are characterized by an extended hypoxic fraction (mean pO_2 level in tumors with a volume of 50–100 mm^3 reached value about 2 mm Hg). Cellular-targeted PDT with F_2BMet (DLI = 72 h) initially leads to disturbances in the structure and function of vessels, and then to the normalization of vascularity (about nine days) in the PDT-treated area. In contrast, therapy directed against tumor vasculature (DLI = 15 min) destroyed the vascular structure in the tumor and led to complete inhibition of their functionality for about 48 h after irradiation. These effects consequently led to strong tumor hypoxia (pO_2 = 0 mm Hg) [251]. Results of following *in vivo* studies per-

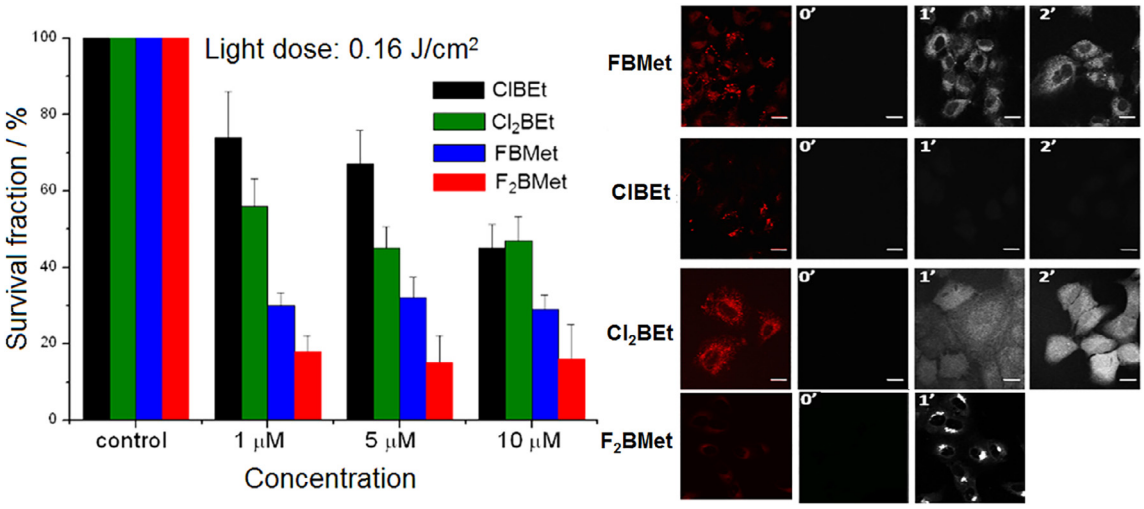

Fig. 29. Comparison of the photodynamic effect (left) with the generation of hydroxyl radicals (right) for four selected bacteriochlorin derivatives (ClBEt, Cl_2BEt, FBMet, F_2BMet) depending on the applied PS concentration with a NIR light dose of 0.16 J/cm^2.

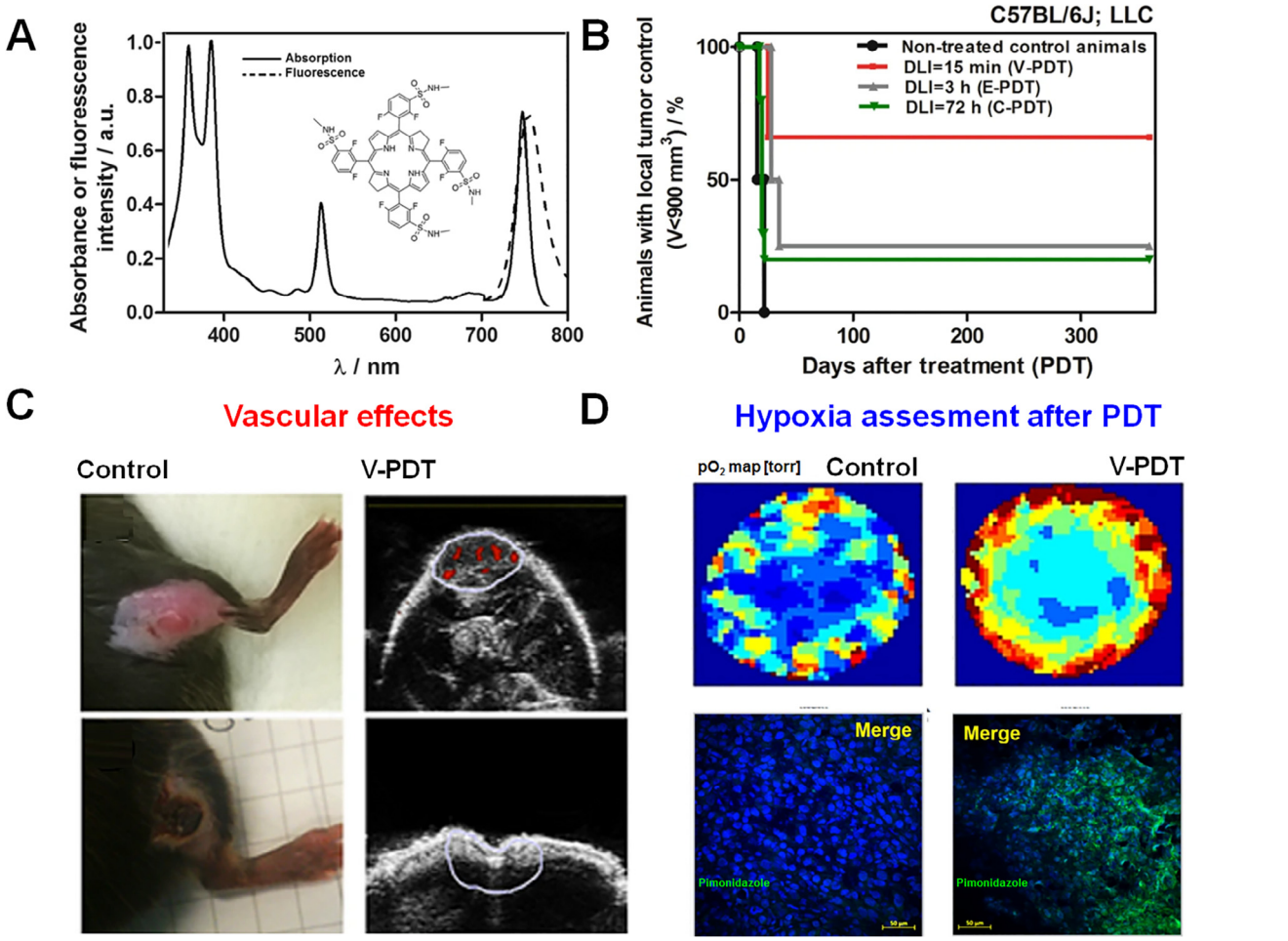

Fig. 30. Effects of redaporfin-PDT on tumor oxygenation and blood flow in C57 mice bearing LLC tumors: (A) electronic absorption and fluorescence spectra of redaporfin; (B) Kaplan–Meier survival plot determined for controls (untreated mice) and animals subjected to redaporfin-PDT; (C) representative examples of treated tumors and power Doppler images of tumors registered before and after PDT; (D) Hypoxia evaluation using tumor oximetry (oxygen maps) and immunohistochemical staining with pimonidazole performed for untreated and photodynamically-treated LLC tumors. Adapted from [192].

formed on LLC tumors also showed that V-PDT led to the development of long-term antitumor response as a consequence of vascular occlusion and tumor starvation. In the case of C57 mice bearing LLC tumors, the complete curative effect was observed in 67% of animals followed for over a year after PDT treatment. This significant effect can be mediated by, *i.e.*, bacteriochlorin-based PS properties as well as real-time monitoring of oxygen distribution, its intertissued concentration and controlled density of tumor vasculature before and after treatment, Fig. 30 [192]. These data reveal that in the case of LLC tumors, V-PDT results in more significant therapeutic success than other PDT protocols with longer DLIs (*e.g.*, E-PDT or C-PDT).

5.4. The antitumor immune response after bacteriochlorin-based PDT

It is recognized that PDT can trigger rapid inflammatory responses that are essential for the activation of antitumor immunity and long-lasting protection against metastasis. The generation of post-PDT antitumor response involves the participation of various mechanisms based on the secretion of cytokines and mediators associated with the inflammatory processes, increased level of neutrophils in the blood combined with neutrophil recruitment to the treated areas, and induction of acute-phase proteins and activation of the complement system [252–255]. PDT-induced inflammation is associated with the influx of the cells of the immune system to the treated area, and these cells contribute to the development of an immune response that recognizes cells that survived the therapy [256,257].

The effect of V-PDT on the immune system was investigated with Tookad Soluble as photosensitizer and the antitumor immune response was indicated as the main factor responsible for the observed overall therapeutic efficacy [258]. The long-term systemic antitumor immunity involves both cellular (*e.g.*, activation of lymphocytes) and humoral pathways, including changes in the antigens recognized by the serum immunoglobulins (IgG) and B cells recruitment. The anticancer activity was defined as cross-protective against different tumors (CT26 and 4T1 tumor-bearing BALB/c mice), suggesting that V-PDT-mediated production of both type tumor-derived antigens may be related to endothelial origin. Thus, it can be suggested that locally applied V-PDT can be combined with other antitumor strategies (*e.g.*, immunotherapy) for the enhancement of antitumor immunity in the treatment of both local tumors as well as distant metastases [258].

Pd-Bacteriopheophorbide-mediated PDT (5 mg/kg, 650–800 nm light dose of 360 J/cm^2) against established C6 tumors (rat glioma) growth in CD1 nude mice resulted in complete tumors regression. Moreover, PDT decreased the kinetics of tumor growth and reduced possible lung metastases which was not observed after surgery [107]. V-PDT against renal cell carcinoma also potentiated systemic antitumor immune response by PD-1/PD-L1 immune

checkpoint inhibition [230]. Mice bearing primary renal tumors were treated with either V-PDT alone, with PD-1/PD-L1 antagonistic antibodies alone, or with a combination of V-PDT and antibodies. The results confirmed that only V-PDT in combination with systemic PD-1/PD-L1 pathway inhibition, resulted in the regression of primary tumors, prevented growth of lung metastases, and significantly increased prolonged survival. It also demonstrates the crucial role of local immune modulation with PDT in combination with PD-1/PD-L1 pathway inhibition for the generation of systemic antitumor response [230]. Elimination of primary tumors and control of metastasis after PDT was also reported for redaporfin. The antitumor immune memory of CT26 tumor-bearing BALB/c mice cured with the V-PDT was compared with the group cured by surgery, Fig. 31A. It was observed that all the mice treated with surgery developed tumors in contrast to animals rechallenged with CT26 cells in the contralateral thigh. Accordingly, in this group, 67% of redaporfin-PDT treated mice remained cured for more than three months. This immune memory effect

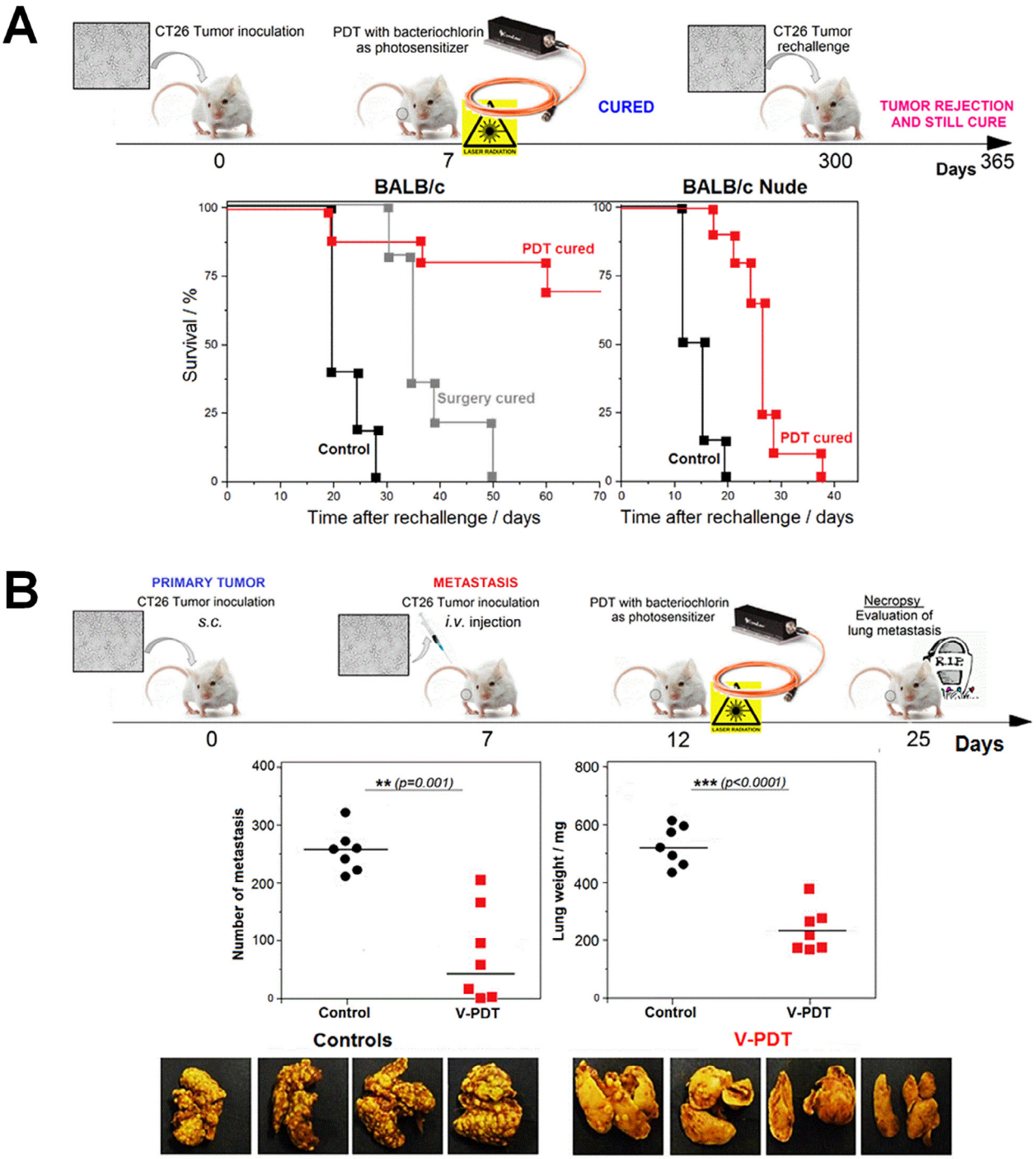

Fig. 31. Impact of redaporfin-V-PDT on long-term antitumor immune response generation: survival analysis of BALB/c mice after rechallenge with CT26 cells of mice treated and cured with V-PDT (PS dose of 0.75 mg/kg, DLI = 15 min, 50 J/cm^2, 130 mW/cm^2, margin 13 mm) or surgical tumor resection (A); the impact of V-PDT on distant lung metastasis determined by the number of developed lung metastasis as well as the weight of the lungs (B). Adapted and modified from [242].

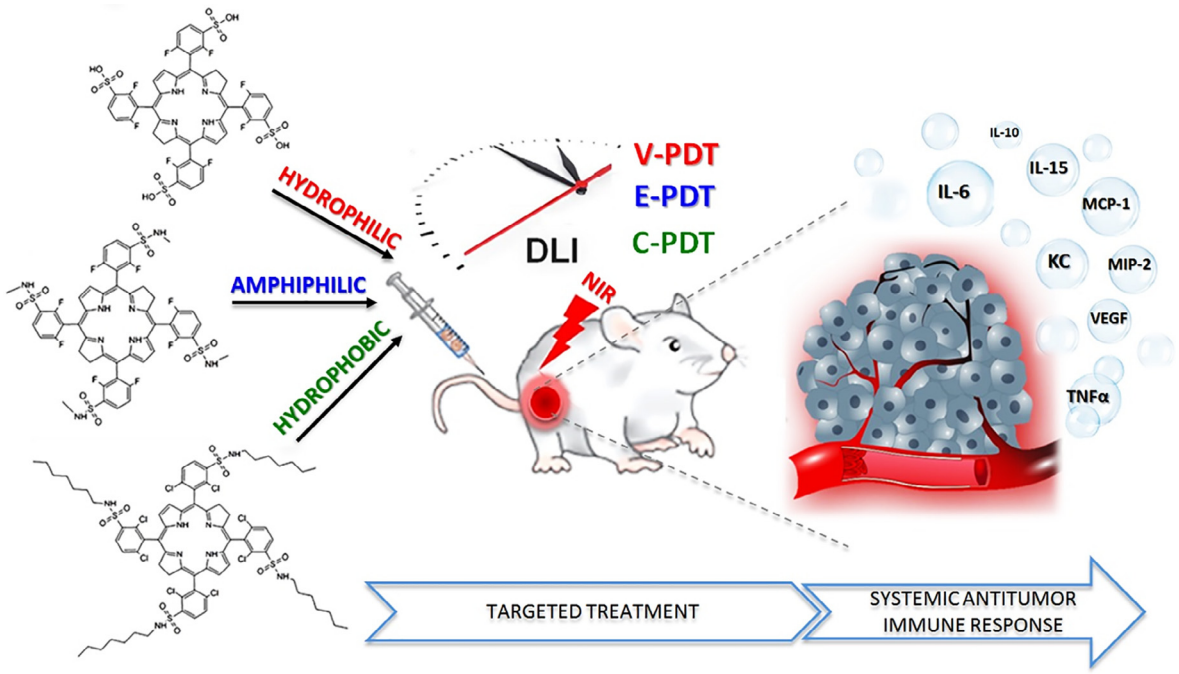

Fig. 32. The role of the lipophilicity of photosensitizer in selection of phototherapeutic protocol (V-PDT, E-PDT, C-PDT) and its impact on the biological response activation with generation systemic antitumor immune response *via* local inflammatory reaction and cytokines expression [156].

also reveals that the optimized PDT protocol was effective in stimulating the immune system *via* activation of T cell adaptive immunity and long-lasting protection against metastases, Fig. 31B [242].

More recently, it was reported that the PDT regimes with polarity-tunable bacteriochlorin lead to different biological responses with the activation of distinct immunological components, Fig. 32 [156]. Various degrees of local inflammation is observed after different PDT regimes. The analysis of selected cytokines present in the blood before and 24 h after the PDT showed increased IL-6 concentration in plasma after PDT, as expected from the observed inflammation. The enhanced concentration of KC and MIP-2 chemokines after PDT suggests that tumor response may involve an influx of neutrophils to the tumor. Moreover, the optimal protocols with sulfonamide bacteriochlorins (F_2-BMet-V-PDT and Cl_2BHep-C-PDT) are characterized by increased secretion of MIP-1, which is also involved in neutrophilic inflammation. The optimal protocols also indicated the increased level of TNFα activity and decreased VEGF expression, especially after anti-vascular treatment. These findings offer the molecular basis of how the changes in selected biomarkers after PDT contribute to mounting an adaptive immune response capable of inducing immunological memory and recognition of tumor cells that have survived the local PDT treatment [156].

5.5. Photodynamic efficacy enhancement by PS functionalization

The direction of the research consisting of the construction of phototherapeutic systems dedicated to targeted therapies has also contributed to the use of nanotechnology in the design of photosensitizers with higher pharmacological activity and simultaneous minimization of side effects (allergic reactions, long retention time in the body). Additionally, the use of new formulations and selective systems for the supply of bacteriochlorins allows to increase their (photo)stability, accumulation in cells, reduces the aggregation in the biological media, and eventually increases *in vitro* and *in vivo* efficacy [259–262]. They also affect significantly the pharmacokinetics and pharmacodynamic parameters ensuring preferred tissue distribution in the body [263–266]. Moreover, they influence not only the photophysical properties allowing the control of the electron and energy transfer processes but also the localization of induced photodamages. The use of various functionalization pathways enables determination of the relationship between the structure and physicochemical properties as well as biological activity of bacteriochlorins in the context of their application in photomedicine [53,174,175].

5.5.1. Polymeric micelles and nanoparticles

Several drug delivery nanosystems have been designed to target many tetrapyrrolic-based photosensitizers towards cancer cells and tumor microenvironment [265,267,268]. Considering the hydrophobicity of bacteriochlorophyll derivatives, Gomes *et al.* have evaluated the photophysical and photochemical behavior of BChl *a*, when loaded into a drug delivery system (DDS) such as poly(D, L-lactide-co-glycolide) (PLGA) nanoparticles. Nanoparticles of biodegradable poly(D, L-lactide-co-glycolide) loaded with BChl *a* were successfully synthesized with high yield and satisfactory incorporation efficiency using a solvent evaporation technique. The authors described the method suitable for the encapsulation of BChl *a* and enabling safe *in vivo* administration [269]. BChl *a* has shown to be a promising alternative to the molecules currently being used in PDT due to its spectroscopic properties, such as a NIR absorption at 770 nm (in toluene) and 782 nm in an aqueous solution of nanoparticles, respectively. Moreover, the increased singlet oxygen generation quantum yield (Φ=0.31) is related to the ROS formation mainly *via* type II photoreactions.

The functionalization of redaporfin with Pluronic® copolymers increased the effectiveness of the therapeutic regimens [180]. The pharmacokinetic profile and photodynamic efficacy of redaporfin-CrEL, redaporfin-F127, and redaporfin-P123 in animal models (B16 melanoma-bearing C57BL/6J mice) were determined. The results of the conducted research indicate the possibility of a significant increase in the selectivity of the applied photosensitizer and the possibility of obtaining a 100% long-term cure for animals

after the application of the F_2BMet-P123-V-PDT therapeutic protocol [180].

5.5.2. Lipoproteins

Lipoproteins represent the class of biocompatible, nonimmunogenic complexes containing the lipids and proteins, which are ideal for efficient drug loading and delivery. Many lipoprotein-based nanoparticles create the opportunities for enhanced therapeutic and theranostic effect through mimicking the shape and structure of endogenous lipoproteins. Due to the small size (>30 nm) of the low- and high-density lipoproteins (LDL and HDL, respectively), they can avoid the reticuloendothelial system (RES) and penetrate the tumor tissue more deeply. In addition, they are characterized by longer circulation time in the body. Moreover, lipoproteins are useful in cancer treatment because many tumors (*e.g.*, colon, breast, prostate) indicate increased expression of LDL receptors. Furthermore, LDLs may also be re-targeted to folate receptors that are more specific to the selected type of human tumors [270,271].

Marotta and coworkers have developed the LDL-based delivery system for lipophilic bacteriochlorophyll derivative – bacteriochlorin e6 bisoleate (abbreviated as r-Bchl-BOA-LDL) for its used in PDT. Bis-oleate or bis-stearate moieties have also been applied for loading of hydrophilic dyes (like tricarbocyanines) and Gd-chelating substituents into the phospholipid monolayer of LDL [272]. The biological activity profile of r-Bchl-BOA-LDL was investigated *in vivo* on human hepatoblastoma G2 (HepG2) tumors. When compared with untreated control mice, the kinetics of tumor growth was significantly delayed after PDT with PS dose of 2 μmol/kg and different light doses (125, 150 or 175 J/cm^2). Moreover, assessed phototoxicity against tumor as well as minimized healthy tissue damages confirm that r-Bchl-BOA-LDL may be used as an effective PDT agent [272].

5.5.3. Metal-based nanoparticles

Nanoparticles (NPs) and, more specifically, noble metal NPs are widely-known agents for many biomedical applications, including promising drug delivery systems and diagnostics tools. In general, noble metal NPs (*e.g.*, Au, Ag) indicate the high surface-to-volume ratio and appropriate, tunable spectroscopic properties that may be modulated to desired wavelengths. Such tuning is possible due to their shapes (nanorods, nanoshells, *etc.*), size (up to 100 nm), composition (core/shell or alloys) and potential surface modification and functionalization [273]. Pantiushenko and coworkers have described the comprehensive characteristics of a new type of materials containing bacteriochlorophyll isolated from non-sulfur bacteria *Rh. capsulatus*. This derivative posseses the disulfide moiety derived from lipoic acid. Such types of bacteriopurpurinimides-based photosensitizers are characterized by aurophilicity (a phenomenon referring to the aggregation of gold complexes). Due to the possibility of the formation of S–Au bonds, such properties allow obtaining the conjugates with gold nanoparticles (NP-Au). The conjugation is related to the red-shifted NIR absorption (at λ_{max} = 824 nm) and fluorescence emission at λ_{max} = 830 nm. The biological tests performed *in vivo* in rats bearing M1 sarcoma indicated the favorable biodistribution of PS-Au estimated by real-time dynamic fluorescence imaging. The authors have reported that PS-Au conjugates exhibited a longer circulation time in the blood than free bacteriochlorophyll *a* as well as enhanced accumulation in tumor tissue that makes it a more effective nanoformulated theranostic agent [274].

The other type of NPs are magnetic nanoparticles consist of a metal/metallic oxide core, encapsulated in an inorganic or a polymeric coating shell. This shell renders the properties of the particles, such as their biocompatibility and stability, as well as may act as a support for many biomolecules. Their magnetic properties enables their application as MRI contrast agents, hyperthermia agents, magnetic wand vectors controlled by magnetic field gradient towards a selected location similar to targeted drug delivery systems [275]. The bacteriochlorin-loaded magnetic nanoparticles dedicated to personalized MRI-guided PDT were recently described. The bacteriochlorin derivative with a positive charge and various-lengths linker between the amine group and macrocyclic ring was efficiently encapsulated in HSA coated metal NPs *via* electrostatic and hydrophobic binding. After successful encapsulation, magnetic NPs-HSA-PEG nanoparticles provide long-term stability as well as effectiveness in delivering PS to cancer cells in both *in vitro* and *in vivo* systems. Moreover, this kind of conjugates reveals that they can be applied in *in vivo* MRI imaging for efficient drug delivery into the tumor milieu [276].

The same research group performed a primary screening of bacteriochlorin-based photosensitizers containing aminoamide, propyl, and peripheral carbohydrate substituents. The authors performed the comprehensive spectroscopic characteristics of these compounds, determined their stability as well as dark and phototoxicities against HepG2 cancer cells [277]. All studied photosensitizers except the bacteriochlorin substituted with carbohydrate moiety in the exocycle E were not cytotoxic in the dark and led to the strong photodynamic effect. The highest photoactivity was noticed for aminoamide-bearing photosensitizer, for which two hours of incubation led to the IC50 in the range of 17–49 nM). Based on all of the determined physicochemical and biological properties for this group of agents, O-propyloxime-N-propoxybacteriopurinimide methyl ester was ranked as the most promising agent in the treatment of tumors [277]. These studies were further continued by Plotnikova *et al.* in order to develop the formulation for O-propyloxime-N-propoxy-bacteriopurpurinimide methyl ester. The CrEL micellar emulsion was indicated as a promising formulation of this photosensitizer and was of great interest for further studies in the field of PDT [277].

5.5.4. Metal-organic frameworks (MOFs)

Nanovehicles designed for therapeutics have gained increasing interest, as these systems allow to avoid many disadvantages of traditional treatments. A new class of hybrid organic-inorganic materials is represented by metal-organic frameworks (MOFs), containing selected metal ions and organic bridging ligands. MOFs may be promising nanoplatform for selective drug delivery, with the opportunity of high drug loading, biocompatibility as well as wide-spectrum functionality and applications [278]. The hydrophobic character of many tetrapyrrolic derivatives may be a reason not only for insufficient selectivity towards tumors but also may cause aggregation and reduce the efficacy of PDT. However, this makes them very attractive examples of organic ligands in the MOF structure [279]. The use of tetrapyrrole-based MOFs designed for PDT application have been investigated. However, in many cases, they are conjugated with other nanoparticles forming dual-agents for synergistic strategy (including PDT-photothermal therapy, PDT-radiotherapy). Recently, bacteriochlorin-based MOF was prepared as a NIR-absorbing dual-mode photoagent for photoacoustic imaging PAI-guided PDT [279]. This MOF contains the 5,15-di(*p*-benzoato)bacteriochlorin (H_2DBBC) as blocks and central clusters, including $Hf_6(\mu_3\text{-}O)_4(\mu_3\text{-}OH)_4$ (abbreviated as DBBC-UiO). This hybrid material was dedicated to the treatment of hypoxic tumors due to the ability of ROS generation *via* both types of photoreaction with singlet oxygen as well as oxygen-centered radicals formation, Fig. 33. It was reported that the DBBC-UiO MOF could generate superoxide anion within a severe hypoxic microenvironment, and, that the part of the generated amount of $O_2^{\cdot-}$ is converted into hydroxyl radicals *via* SOD-induced catalytic process upon irradiation with NIR light [279]. This effect suggests that the photoactivity of DBBC-UiO may also be oxygen-independent and effective against hypoxic tumors. In the following studies,

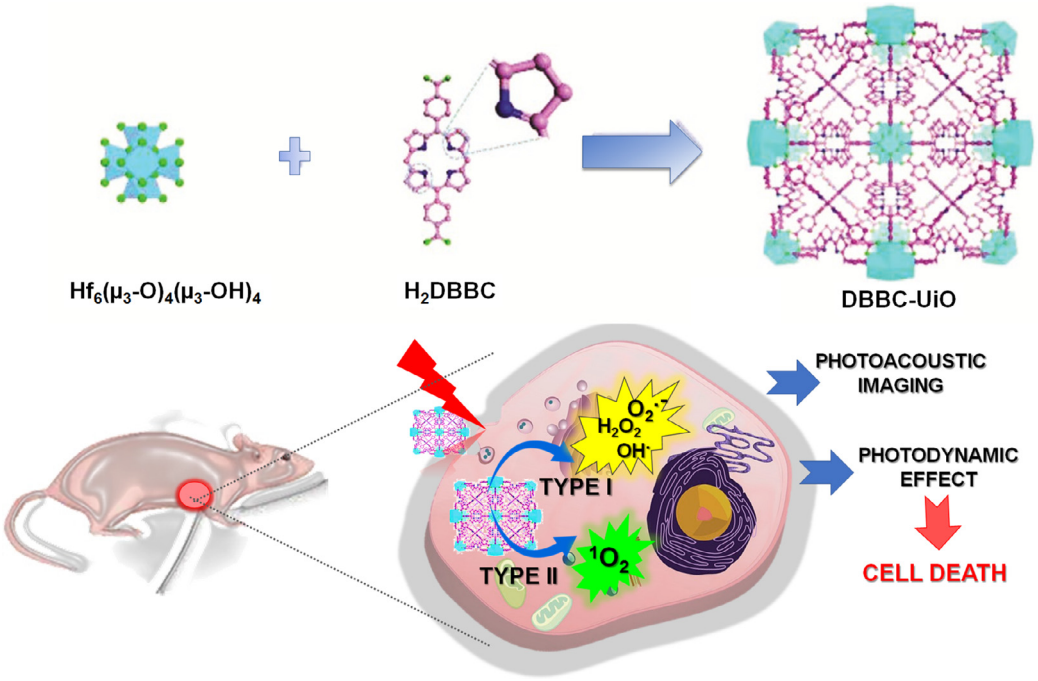

Fig. 33. The scheme of the synthetic procedure for metal-organic framework DBBC-UiO formation and its potential application for photoacoustic imaging and photodynamic therapy. Adapted and modified from [279].

the ability of MOF application in tumor-specific PAI was verified and these data indicate that it could also be used as an agent for diagnosis of cancer with deeper tissue penetration and increased resolution [279].

6. Application of (metallo)bacteriochlorins in photodiagnosis (PD) and imaging

The growing interest in cancer detection focuses on the ability for better visualization of selected probes that target diseased tissues. Real-time imaging of designed fluorescent probes enables the improvement of both basic and preclinical research. The photons from the near-infrared region are able to penetrate biological tissues more efficiently than visible light [3]. However, at wavelengths λ>950 nm, these effects are reduced due to increased absorption of water and lipids. Thus, the phototherapeutic window used in PDT (630–850 nm) is not optimal for photodiagnosis, considering the higher background signal from tissue autofluorescence as well as limited light penetration through tissue (1–2 cm). Therefore, in photodiagnosis the optical window covers the range from 700 nm to 900 nm [280]. In this region, the endogenous pigments do not absorb and, consequently, do not interfere with the NIR-fluorescent molecules [281–284]. Moreover, NIR photons indicate a lower ability to generate ROS due to the lower energies in this part of spectra [3,6]. The spectroscopic properties of bacteriochlorin derivatives indicated the strong absorption band between 700 and 800 nm is of particular interest because it allows higher tissue penetration depth and avoids the optical interferences with endogenous pigments. The ability to distinguish multiple-color molecular markers during fluorescence imaging is one of the most appropriate feature. Such an effect can be achieved by using an appropriate probe or in combination of selected labelling-agents. These fluorophores should indicate significant Stokes shifts derived from well-separated absorption and fluorescence emission bands. Moreover, this property reduces the signal of the scattered excitation light, and consequently, to improve the quality and resolution of registered images [36,285].

Several NIR fluorophores, like cyanine dyes (Cy5, Cy7), indocyanine green (ICG), Alexa Fluor compounds as well as tetrapyrrole-based fluorochromes have been extensively developed for biomedical applications [38]. Despite the fact that some commercial probes are based on these structures, several new classes of labelling agents, including bacteriochlorophyll- or bacteriochlorin framework are still being developed. Besides the favorable characteristics, some of the studied bacteriochlorins demonstrated limitations for their successful application. The major limitations are due the reduced stability of bacteriochlorins. As previously described, many efforts have been taken to modulate the stability of BChls, including peripheral modification of the macrocycle, the introduction of the serine or halogen atoms as substituents, insertion of central metal ion, or encapsulation in selected drug delivery systems. For instance, Ptaszek and coworkers have described several promising dyads with potential use as optical imaging probes [37,38]. The chlorin-bacteriochlorin, as well as BODIPY-bacteriochlorin complexes are able to take part in the efficient energy transfer, and thus, are considered as promising fluorescence probes. In such a chlorin-bacteriochlorin system, chlorin acts as an energy donor and bacteriochlorin plays an energy acceptor role. Excitation of the chlorin leads to stronger fluorescence emission derived from bacteriochlorin [37,38]. This complex exhibits several desirable properties, including strong absorption and fluorescence, narrow bands with FWHM <20 nm and large Stokes shift over 85 nm. Moreover, these chlorin-bacteriochlorin dyads are characterized by relatively long-lived excited singlet state *ca.* ~5 ns [38]. Additionally, the fluorescence properties can be tuned by a structural modification and changes in the peripheral substitution patterns. In other studies, the BODIPY-bacteriochlorin complex was synthesized and characterized, Fig. 34 [286].

In this type of bioconjugates, the BODIPY molecule, contrary to chlorins, possesses increased hydrophilicity and high molar absorption coefficient in the green range of spectra. However, due to the bulky aromatic structures and overall hydrophobicity,

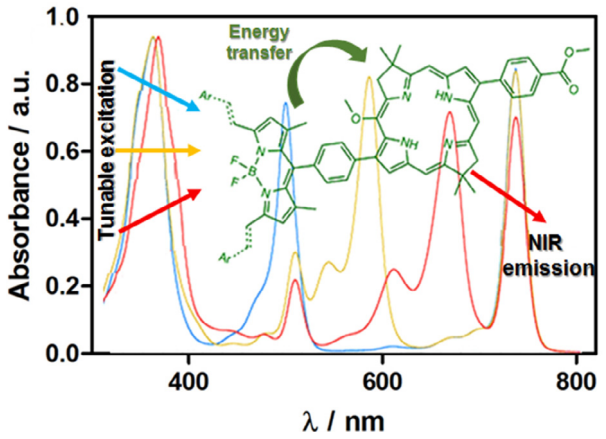

Fig. 34. Electronic absorption and fluorescence spectra as well as the chemical structure of boron-dipyrromethene (BODIPY)-bacteriochlorin energy-transfer dyads with activatable near-infrared fluorescence. Adapted and modified from [286].

PEG formulation was used to improve the water solubility and alter their pharmacokinetics *in vivo* [287]. To achieve enhanced selectivity and active targeting of fluorescent probes, many efforts were undertaken, including the conjugation with antibodies. Unfortunately, probe-antibody complexes (*e.g.*, panitumumab-bacteriochlorin conjugates) were characterized by increased hydrophobicity and were prone to aggregation [287].

Moreover, the synthesis and characterization of the other bacteriochlorin derivatives (named as NMP4 and NMP5) were reported in terms of their use as targeted photodiagnostic agents [285]. These compounds, after excitation with a green light indicate the fluorescence emission in the NIR (λ ~ 739 nm for NMP4 and λ ~ 770 nm for NMP5, respectively) [285]. In the subsequent studies, these bacteriochlorins were conjugated to galactosyl-human serum albumin (hGSA) or glucosyl-human serum albumin (glu-HSA), which are the molecules with affinity to H-type lectins. Thus, these complexes were enabled to target, *i.e.*, β-D-galactose receptors, which are expressed on ovarian cancer, Fig. 35.

The *in vivo* multicolor imaging was performed in mice bearing ovarian cancer metastases. The excitation of bacteriochlorin with green light results in various NIR fluorescence emissions that may be detected apparently from each fluorophore. The selectivity towards targeted receptors was achieved and also enhanced due to the unique fluorescence properties. The fluorescence emission of bacteriochlorin conjugated to hGSA are normally quenched [285]. Nevertheless, after binding to H-type lectin on the surface of cancer cells, the fluorescence signal was observed showing the tumor localization. The described activity of these compounds was reported only in the case of peritoneal metastases. Based on single excitation, two-color NIR fluorescence imaging with bacteriochlorin-based photoactivatable complexes was developed and reveal that they are worth further investigation [285].

In other studies, Liu *et al.* have described the bacteriochlorophyll derivative that might be used in multimodal theranostics [288]. The molecular design of this probe consists of bacteriochlorophyll molecule conjugated with a targeting peptide that enables modifying the pharmacokinetic profile as well as recognition of folate receptors on the cancer cells surface. Moreover, this probe indicated significant, red-shifted fluorescence emission

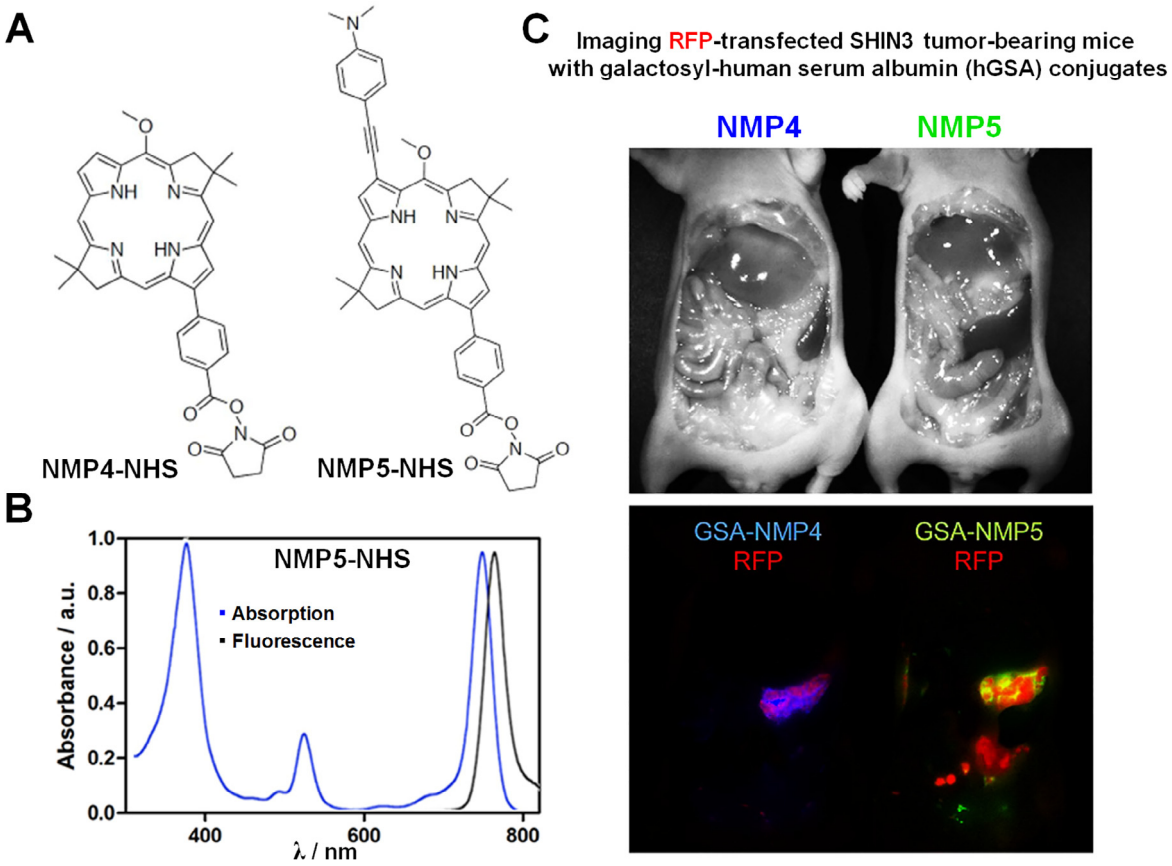

Fig. 35. Chemical structures of the bacteriochlorin derivatives named NMP4-NHS ester and the NMP5-NHS ester (A), the absorption and emission spectra of NMP5-NHS, and fluorescence imaging of ovarian cancer (SHIN3) after *i.p.* administration with hGSA-NMP4 or hGSA-NMP5. Adapted from [285].

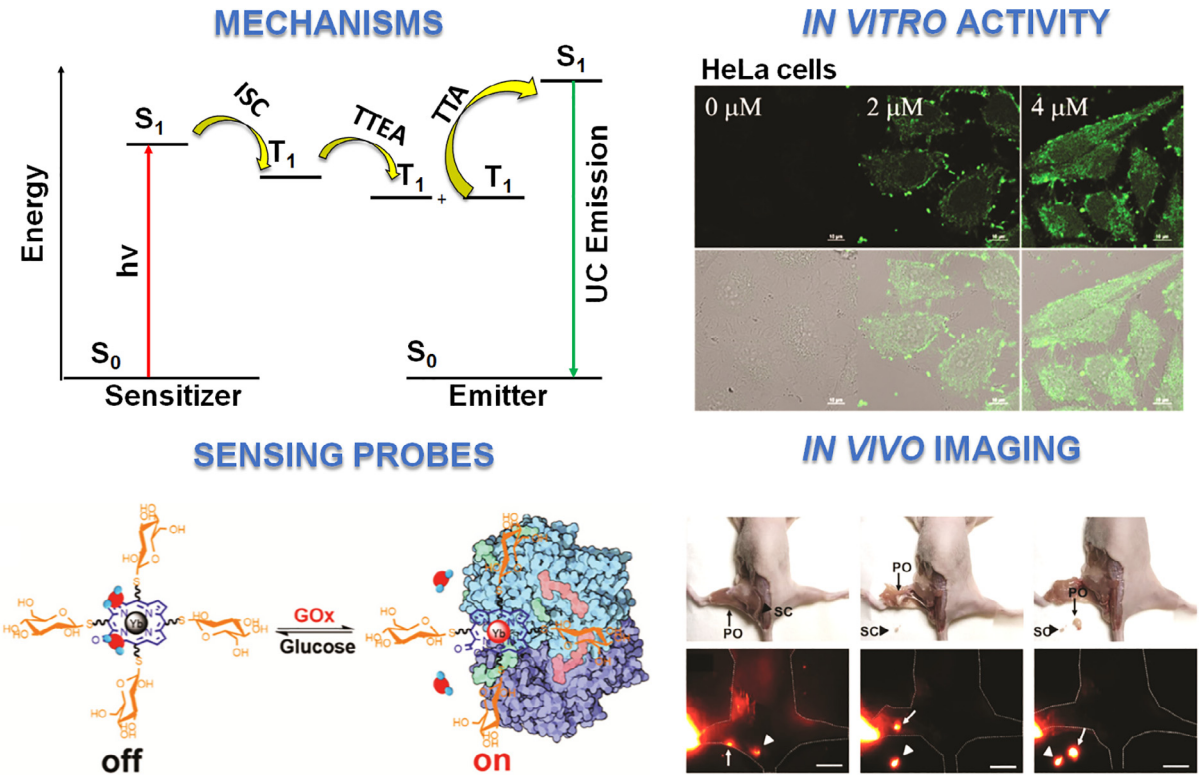

Fig. 36. Lanthanide complexes of porpholactone derivatives as efficient photodiagnostic tool: (a) scheme for TTA-UC *via* conventional triplet sensitization routes; (b) H_2DCFDA fluorescence images of HeLa cells after treatment with Gd-derivatives; (c) the structure of the Yb^{3+} porpholactone complex and its sensing for glucose oxidase; (d) β-fluorinated Yb^{3+} complexes applied in *in vivo* imaging (fluorescence-guided sentinel lymph node surgery). Adapted from [290].

($\lambda_{ex}/\lambda_{em}$ 748/766 nm). To confirm the selectivity of the prepared probe and the possibility of targeting the folate receptor-expressing cancer cells, its accumulation of tumor tissue was investigated *in vivo* in KB- and HT1080- tumor-bearing nude mice. In these animal models, KB tumors were characterized by high folate receptor expression and HT1080 with low expression, respectively. Besides the fluorescence imaging, performed studies revealed high *in vitro* phototoxicity as well as significant photoactivity *in vivo* resulted in complete tumors regression. Thus, these findings provide that the modified BChl derivative can be a promising dual-mode agent for NIR fluorescence imaging and PDT purposes [288].

In the context of photodynamic treatment, the new frontier is related to selective and controlled light delivery with possible visualization of the administered photosensitizer. Even though the insertion of the optic-fiber into the body and selected internal organs is usually supported and controlled by standard techniques including ultrasonography, optical, or X-ray imaging, the complete and real-time monitoring of the delivered light and the direct impact on tissue response during PDT is currently unavailable [289]. This limitation may be dangerous in the case of tumors localized closely to vital organs, major blood vessels or nerves, because then the light must be spared to avoid the damages or medical complications [289]. In such cases, the precise light delivery during PDT is desirable. For instance, Scherz with collaborators have evaluated the opportunity of the use of blood oxygenation level-dependent (BOLD) contrast MRI for real-time and dynamic monitoring of PDT procedure. They developed this technique using Tookad-PDT against prostate cancer and indicated that during photodynamic treatment, the significant attenuation (*ca.* 25–40%) of the magnetic resonance signal might be observed only in tumor area subjected to the irradiation [257]. All of the described results reveal that photosensitized BOLD-contrast MRI may be applied intraoperatively as interactive guidance for monitoring antivascular cancer therapy, cardiology, PDT for age-related macular degeneration (AMD) as well as other biomedical purposes [289].

Lanthanide complexes are characterized by strong luminescence in the NIR, with an extremely narrow band, making them ideally suited for use in developing new multifunctional luminescent materials. Unfortunately, these complexes exhibit low molar absorption coefficients due to forbidden *f–f* transitions. This problem may be omitted by using tetrapyrrolic ligands, characterized by strong absorption and efficient energy transfer from its triplet state, which lay higher than excited state of the lanthanides. The complexation of lanthanide metal ion by tetrapyrrolic ligand enhances the NIR emission and extends the phosphorescence lifetime by narrowing the energy gap between the triplet state of ligand and the excited state of the metal ion (triplet-triplet annihilation upconversion mechanism, TTA-UC, Fig. 36A). The properties of free-base porpholactone ligands and lanthanide(III) metal complexes (Ln = Lu^{3+}, Gd^{3+}, Yb^{3+}) and their biological activity studies including cellular-uptake as well as photocytotoxicity was performed by Zhang and co-workers [169,170,290]. The comparison of free-base tetrapentafluorophenylporphyrin (F_{20}TPP), porpholactone (F_{20}TPPL), cis/trans porphodilactone and their Gd^{3+} complexes show, that especially in case of *trans*-isomers the phosphorescence is red-shifted with decreased lifetimes and phosphorescence quantum yields [290]. Moreover, the incorporation of the heavy atom (Gd^{3+}) enhanced photocytotoxicity of these compounds upon red light irradiation that makes them most promising for PDT, Fig. 36B. Furthermore, the presence of Gd^{3+} in porpholactone structure allows the rational design of dual-mode photosensitizers due to both therapeutic and diagnostic agents within the same molecular scaffold [290]. Similarly to free-base, the cis/trans isomers of porphodilactones have significant differences in quantum yields of the triplet state of Yb^{3+} complexes. Due to this fact, Zhang

et al. also constructed a sensitive glucose-oxidase dependent lanthanide poprholactone-based luminescent sensor. In this probe, the NIR emission of Yb^{3+} is specifically switched-on by glucose oxidase and then switched-off in the presence of glucose (Fig. 36C). This phenomenon indicates that porphodilactone-based ligands enhance the quantum yield of Ln luminescence and may be used in several biomedical applications, Fig. 36 [290]. The upconversion fluorescence imaging is a promising method due to their biological and technical specification, including excellent photostability, narrow emissions bands, absence of photodamage to living organisms, absence or very low auto-fluorescence, high sensitivity, and high penetration into biological tissues. Upconversion is a non-linear optical process, which involves the conversion of two or more low energy photons (from the NIR) and emits radiation with higher energy [291]. Thus, its potential is commonly used not only in diagnostics but also in PDT [292]. The functionalization of these fluorescent probes may be combined with other imaging methods such as magnetic resonance imaging, positron emission tomography and computed tomography. Porphodilactone complexes with Lu^{3+} are suitable for upconversion based on triplet-triplet annihilation [290]. Moreover, they display much longer phosphorescence decay lifetimes (μs scale) than the Pt^{2+}, Pd^{2+} complexes (ms), and thus can be applied in upconversion-based imaging [169].

Other examples of upconversion probes are nanoparticles and nanocrystals doped with metal ions, especially by *f*-block metals [291,292]. Moreover, the immobilization of nanoparticles with lanthanide porphyrinoids allows to overcome the major limitation of traditional porphyrin-based photosensitizers for practical application of PDT such as weak absorption in the red region and poor biocompatibility [292]. Similarly to bacteriochlorins, the porpholactones and their metal complexes possess higher cellular uptake than porphyrin, which is crucial for their *in vivo* evaluation [169]. Furthermore, porpholactones are characterized by a high binding affinity to low-density lipoproteins (LDL). The cytotoxicity tests also reveal that β-lactonization of porphyrin leads to a more prominent photodynamic effect against HeLa cells with photodynamically-induced cell death *via* apoptosis [169].

7. Application of bacteriochlorins in photodynamic inactivation of microorganisms (PDI)

The bacteria-related diseases are becoming a serious worldwide health problem due to the increased multi-drug resistance [293]. Although many antibiotics are effective against Gram-positive bacteria, the clinical manifestation of multi-resistant bacterial infections, especially caused by Gram-negative bacteria, is still unsatisfactory. Moreover, microorganisms are capable of developing complex mechanisms of defense against the damages and antimicrobial drugs by, for instance, creating their matrix named biofilm as well as several virulence factors. Thus, the development of new antibacterial strategies is urgently needed [294–297]. Among them, the photodynamic inactivation of microorganisms (PDI) represents one of the most promising method that involves the excitation of a photosensitizer to generate ROS. Due to the lack of resistance to singlet oxygen, this highly reactive molecule may initiate further oxidative reactions in the nearest environment, such as nucleic acids, lipids, proteins, or enzymes [59,298]. Therefore, PDI is based on the concept that a photosensitizer can accumulate in the cytoplasmic membrane, which is the critical target for damages after irradiation [298], Fig. 37 [299–301].

Many classes of photosensitizers were developed for efficient PDI of bacteria, viruses and fungi [157,294,295,298,302–308]. It appears that the most appropriate PDI photosensitizers are positively-charged, water-soluble and photostable compounds [309]. Moreover, affinity to bacterial cell wall is a crucial factor which influences PDI efficacy. The differences in morphology between the Gram-negative and Gram-positive bacteria are responsible for PS interaction with the bacterial cell walls. The presence of lipopolysaccharide (LPS) in the outer membrane of Gram-negative bacteria provides an additional barrier to many molecules in the external environment. It contributes to the observed drug-resistance of these organisms. In contrast, Gram-positive bacteria contain a single peptidoglycan layer with specific proteins on the cell surface. The PDI effectiveness against fungal yeast is limited by low diffusion of the drug into the fungal cytoplasm because of their cell walls, which also contain β-glucan. Thus, PS with positively charged groups or the addition of substances able to increase the permeability of the outer membrane outstanding enhance the efficacy of Gram-positive bacteria inactivation.

As it has been claimed earlier, the most promising photosensitizers for anticancer PDT are chlorins and bacteriochlorins. Porphyrins, however, can still be considered as efficient agents for antimicrobial approach. Anyway, bacteriochlorins still seem to be more promising for the treatment of biofilm, localized infections and deeper wounds, due to the sufficient NIR light penetration through tissues [310]. Besides the appropriate spectroscopic properties, a photoactive agent should have a high affinity to the bacterial cell wall and allows penetration into bacterial cells [238]. The examples of three mono-substituted cationic bacteriochlorins with quaternary ammonium substitution (named BC37, BC38, BC39,

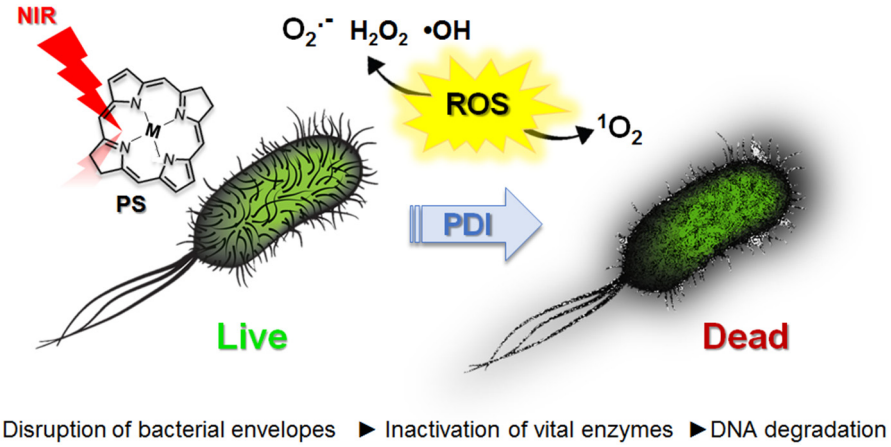

Fig. 37. Scheme of photodynamic inactivation of microorganisms (PDI) and its basic mechanims of action.

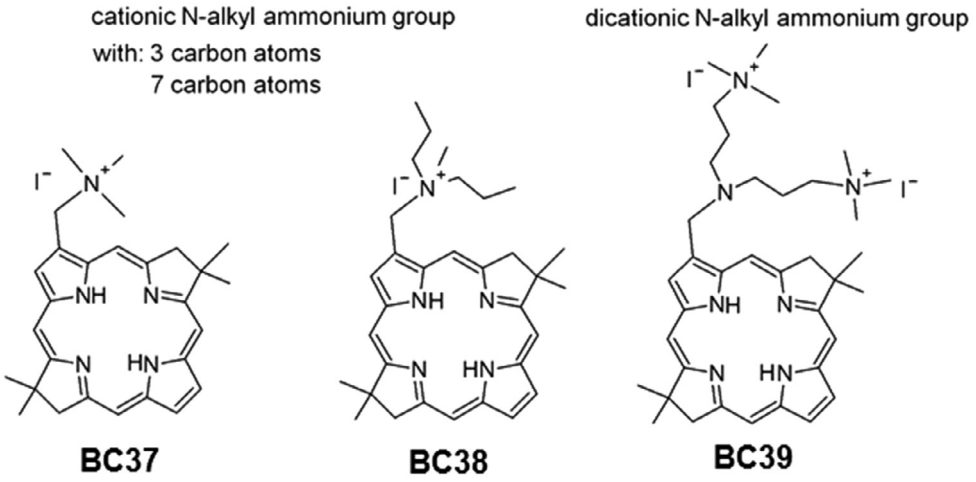

Fig. 38. Chemical structures of positively-charged bacteriochlorin derivatives designed for PDI application.

Fig. 38.) were synthesized and tested as antimicrobial photosensitizers [311].

High effectiveness at nanomolar concentrations and low light dose (10 J/cm^2) against Gram-positive bacteria was reported for bacteriochlorins presented in Fig. 38, with a different number of positively-charged groups. The bacteriochlorin bearing two cationic moieties indicates the highest activity against the resistant bacteria (at micromolar concentrations), whereas the hydrophobic one was more effective against the fungi [311]. According to these studies, it can be concluded that Gram-positive bacteria are more susceptible to PDI by neutral photosensitizers or those with a moderate number of positive charges with relatively low hydrophobicity [311]. In contrast, effective photoinactivation of Gram-negative bacteria requires more hydrophobic photosensitizers with many positive charges in the structure [303]. In turn, fungal cells should be treated with photosensitizers that have little or no positive charge with relatively higher hydrophobicity [311].

It should also be highlighted that efficient photodynamic inactivation of a broad-spectrum of pathogens can be achieved by a protocol involving short photosensitizer-cell incubation time (up to 2 h) and relatively low light dose (*i.e.*, 10 J/cm^2). Thus, in the following studies, the authors also showed that a short incubation time (up to 30 min) might also result in increased selectivity for microbial cells over human cells (HeLa cancer cell line) [311]. The possibility to use shorter incubation times in PDI than for typical photodynamic effect against cancer or eukaryotic cells is a consequence of the fast-electrostatic interaction occurring between cationic functional groups in PS structure and the negatively charged teichuronic and lipoteichoic acids located in the outer wall of bacterial and fungal cells [303].

In other studies, Hamblin with coworkers tested the next set of bacteriochlorins containing a various number of cationic charges against the different species of microorganisms, Fig. 39 [238]. It was reported that all four derivatives indicate the PDI activity against Gram-positive *S. aureus*. The most significant antibacterial effect was achieved for the bis-quaternized derivative (5 logs reduction after PDI with 100 nM PS). However, other bacteriochlorins (basic, tetrakis- as well as hexakis-quaternized) showed similar but relatively lower than the best one, activity in bacteria inactivation procedure (up to 5 logs of killing after PDI with 1 μM PS) [238]. The observed effect may be explained by the statement, that there is an optimum number of cationic charges in the photosensitizer structure, which is responsible for: (i) PS binding to anionic phosphate groups present on the bacteria cell wall and (ii) efficient penetration into the bacterial cell wall, where ROS are produced upon irradiation leading to photodamages. The lower than the optimal number of positive charges (for instance, neutral bacteriochlorin derivative with two basic amino groups) dimin-

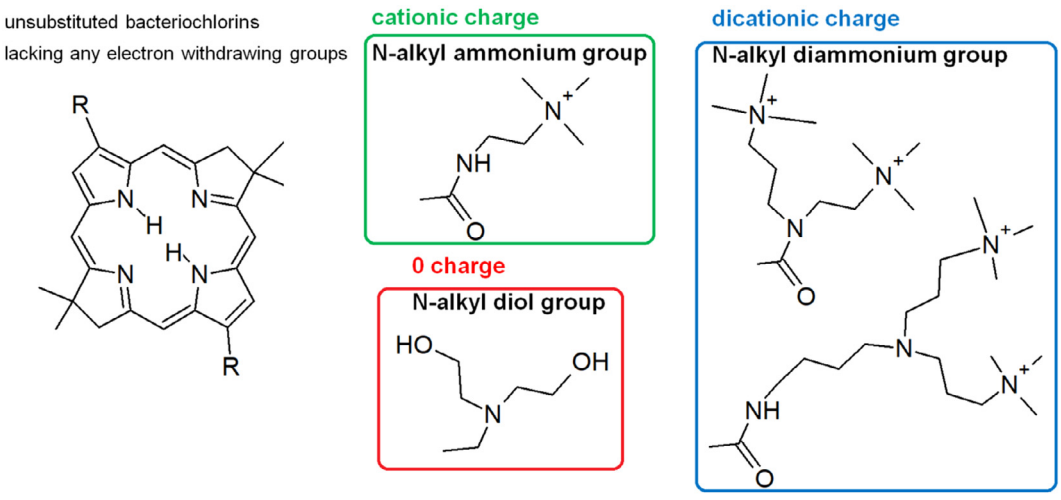

Fig. 39. Examples of disubstituted positively-charged bacteriochlorins designed for photodynamic inactivation of bacteria.

ishes the sufficient binding. In contrast, the respective higher number of cationized groups like in bacteriochlorin containing 4–6 positive charges) result in too strong binding, which reduced the PS penetration into the cell wall [238]. A similar finding has also been reported for PDI with chlorin *e6* conjugates with different-sized poly-L-lysine [312,313] or polyethylenimine [313] chains as well as porphyrin derivative [157,309,314]. Maisch *et al.* have confirmed that porphyrin-based photosensitizer with two cationic groups indicated higher activity against *S. aureus* than an analog molecule with four positively-charged substituents [314].

The observed results for cationic bacteriochlorins were also supported by the photophysical studies and DFT calculation undertaken in the following studies [238]. The theoretical analysis revealed that the excited triplet state quantum yield, which is the precursor of ROS, for the four bacteriochlorins is similar and reached *ca.* 0.48–0.53 [238]. Moreover, any correlation between the redox properties of photosensitizers was observed [238]. The only noticeable trend is that mono-substituted bacteriochlorins are more effective than di-substituted derivatives, which may suggest that their photoactivity is associated with an increased probability of the electron transfer processes [238]. Thus, it can be suggested that overall PDI activity observed among the set of bacteriochlorins must be related to both cellular binding and accumulation rather than photochemical features. All of these data present the basic information about the structure-activity relationship for analyzed cationic bacteriochlorins and indicate the major factors that influence their photodynamic activity [238].

Other authors also investigated the bacteriochlorin-based PDI-photosensitizers. For instance, Meerovich *et al.* have also studied the effect of cationic charges in the photosensitizer structure. It appeared that the investigated tetracationic photosensitizers, based on synthetic bacteriochlorins with reduced molecular size and molecular weight, were highly efficient in photodynamic inactivation of Gram-positive bacteria (*S. aureus*) and Gram-negative bacteria (*P. aeruginosa*) and against their biofilms [315]. The *E. coli* photoinactivation profile by cationic isobacteriochlorin described by Faustino *et al.* also proved that by using adequate PS, the PDI could be used in clinical applications. The results obtained for the series of modified isobacteriochlorins confirm that the trend of inactivation efficiency proceeds with the increasing number of cationic groups in the PS structure. The synergistic effect of red-shifted absorption and a positive charges in investigated isobacteriochlorin led to a 6 logs reduction and indicated that cationic isobacteriochlorins seem to be a promising agents for photodynamic inactivation of Gram-negative bacteria.

The future outlook of the treatment of resistant pathogens is the design and development of hybrid materials with multiple mechanisms of action. For these reasons, nanotechnology-based strategies in combination with PDI are more frequently explored [295,304,305]. Properly designed hybrid nanosystems may increase the affinity to microorganisms, enhanced ROS generation as well as are able to overcome the multidrug resistance mechanisms. The last one seems to be most important, due to the fact that the present time is named as the "end of the antibiotic era" [294]. This motivated a search for alternative antimicrobial strategies, including PDI to overcome multidrug-resistance mechanisms [294,302].

8. Other applications of bacteriochlorins beyond the medicine

8.1. Application of (metallo)bacteriochlorins conjugates as a light-harvesting antennas

The primary function of metallobacteriochlorins is to participate in the photosynthesis reactions consisting of, among others, the NIR photons absorption that leads to charge separation and efficient transformation of solar energy into chemical energy in the forms of sugars that later serve as fuel for leaving organisms. Therefore, an increasing number of studies are being conducted on the use of similar compounds as the potential light-harvesting antenna (LHA) models. LHA that captures light energy and then funnels excitation energy to the reaction center is very important for natural photosynthesis. Among the reported natural or artificial LHAs, porphyrins or their derivatives have been widely used as donors or acceptors. However, the absorption spectra of porphyrins cover only a limited portion of the visible region, which is a big barrier to light harvesting. The design of the bioinspired light-harvesting devices using well organized supramolecular arrays must be considered as one of the most promising system. The requirements for ideal supramolecular assemblies are *i.e.*, strong absorption, efficient solar energy storage and easily transferred without energy loss [316]. Metal-coordinated chromophores assemblies are widely studied for antenna systems due to their large molar absorption coefficients. In addition, metal ion coordination ensures a strong impact through ion interaction as well as through the formation of a hydrogen bond [316]. The construction is based on metallotetrapyrolles linked with free-base molecule by linker with different hindrances and in different positions, which provide changes in the HOMO-LUMO gap. Excellent energy transfer and weak electronic coupling may be obtained by using such a linker because the distance between linked chromophores as well as a hindrance is crucial to ensure efficient excitation and energy transfer.

In the systems containing Mg^{2+} or Zn^{2+} complexes as energy donors and free-base acceptor, the energy transfer process is characterized by short lifetime (τ~25–115 ps) and high quantum yield (Φ~95%) [317]. Another class of extensively studied artificial antennas is encompassed synthetic tetrapyrroles, likely zinc bacteriochlorin-bacteriochlorin (ZnBC-BC) complexes. Shoji, Nomura, and Tamiaki have investigated covalently linked heterodimers of porphyrin, chlorin, or bacteriochlorin with or without zinc ion [124]. They have also compared the axial ligation of Zn^{2+} in porphyrins, chlorins and bacteriochlorins, concluding that the more flexible and less π-conjugated bacteriochlorins bind axial pyridine stronger than the corresponding chlorins or porphyrins. They have reported several Zn^{2+} bacteriochlorins that, upon self-aggregation, exhibit significant red-shifts in their absorption spectra [318–320]. Based on naturally-occurring photosynthetic systems with a large number of excitonically coupled tetrapyrrolic arrays or strongly conjugated by a linker (double and triple C–C bonds) with faced model assembly were investigated [321] Fig. 40 [117,122,322].

Ptaszek with co-authors have found out that the dimer of chlorin (*cis*-2C), bacteriochlorin-chlorin (*cis*-2BC), and zinc-bacteriochlorin-chlorin (*cis*-2ZnC) linked *via* enediyne bond exhibited thermally stable isomers. The slipped co-facial arrangement of the macrocycles, in which the structure may be stabilized through space- and bond-interactions were studied [40]. Nevertheless, the computational of the trans arrangement along linkage double bond has no splitting. NMR spectra and DFT calculations predict the antiparallel arrangement of macrocycles. In addition, theoretical calculation confirms that the anti-parallel configuration of chromophores provides the lowest energy for cis configuration of the linking bridge. The introduction of Zn^{2+} into the system indicates strong excitonic coupling in contrast to the identical free-base supramolecular arrangement. The excited state of *cis*-2ZnC tends to decay with reduced fluorescence. Additionally, the dimers of the tetrapyrrolic core possess lower fluorescence quantum yield (Φ_F) compared to their monomers. This study shows that the geometry and spectral properties of the investigated dyad are similar to those observed in particular pairs involved in photosynthetic

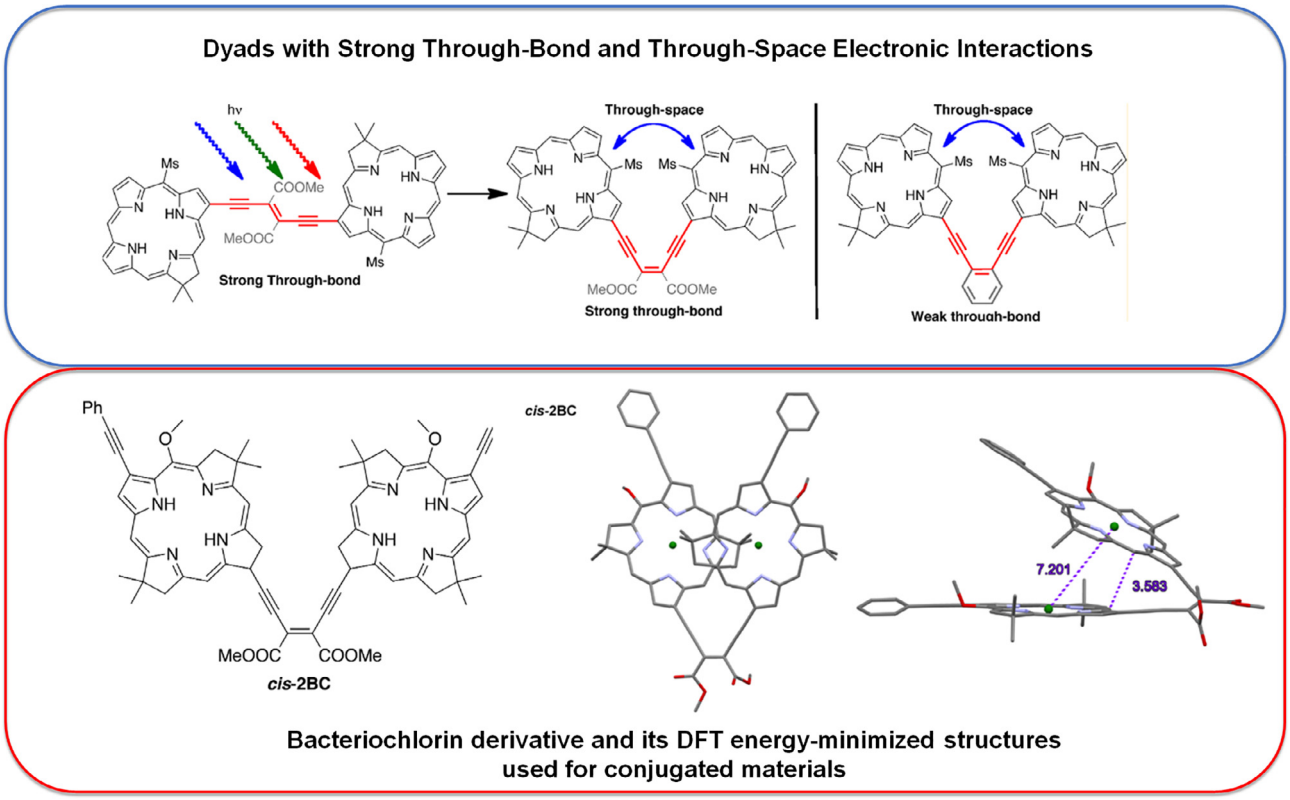

Fig. 40. Example of dyads composed of two identical bacteriochlorin derivatives with different linker (top panel); and *cis* isomers structures calculated with DFT level of theory approach (bottom panel). Adapted and modified from [321].

reaction centers [40]. Thus, they may be constructed components of energy and electron transfer for modeling the photosynthetic reaction pathway. In addition, the chromophores coupled with enediine connector, able to subsequent photoisomerization to trans-cis conjugates, seems to be useful elements for designing the energy conversion systems and photonic materials with new optical properties.

In the co-assembly model containing an aggregative zinc 3[1]-hydroxy-13[1]-oxo-chlorin and free-base bacteriochlorin with appropriate energy level, the covalently linked BChl heterodimer was arranged in chlorosomal chlorin J-aggregates. In particular, co-assemblies of porphyrin J-aggregates with heterodimers were first developed, and the J-aggregates with zinc-chlorin with bacteriochlorin (ZnC-B) or zinc-porphyrin with bacteriochlorin (ZnP-B) exhibited relatively higher intense emission than the free-base bacteriochlorin conjugated with chlorin. The Zn^{2+} complexes possess a particularly narrow HOMO-LUMO gap. Thus, the intramolecular photoinduced electron transfer processes to the nearest molecule can easily occur. Zinc-bacteriochlorin linked by the alkyne linker group with the sterically unhindered alkyne linker (strong interactions) attached in the different sites is characterized by a strongly reduced in the HOMO-LUMO gaps, and low tetrapyrrolic-linker rotational barriers, Fig. 41 [123,323].

In contrast, bulky aryl linkers have limited interaction between linked macrocycle resulting in increased HOMO-LUMO gap energy and higher ZnBC-linker rotational barriers. The design of supramolecular conjugates based on linker interaction is important for development of efficient light-harvesting arrays [324]. Computational studies of these systems are very feasible and can be helpful for further prediction of their application as a components of the antenna system. Okuno and Mashiko have proposed the mechanism of the interaction with different linkers and chromophores in porphyrin arrays. The comparison of excitation energy with rotational energy barrier for Zn-porphyrin shows strong dependence, in contrast to the free-base analog, in which the HOMO-LUMO energy gap is independent of π conjugation [324].

8.2. Application of bacteriochlorins as chemical sensors

It is commonly recognized that optical sensors relying on fluorescence detection indicate higher sensitivity than absorption-based ones. For fluorescent optical sensors with optimized performance and sensitivity, the use of a single-excitation and dual-emission fluorophore allows for ratiometric signal processing. It is essential to overcome some disadvantages (photobleaching, indicator leaching, light source intensity fluctuations, etc.) of single wavelength fluorescence intensity approaches. Suzuki, Tamiaki *et al.* have described the use of bacteriochlorin derivative as a fluorescent ratiometric optical, chemical sensor (optode) for alcohol detection [325]. In previous studies, the same authors reported the synthesis of a trifluoroacetylchlorin as the first example of a fluorescent probe for alcohols and amines using a chlorophyll derivative as the central dye unit.

Due to the fact that optical sensors with spectral sensitivity in the long-wavelength range are less prone to optical interference (light absorption, autofluorescence), the authors appllied a lipophilic derivative of 8-oxo-bacteriochlorin incorporated into a plasticized poly(vinyl chloride) membrane. With this fluorophore, sensitive and reversible ratiometric ethanol sensing in the NIR range with reversible signal changes was achieved. Immobilization of the fluorophore into a plastic membrane of the poly(vinyl chloride) dramatically change both, their absorption and emission properties. The blue-shifted of fluorescence from 750 nm to 701 nm in the presence of ethanol may be used as an ethanol sensing probe for beverage and industrial analyses [325].

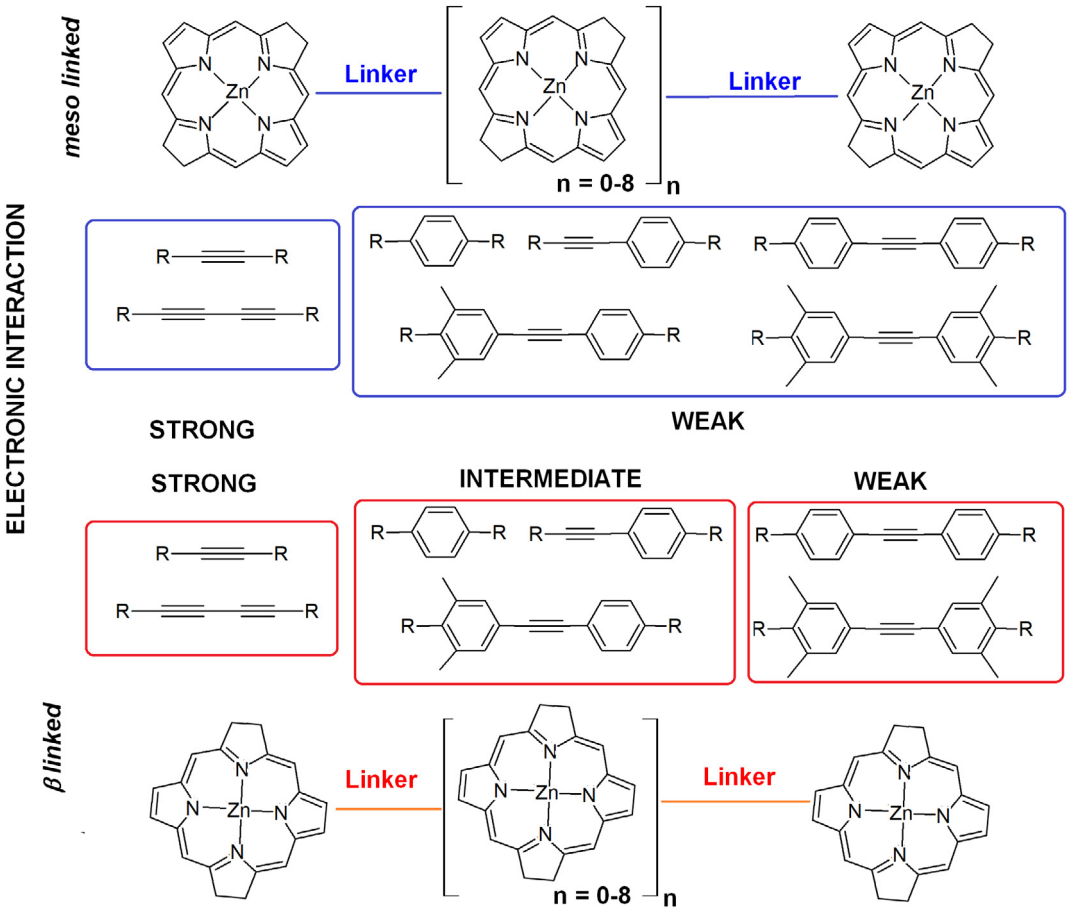

Fig. 41. Spatial-arrangement of Zn-bacteriochlorin oligomer with linker in *meso* and *β* positions and their different electronic interactions [40].

8.3. Bacteriochlorin based organic-solar cells for efficient energy conversion

Metal complexes with tetrapyrrolic ligands, due to appropriate excitation energy and high molar absorption coefficients in Vis/NIR, are particularly interesting in terms of their possible application in dye-sensitized solar cells (DSSC). The functioning of DSSCs depends on the efficiency of the electron injection from a photoexcited sensitizer molecule to the conduction band of the semiconductor, yielding mobile electrons and the oxidized dye. The electron injection and recombination of separated charges at the sensitizer-semiconductor interface are the crucial processes influencing the efficiency of solar energy conversion [326,327]. Metallotetrapyrroles, mainly with coordinated Zn^{2+}, were successfully used to sensitize TiO_2 in DSSC [328]. Due to the strong absorption within the green (*ca.* 500–550 nm) and NIR regions of spectra, the bacteriochlorin derivatives are indicated as versatile molecules for the construction of photovoltaic devices. So far, the most popular DSSCs are these containing ruthenium complexes adsorbed at the surface of nanocrystalline TiO_2 to collect photons up to 650 nm. However, their main limitation is the energy conversion efficiency of 11%. Extending the absorption to 800 nm could increase the maximum global solar radiation from 24% to 40%.

Organic solar cells are a prospective alternative for classical solar energy conversion into electrical energy due to the effective heterojunction of electrons in the active layer [329,330]. Among the several types of polymers or small molecules based on donor-acceptor, the conjugates with bacteriochlorin as a core with two electron-withdrawing terminal units linked by two π-linkers, are characterized by remarkable photovoltaic productivity. However, power conversion efficiency (PCE) of the OSCs depends on the strong absorption of the solar spectrum region and efficient electron transfer by the active layer. In this context, Ponsot and colleagues have designed a molecule based on the electro-donor central core of bacteriochlorin linked with two different electron-acceptors groups *via* π linker bridges for heterofunctional organic solar cells [330]. The use of small-molecule ligand as a complementary donor enables to increase of the efficacy of this binary system up to 9.88%, which is probably related to a deeper HOMO ligand energy level. In addition, the respective LUMO offset reaches only ~0.30 eV, which is very similar to the threshold value necessary for exciton dissociation and charge transfer in mass group substitution causes heterojunction to the active layer with minimal energy loss [330]. The authors indicated that the bacteriochlorin with a more extended π-system exhibits a narrow HOMO-LUMO energy gap, which is desirable properties for light-harvesting in the NIR region of the solar spectrum [330].

9. Summary and conclusions

Near-infrared (NIR) part of the electromagnetic radiation, despite its advantages, has been relatively poorly used in medicine, optoelectronics and photocatalysis due to the lack of thermally and photochemically stable chromophores, that strongly absorb electromagnetic radiation of this range. Bacteriochlorins are an exceptional example of NIR-absorbing compounds. They have been chosen by nature to conduct photosynthesis without the produc-

tion of oxygen in various phototropic bacteria. The reason for this selection is that these molecules efficiently absorb photons in the range of 700–900 nm and have appropriate redox properties. The best-known example of bacteriochlorin is bacteriochlorophyll *a*, a natural pigment structurally similar to chlorophyll *a*, but containing two reduced pyrrole rings. This is the main reason why its naturally occurring derivatives are characterized by reduced stability and high cost of production. Therefore, in recent years there has been an increased interest in obtaining rationally designed synthetic bacteriochlorins, with more favorable photochemical properties and increased stability. The absorption spectra of bacteriochlorins reveal an extraordinary high absorption in the infrared ($\varepsilon \sim 100{,}000\ M^{-1}cm^{-1}$), a very high absorption in the near UV, and relatively low absorption in the green part of the visible light. The stability of synthetic bacteriochlorins is assigned to the presence of desired metals ions, electron-withdrawing groups (*e.g.*, cyano, geminal dimethyl and halogen substituents) and steric protection. The presence of such substituents in the bacteriochlorin structure results in a marked increase in oxidation potentials and thus, in a lower tendency of these compounds to photodegradation. The proper control of oxidation potentials is also important for the determination of ROS generation mechanisms, and more precisely, for the engineering of photoinduced electron transfer and energy transfer processes.

The possibility of introducing various functional groups and metal ions into the bacteriochlorin core for fine-tuning of optical properties and polarity and the increased possibility to obtain large quantities of substantially pure metallobacteriochorins led to a wide range of practical applications. They are useful antennae systems for light-harvesting in the near-infrared (NIR) and are considered as effective agents in the photodynamic therapy (PDT) of cancer, photodynamic inactivation of microorganisms (PDI), *in vivo* oxygen imaging, fluorescent labeling of biomolecules, photodiagnosis (PD), solar energy conversion, optical sensing, and photocatalysis. The recent results from various scientific groups, including our, have shown that bacteriochlorins are promising compounds for PDT because they can use NIR radiation that deeply penetrates through the tissues and convert it very effectively to highly reactive oxygen species such as singlet oxygen, superoxide ion, hydrogen peroxide and hydroxyl radicals. *In vitro* studies with several families of (metallo)bacteriochlorins generally revealed their low cytotoxicity in the dark and high phototoxicity to various cancer cells. In a few independent studies, it was demonstrated that the photodynamic effect does not depend on the quantum yields of singlet oxygen formation, but it is strictly correlated with the production of oxygen-centered radicals. Bacteriochlorins that generate free radicals more efficiently lead to a more effective photodynamic effect than photosensitizers generating only singlet oxygen. The experiments performed on different animal models showed favorable pharmacokinetics, biodistribution and photodynamic efficacy. It was also demonstrated that the functionalization of bacteriochlorins may increase the effectiveness of the applied therapeutic protocols with polymeric micelles, lipoproteins, nanoparticles and metal-organic frameworks.

The best example of a bacteriochlorin containing metal ion, that has been successful in clinical trials, is Tookad Soluble (padeliporfin). After passing stage III and undergoing phase IV clinical trials, it is finally approved in the European Union and in Mexico for the treatment of low-risk early prostate cancer. Another bacteriochlorin-based photosensitizer discussed in this work, which is currently in Phase I/II of clinical trials, is redaporfin. Redaporfin is a photosensitizer from the family of halogenated bacteriochlorins that absorbs NIR photons efficiently and convert them into cytotoxic ROS. Its efficacy in the treatment of various types of tumors, including lung, colon, prostate, breast and melanoma has already been confirmed in preclinical tests. The promising results of Phase I/II clinical trials for the treatment of advanced head and neck cancer clearly reinforce the beneficial results of non-clinical studies. PDT with redaporfin as photosensitizer offers a number of advantages over existing anticancer regimes, such as improved efficacy, good tolerability, ease-of-use, and low-cost efficiency. Some of (metallo)bacteriochlorin described herein are also characterized by an intense fluoresce at 750–900 nm, where tissues are most transparent, and a large Stokes shift, offering opportunities for photodiagnosis and for their use as sensors. Needless to say, the development of NIR-absorbing materials for therapy and diagnosis may have a large impact on health care. Ongoing research in this area may lead not only to the use of novel compounds with increased performance in currently available treatments but also to the discovery of innovative therapeutic approaches.

Novel stable bacteriochlorins and their metal complexes are constantly and comprehensively characterized by advanced spectroscopic, photophysical, photochemical, electrochemical, and biochemical techniques. Hybrid materials obtained as a result of their combination with semiconductors and other nanostructures offer new interesting photochemical, photophysical, and redox properties. Smart control of these features is possible by the choice of proper metal, ligand modification, supramolecular architecture and anchored nanoparticles. Clearly, stable (metallo)bacteriochlorins have opened a new window to the NIR region of the electromagnetic spectrum, which has never before been so widely exploited in chemistry, biology, medicine and industry.

Declaration of Competing Interest

The authors declare that they have no known competing financial interests or personal relationships that could have appeared to influence the work reported in this paper.

Acknowledgments

This research was funded by the National Science Center (NCN), Poland, Sonata Bis grant number 2016/22/E/NZ7/00420 given to JMD. BP thanks Foundation for Polish Science for START 071.2019 program.

References

[1] A. Sakudo, Near-infrared spectroscopy for medical applications: current status and future perspectives, Clin. Chim. Acta 455 (2016) 181–188.
[2] R. Weissleder, V. Ntziachristos, Shedding light onto live molecular targets, Nat. Med. 9 (2003) 123.
[3] A.M. Smith, M.C. Mancini, S. Nie, Bioimaging: second window for in vivo imaging, Nat. Nanotechnol. 4 (2009) 710.
[4] X. Xia, N. Deng, G. Cui, J. Xie, X. Shi, Y. Zhao, Q. Wang, W. Wang, B. Tang, NIR light induced H 2 evolution by a metal-free photocatalyst, Chem. Commun. 51 (2015) 10899–10902.
[5] M.R. Hamblin, Shining light on the head: photobiomodulation for brain disorders, BBA Clin. 6 (2016) 113–124.
[6] J.V. Frangioni, In vivo near-infrared fluorescence imaging, Curr. Opin. Chem. Biol. 7 (2003) 626–634.
[7] S.A. Hilderbrand, R. Weissleder, Near-infrared fluorescence: application to in vivo molecular imaging, Curr. Opin. Chem. Biol. 14 (2010) 71–79.
[8] S. Luo, E. Zhang, Y. Su, T. Cheng, C. Shi, A review of NIR dyes in cancer targeting and imaging, Biomaterials 32 (2011) 7127–7138.
[9] B. Grimm, R.J. porra, W. Rüdiger, H. Scheer, Chlorophylls and Bacteriochlorophylls: Biochemistry, Biophysics, Functions and Applications, Springer Science & Business Media, 2007.
[10] Y. Tang, W. Di, X. Zhai, R. Yang, W. Qin, NIR-responsive photocatalytic activity and mechanism of NaYF4: Yb, Tm@ TiO2 core–shell nanoparticles, ACS Catal. 3 (2013) 405–412.
[11] M.O. Senge, K.R. Gerzevske, M.G.H. Vicente, T.P. Forsyth, K.M. Smith, Models for the photosynthetic reaction center—synthesis and structure of porphyrin dimers with cis-and trans-ethene and skewed hydroxymethylene bridges, Angew. Chem., Int. Ed. Engl. 32 (1993) 750–753.
[12] K. Kadish, K.M. Smith, R. Guilard, The Porphyrin Handbook, Elsevier, 2000.
[13] M. da, G.H. Vicente, K.M Smith, Syntheses and functionalizations of porphyrin macrocycles, Curr. Org. Synth. 11 (2014) 3–28.

[14] F. Giuntini, R. Boyle, M. Sibrian-Vazquez, M. Graça, H. Vicente, Porphyrin conjugates for cancer therapy, in: Handbook of Porphyrin Science (Volume 27) With Applications to Chemistry, Physics, Materials Science, Engineering, Biology and Medicine—Volume 27: Erythropoiesis, Heme and Applications to Biomedicine, World Scientific, 2014, pp. 303–416.

[15] N. Mochizuki, R. Tanaka, B. Grimm, T. Masuda, M. Moulin, A.G. Smith, A. Tanaka, M.J. Terry, The cell biology of tetrapyrroles: a life and death struggle, Trends Plant Sci. 15 (2010) 488–498.

[16] A.R. Battersby, Tetrapyrroles: the pigments of life, Nat. Prod. Rep. 17 (2000) 507–526.

[17] R. Luguya, L. Jaquinod, F.R. Fronczek, M.G.H. Vicente, K.M. Smith, Synthesis and reactions of meso-(p-nitrophenyl) porphyrins, Tetrahedron 60 (2004) 2757–2763.

[18] J.M. Dąbrowski, B. Pucelik, A. Regiel-Futyra, M. Brindell, O. Mazuryk, A. Kyzioł, G. Stochel, W. Macyk, L.G. Arnaut, Engineering of relevant photodynamic processes through structural modifications of metallotetrapyrrolic photosensitizers, Coord. Chem. Rev. 325 (2016) 67–101.

[19] M. Graça, H. Vicente, I.N. Rezzano, K.M. Smith, Efficient new syntheses of benzochlorins, benzoisobacteriochlorins, and benzobacteriochlorins, Tetrahedron Lett. 31 (1990) 1365–1368.

[20] M. Krayer, E. Yang, J.R. Diers, D.F. Bocian, D. Holten, J.S. Lindsey, De novo synthesis and photophysical characterization of annulated bacteriochlorins. Mimicking and extending the properties of bacteriochlorophylls, N. J. Chem. 35 (2011) 587–601.

[21] C.-Y. Chen, E. Sun, D. Fan, M. Taniguchi, B.E. McDowell, E. Yang, J.R. Diers, D.F. Bocian, D. Holten, J.S. Lindsey, Synthesis and physicochemical properties of metallobacteriochlorins, Inorg. Chem. 51 (2012) 9443–9464.

[22] M.M. Pereira, C.J. Monteiro, A.V. Simões, S.M. Pinto, A.R. Abreu, G.F. Sá, E.F. Silva, L.B. Rocha, J.M. Dąbrowski, S.J. Formosinho, Synthesis and photophysical characterization of a library of photostable halogenated bacteriochlorins: an access to near infrared chemistry, Tetrahedron 66 (2010) 9545–9551.

[23] S. Ikeda, M. Toganoh, S. Easwaramoorthi, J.M. Lim, D. Kim, H. Furuta, Synthesis and photophysical properties of N-fused tetraphenylporphyrin derivatives: near-infrared organic dye of [18] annulenic compounds, J. Org. Chem. 75 (2010) 8637–8649.

[24] N.K. Davis, A.L. Thompson, H.L. Anderson, A porphyrin fused to four anthracenes, J. Am. Chem. Soc. 133 (2010) 30–31.

[25] T. Goslinski, J. Piskorz, Fluorinated porphyrinoids and their biomedical applications, J. Photochem. Photobiol., C 12 (2011) 304–321.

[26] D.A. Tekdaş, U. Kumru, A.G. Gürek, M. Durmuş, V. Ahsen, F. Dumoulin, Towards near-infrared photosensitisation: a photosensitising hydrophilic non-peripherally octasulfanyl-substituted Zn phthalocyanine, Tetrahedron Lett. 53 (2012) 5227–5230.

[27] J.R. Stromberg, A. Marton, H.L. Kee, C. Kirmaier, J.R. Diers, C. Muthiah, M. Taniguchi, J.S. Lindsey, D.F. Bocian, G.J. Meyer, Examination of tethered porphyrin, chlorin, and bacteriochlorin molecules in mesoporous metal-oxide solar cells, J. Phys. Chem. C 111 (2007) 15464–15478.

[28] J.S. Lindsey, O. Mass, C.-Y. Chen, Tapping the near-infrared spectral region with bacteriochlorin arrays, New J. Chem. 35 (2011) 511–516.

[29] E. Yang, C. Kirmaier, M. Krayer, M. Taniguchi, H.-J. Kim, J.R. Diers, D.F. Bocian, J.S. Lindsey, D. Holten, Photophysical properties and electronic structure of stable, tunable synthetic bacteriochlorins: extending the features of native photosynthetic pigments, J. Phys. Chem. B 115 (2011) 10801–10816.

[30] B. Regan, M. Grätzel, Alow-cost, high-efficiency solar cell based on dye-sensitized colloidal TiO2 films, Nature 353 (1991) 737–739.

[31] C.G. Granqvist, M. Sedlaříková, J. Vondrák, Editorial| Solar Energy Materials and Solar Cells-Volume 90, Issue 4, North-Holland, 2006.

[32] T. Goslinski, E. Tykarska, W. Szczolko, T. Osmalek, A. Smigielska, S. Walorczyk, H. Zong, M. Gdaniec, B.M. Hoffman, J. Mielcarek, Synthesis and characterization of periphery-functionalized porphyrazines containing mixed pyrrolyl and pyridylmethylamino groups, J. Porphyrins Phthalocyanines 13 (2009) 223–234.

[33] T. Rębiś, M. Falkowski, M. Kryjewski, L. Popenda, L. Sobotta, S. Jurga, M.P. Marszall, J. Mielcarek, G. Milczarek, T. Goslinski, Single-walled carbon nanotube/sulfanyl porphyrazine hybrids deposited on glassy carbon electrode for sensitive determination of nitrites, Dyes Pigm. (2019) 107660.

[34] L. Jiao, J. Li, S. Zhang, C. Wei, E. Hao, M.G.H. Vicente, A selective fluorescent sensor for imaging Cu 2+ in living cells, New J. Chem. 33 (2009) 1888–1893.

[35] J. Jiang, A.J. Matula, J.R. Swierk, N. Romano, Y. Wu, V.S. Batista, R.H. Crabtree, J. S. Lindsey, H. Wang, G.W. Brudvig, Unusual stability of a bacteriochlorin electrocatalyst under reductive conditions. A case study on CO2 conversion to CO, ACS Catal. 8 (2018) 10131–10136.

[36] M. Ptaszek, H.L. Kee, C. Muthiah, R. Nothdurft, W. Akers, S. Achilefu, J.P. Culver, D. Holten, Near-infrared molecular imaging probes based on chlorin-bacteriochlorin dyads, reporters, markers, dyes, nanoparticles, and molecular probes for biomedical applications II, Int. Soc. Opt. Photon. (2010) 75760E.

[37] H.L. Kee, J.R. Diers, M. Ptaszek, C. Muthiah, D. Fan, J.S. Lindsey, D.F. Bocian, D. Holten, Chlorin-bacteriochlorin energy-transfer dyads as prototypes for near-infrared molecular imaging probes: controlling charge-transfer and fluorescence properties in polar media, Photochem. Photobiol. 85 (2009) 909–920.

[38] H.L. Kee, R. Nothdurft, C. Muthiah, J.R. Diers, D. Fan, M. Ptaszek, D.F. Bocian, J. S. Lindsey, J.P. Culver, D. Holten, Examination of chlorin-bacteriochlorin energy-transfer dyads as prototypes for near-infrared molecular imaging probes, Photochem. Photobiol. 84 (2008) 1061–1072.

[39] M. Ethirajan, Y. Chen, P. Joshi, R.K. Pandey, The role of porphyrin chemistry in tumor imaging and photodynamic therapy, Chem. Soc. Rev. 40 (2011) 340–362.

[40] A. Meares, Z. Yu, G. Viswanathan Bhagavathy, A. Satraitis, M. Ptaszek, Photoisomerization of enediynyl linker leads to slipped co-facial hydroporphyrin dimers with strong through-bond and through-space electronic interactions, J. Org. Chem. (2019).

[41] E. Yang, J. Wang, J.R. Diers, D.M. Niedzwiedzki, C. Kirmaier, D.F. Bocian, J.S. Lindsey, D. Holten, Probing electronic communication for efficient light-harvesting functionality: dyads containing a common perylene and a porphyrin, chlorin, or bacteriochlorin, J. Phys. Chem. B 118 (2014) 1630–1647.

[42] Y. Chen, G. Li, R.K. Pandey, Synthesis of bacteriochlorins and their potential utility in photodynamic therapy (PDT), Curr. Org. Chem. 8 (2004) 1105–1134.

[43] J.M. Dąbrowski, L.G. Arnaut, Photodynamic therapy (PDT) of cancer: from local to systemic treatment, Photochem. Photobiol. Sci. 14 (2015) 1765–1780.

[44] C.H. Foyer, Reactive oxygen species, oxidative signaling and the regulation of photosynthesis, Environ. Exp. Bot. 154 (2018) 134–142.

[45] B.A. Logan, 10 Reactive oxygen species and photosynthesis, Antioxid. React. Oxygen Spec. Plants (2008) 250.

[46] C. Woehle, T. Dagan, G. Landan, A. Vardi, S. Rosenwasser, Expansion of the redox-sensitive proteome coincides with the plastid endosymbiosis, Nat. Plants 3 (2017) 17066.

[47] D. Frackowiak, The jablonski diagram, J. Photochem. Photobiol., B 2 (1988) 399.

[48] J. Kuncewicz, J.M. Dąbrowski, A. Kyzioł, M. Brindell, P. Łabuz, O. Mazuryk, W. Macyk, G. Stochel, Perspectives of molecular and nanostructured systems with d-and f-block metals in photogeneration of reactive oxygen species for medical strategies, Coord. Chem. Rev. 398 (2019) 113012.

[49] P. Agostinis, K. Berg, K.A. Cengel, T.H. Foster, A.W. Girotti, S.O. Gollnick, S.M. Hahn, M.R. Hamblin, A. Juzeniene, D. Kessel, Photodynamic therapy of cancer: an update, CA Cancer J. Clin. 61 (2011) 250–281.

[50] M. Garcia-Diaz, Y.-Y. Huang, M.R. Hamblin, Use of fluorescent probes for ROS to tease apart Type I and Type II photochemical pathways in photodynamic therapy, Methods 109 (2016) 158–166.

[51] E.F. Silva, C. Serpa, J.M. Dąbrowski, C.J. Monteiro, S.J. Formosinho, G. Stochel, K. Urbanska, S. Simões, M.M. Pereira, L.G. Arnaut, Mechanisms of singlet-oxygen and superoxide-ion generation by porphyrins and bacteriochlorins and their implications in photodynamic therapy, Chem. Eur. J. 16 (2010) 9273–9286.

[52] C.S. Foote, Definition of type I and type II photosensitized oxidation, Photochem. Photobiol. 54 (1991) 659.

[53] J.M. Dąbrowski, Reactive oxygen species in photodynamic therapy: mechanisms of their generation and potentiation, Adv. Inorg. Chem. Elsevier (2017) 343–394.

[54] L.G. Arnaut, M.M. Pereira, J.M. Dąbrowski, E.F. Silva, F.A. Schaberle, A.R. Abreu, L.B. Rocha, M.M. Barsan, K. Urbańska, G. Stochel, Photodynamic therapy efficacy enhanced by dynamics: the role of charge transfer and photostability in the selection of photosensitizers, Chem. Eur. J. 20 (2014) 5346–5357.

[55] J.M. Dąbrowski, L.G. Arnaut, M.M. Pereira, K. Urbanska, S. Simoes, G. Stochel, L. Cortes, Combined effects of singlet oxygen and hydroxyl radical in photodynamic therapy with photostable bacteriochlorins: Evidence from intracellular fluorescence and increased photodynamic efficacy in vitro, Free Radic. Biol. Med. 52 (2012) 1188–1200.

[56] M. Oszajca, M. Brindell, Ł. Orzeł, J.M. Dąbrowski, K. Śpiewak, P. Łabuz, M. Pacia, A. Stochel-Gaudyn, W. Macyk, R. van Eldik, Mechanistic studies on versatile metal-assisted hydrogen peroxide activation processes for biomedical and environmental incentives, Coord. Chem. Rev. 327 (2016) 143–165.

[57] R.R. Allison, K. Moghissi, Photodynamic therapy (PDT): PDT mechanisms, Clin. Endoscopy 46 (2013) 24.

[58] A.P. Castano, T.N. Demidova, M.R. Hamblin, Mechanisms in photodynamic therapy: part one—photosensitizers, photochemistry and cellular localization, Photodiagn. Photodyn. Ther. 1 (2004) 279–293.

[59] L. Huang, Y. Xuan, Y. Koide, T. Zhiyentayev, M. Tanaka, M.R. Hamblin, Type I and Type II mechanisms of antimicrobial photodynamic therapy: an in vitro study on gram-negative and gram-positive bacteria, Lasers Surg. Med. 44 (2012) 490–499.

[60] I.O. Bacellar, T.M. Tsubone, C. Pavani, M.S. Baptista, Photodynamic efficiency: from molecular photochemistry to cell death, Int. J. Mol. Sci. 16 (2015) 20523–20559.

[61] M.S. Baptista, J. Cadet, P. Di Mascio, A.A. Ghogare, A. Greer, M.R. Hamblin, C. Lorente, S.C. Nunez, M.S. Ribeiro, A.H. Thomas, Type I and type II photosensitized oxidation reactions: guidelines and mechanistic pathways, Photochem. Photobiol. 93 (2017) 912–919.

[62] M.L. Circu, T.Y. Aw, Reactive oxygen species, cellular redox systems, and apoptosis, Free Radical Biol. Med. 48 (2010) 749–762.

[63] T. Finkel, Signal transduction by reactive oxygen species, J. Cell Biol. 194 (2011) 7–15.

[64] V.J. Thannickal, B.L. Fanburg, Reactive oxygen species in cell signaling, Am. J. Physiol. Lung Cell. Mol. Physiol. 279 (2000) L1005–L1028.

[65] Z. Zhou, J. Song, L. Nie, X. Chen, Reactive oxygen species generating systems meeting challenges of photodynamic cancer therapy, Chem. Soc. Rev. 45 (2016) 6597–6626.

[66] M. Chen, M. Schliep, R.D. Willows, Z.-L. Cai, B.A. Neilan, H. Scheer, A red-shifted chlorophyll, Science 329 (2010) 1318–1319.

[67] H. Scheer, Structure and occurence of chlorophylls, (1991).
[68] Y. Saga, K. Hirota, H. Asakawa, K. Takao, T. Fukuma, Reversible changes in the structural features of photosynthetic light-harvesting complex 2 by removal and reconstitution of B800 bacteriochlorophyll a pigments, Biochemistry 56 (2017) 3484–3491.
[69] Y. Tsukatani, Y. Hirose, J. Harada, N. Misawa, K. Mori, K. Inoue, H. Tamiaki, Complete genome sequence of the bacteriochlorophyll b-producing photosynthetic bacterium Blastochloris viridis, Genome Announc. 3 (2015) e01006–e1015.
[70] H. Scheer, G. Hartwich, Bacterial Reaction Centers with Modified Tetrapyrrole Chromophores, Anoxygenic Photosynthetic Bacteria, Springer, 1995, pp. 649–663.
[71] G. Hartwich, L. Fiedor, I. Simonin, E. Cmiel, W. Schäfer, D. Noy, A. Scherz, H. Scheer, Metal-substituted bacteriochlorophylls. 1. Preparation and influence of metal and coordination on spectra, J. Am. Chem. Soc. 120 (1998) 3675–3683.
[72] J. Fiedor, L. Fiedor, N. Kammhuber, A. Scherz, H. Scheer, Photodynamics of the bacteriochlorophyll-carotenoid system. 2. Influence of central metal, solvent and β-carotene on photobleaching of bacteriochlorophyll derivatives, Photochem. Photobiol. 76 (2002) 145–152.
[73] Y. Tsukatani, J. Harada, T. Mizoguchi, H. Tamiaki, Bacteriochlorophyll homolog compositions in the bchU mutants of green sulfur bacteria, Photochem. Photobiol. Sci. 12 (2013) 2195–2201.
[74] A. Oren, Characterization of pigments of prokaryotes and their use in taxonomy and classification, Methods Microbiol. Elsevier (2011) 261–282.
[75] Ł. Orzeł, A. Kania, D. Rutkowska-Zbik, A. Susz, G. Stochel, L. Fiedor, Structural and electronic effects in the metalation of porphyrinoids. Theory and experiment, Inorg. Chem. 49 (2010) 7362–7371.
[76] A.N. Kozyrev, Y. Chen, L.N. Goswami, W.A. Tabaczynski, R.K. Pandey, Characterization of porphyrins, chlorins, and bacteriochlorins formed via allomerization of bacteriochlorophyll a. Synthesis of highly stable bacteriopurpurinimides and their metal complexes, J. Org. Chem. 71 (2006) 1949–1960.
[77] M. Galezowski, D.T. Gryko, Recent advances in the synthesis of hydroporphyrins, Curr. Org. Chem. 11 (2007) 1310–1338.
[78] M.A. Grin, A.F. Mironov, A.A. Shtil, Bacteriochlorophyll a and its derivatives: Chemistry and perspectives for cancer therapy, Anti-Cancer Agents Med. Chem. (Formerly Current Medicinal Chemistry-Anti-Cancer Agents) 8 (2008) 683–697.
[79] D. Holten, D.F. Bocian, J.S. Lindsey, Probing electronic communication in covalently linked multiporphyrin arrays. A guide to the rational design of molecular photonic devices, Acc. Chem. Res. 35 (2002) 57–69.
[80] A. Osuka, S. Saito, Expanded porphyrins and aromaticity, Chem. Commun. 47 (2011) 4330–4339.
[81] A.S. Brandis, Y. Salomon, A. Scherz, Bacteriochlorophyll Sensitizers in Photodynamic Therapy, Chlorophylls and Bacteriochlorophylls, Springer, 2006, pp. 485–494.
[82] S. Fukuzumi, K. Ohkubo, X. Zheng, Y. Chen, R.K. Pandey, R. Zhan, K.M. Kadish, Metal bacteriochlorins which act as dual singlet oxygen and superoxide generators, J. Phys. Chem. B 112 (2008) 2738–2746.
[83] P. Vairaprakash, E. Yang, T. Sahin, M. Taniguchi, M. Krayer, J.R. Diers, A. Wang, D.M. Niedzwiedzki, C. Kirmaier, J.S. Lindsey, Extending the short and long wavelength limits of bacteriochlorin near-infrared absorption via dioxo-and bisimide-functionalization, J. Phys. Chem. B 119 (2015) 4382–4395.
[84] G. At, M. Tsvirko, Probabilities of intercombination transitions in porphyrin and metalloporphyrin molecules, Opt. Spectroscopy-USSR 31 (1971) 291–1000.
[85] D. Eastwood, M. Gouterman, Porphyrins: XII. Luminescence of copper complexes at liquid nitrogen temperature, J. Mol. Spectrosc. 30 (1969) 437–458.
[86] D. Eastwood, M. Gouterman, Porphyrins: Xviii. luminescence of (co),(ni), pd, pt complexes, J. Mol. Spectrosc. 35 (1970) 359–375.
[87] H. Scheer, An Overview of Chlorophylls and Bacteriochlorophylls: Biochemistry, Biophysics, Functions and Applications, Chlorophylls and Bacteriochlorophylls, Springer, 2006, pp. 1–26.
[88] D. Noy, L. Fiedor, G. Hartwich, H. Scheer, A. Scherz, Metal-substituted bacteriochlorophylls. 2. Changes in redox potentials and electronic transition energies are dominated by intramolecular electrostatic interactions, J. Am. Chem. Soc. 120 (1998) 3684–3693.
[89] K. Teuchner, H. Stiel, D. Leupold, I. Katheder, H. Scheer, From chlorophyll a towards bacteriochlorophyll a: excited-state processes of modified pigments, J. Lumin. 60 (1994) 520–522.
[90] L. Fiedor, A. Kania, B. Myśliwa-Kurdziel, Ł. Orzeł, G. Stochel, Understanding chlorophylls: central magnesium ion and phytyl as structural determinants, Biochim. Biophys. Acta 1777 (2008) 1491–1500.
[91] A. Drzewiecka-Matuszek, A. Skalna, A. Karocki, G. Stochel, L. Fiedor, Effects of heavy central metal on the ground and excited states of chlorophyll, J. Biol. Inorg. Chem. 10 (2005) 453–462.
[92] D. Zigmantas, E.L. Read, T. Mančal, T. Brixner, A.T. Gardiner, R.J. Cogdell, G.R. Fleming, Two-dimensional electronic spectroscopy of the B800–B820 light-harvesting complex, Proc. Natl. Acad. Sci. 103 (2006) 12672–12677.
[93] G.S. Schlau-Cohen, E. De Re, R.J. Cogdell, G.R. Fleming, Determination of excited-state energies and dynamics in the B band of the bacterial reaction center with 2D electronic spectroscopy, J. Phys. Chem. Lett. 3 (2012) 2487–2492.
[94] A. Konar, R. Sechrist, Y. Song, V.R. Policht, P.D. Laible, D.F. Bocian, D. Holten, C. Kirmaier, J.P. Ogilvie, Electronic interactions in the bacterial reaction center revealed by two-color 2D electronic spectroscopy, J. Phys. Chem. Lett. 9 (2018) 5219–5225.
[95] N.S. Ginsberg, Y.-C. Cheng, G.R. Fleming, Two-dimensional electronic spectroscopy of molecular aggregates, Acc. Chem. Res. 42 (2009) 1352–1363.
[96] M.J. Guberman-Pfeffer, R.F. Lalisse, N. Hewage, C. Brückner, J.A. Gascón, Origins of the electronic modulations of bacterio-and isobacteriodilactone regioisomers, J. Phys. Chem. A 123 (2019) 7470–7485.
[97] D. Rutkowska-Zbik, M. Witko, Metallobacteriochlorophylls as potential dual agents for photodynamic therapy and chemotherapy, J. Mol. Model. 19 (2013) 4155–4161.
[98] Y. Chen, A. Graham, W. Potter, J. Morgan, L. Vaughan, D.A. Bellnier, B.W. Henderson, A. Oseroff, T.J. Dougherty, R.K. Pandey, Bacteriopurpurinimides: highly stable and potent photosensitizers for photodynamic therapy, J. Med. Chem. 45 (2002) 255–258.
[99] Y. Chen, W.R. Potter, J.R. Missert, J. Morgan, R.K. Pandey, Comparative in vitro and in vivo studies on long-wavelength photosensitizers derived from bacteriopurpurinimide and bacteriochlorin p6: fused imide ring enhances the in vivo PDT efficacy, Bioconjug. Chem. 18 (2007) 1460–1473.
[100] A. Kozyrev, M. Ethirajan, P. Chen, K. Ohkubo, B.C. Robinson, K.M. Barkigia, S. Fukuzumi, K.M. Kadish, R.K. Pandey, Synthesis, photophysical and electrochemistry of near-IR absorbing bacteriochlorins related to bacteriochlorophyll a, J. Org. Chem. 77 (2012) 10260–10271.
[101] C. Saenz, R.R. Cheruku, T.Y. Ohulchanskyy, P. Joshi, W.A. Tabaczynski, J.R. Missert, Y. Chen, P. Pera, E. Tracy, A. Marko, Structural and epimeric isomers of HPPH [3-devinyl 3-{1-(1-hexyloxy) ethyl} pyropheophorbide-a]: effects on uptake and photodynamic therapy of cancer, ACS Chem. Biol. 12 (2017) 933–946.
[102] K. Ohkubo, H. Imahori, J. Shao, Z. Ou, K.M. Kadish, Y. Chen, G. Zheng, R.K. Pandey, M. Fujitsuka, O. Ito, Small reorganization energy of intramolecular electron transfer in fullerene-based dyads with short linkage, J. Phys. Chem. A 106 (2002) 10991–10998.
[103] S. Fukuzumi, K. Ohkubo, Y. Chen, R.K. Pandey, R. Zhan, J. Shao, K.M. Kadish, Photophysical and electrochemical properties of new bacteriochlorins and characterization of radical cation and radical anion species, J. Phys. Chem. A 106 (2002) 5105–5113.
[104] A. Rosenfeld, J. Morgan, L.N. Goswami, T. Ohulchanskyy, X. Zheng, P.N. Prasad, A. Oseroff, R.K. Pandey, Photosensitizers derived from 132-oxo-methyl pyropheophorbide-a: enhanced effect of indium (III) as a central metal in in vitro and in vivo photosensitizing efficacy, Photochem. Photobiol. 82 (2006) 626–634.
[105] I. Ashur, R. Goldschmidt, I. Pinkas, Y. Salomon, G. Szewczyk, T. Sarna, A. Scherz, Photocatalytic generation of oxygen radicals by the water-soluble bacteriochlorophyll derivative WST11, noncovalently bound to serum albumin, J. Phys. Chem. A 113 (2009) 8027–8037.
[106] C. Brückner, L. Samankumara, J. Ogikubo, Syntheses of bacteriochlorins and isobacteriochlorins, Handbook Porphyrin Sci. 17 (2012) 1–112.
[107] S. Schreiber, S. Gross, A. Brandis, A. Harmelin, V. Rosenbach-Belkin, A. Scherz, Y. Salomon, Local photodynamic therapy (PDT) of rat C6 glioma xenografts with Pd-bacteriopheophorbide leads to decreased metastases and increase of animal cure compared with surgery, Int. J. Cancer 99 (2002) 279–285.
[108] A. Brandis, O. Mazor, E. Neumark, V. Rosenbach-Belkin, Y. Salomon, A. Scherz, Novel water-soluble bacteriochlorophyll derivatives for vascular-targeted photodynamic therapy: synthesis, solubility, phototoxicity and the effect of serum proteins, Photochem. Photobiol. 81 (2005) 983–992.
[109] N.V. Koudinova, J.H. Pinthus, A. Brandis, O. Brenner, P. Bendel, J. Ramon, Z. Eshhar, A. Scherz, Y. Salomon, Photodynamic therapy with Pd-bacteriopheophorbide (TOOKAD): successful in vivo treatment of human prostatic small cell carcinoma xenografts, Int. J. Cancer 104 (2003) 782–789.
[110] O. Mazor, A. Brandis, V. Plaks, E. Neumark, V. Rosenbach-Belkin, Y. Salomon, A. Scherz, WST11, a novel water-soluble bacteriochlorophyll derivative; cellular uptake, pharmacokinetics, biodistribution and vascular-targeted photodynamic activity using melanoma tumors as a model, Photochem. Photobiol. 81 (2005) 342–351.
[111] Y. Vakrat-Haglili, L. Weiner, V. Brumfeld, A. Brandis, Y. Salomon, B. Mcllroy, B. C. Wilson, A. Pawlak, M. Rozanowska, T. Sarna, The microenvironment effect on the generation of reactive oxygen species by Pd-bacteriopheophorbide, J. Am. Chem. Soc. 127 (2005) 6487–6497.
[112] M. Kobayashi, E.J. van de Meent, C. Erkelens, J. Amesz, I. Ikegami, T. Watanabe, Bacteriochlorophyll g epimer as a possible reaction center component of heliobacteria, Biochim. Biophys. Acta 1057 (1991) 89–96.
[113] H. Tamiaki, S. Yagai, T. Miyatake, Synthetic zinc tetrapyrroles complexing with pyridine as a single axial ligand, Bioorg. Med. Chem. 6 (1998) 2171–2178.
[114] A. Osuka, S. Nakajima, K. Maruyama, N. Mataga, T. Asahi, I. Yamazaki, Y. Nishimura, T. Ohno, K. Nozaki, 1, 2-Phenylene-bridged diporphyrin linked with porphyrin monomer and pyromellitimide as a model for a photosynthetic reaction center: synthesis and photoinduced charge separation, J. Am. Chem. Soc. 115 (1993) 4577–4589.
[115] M.R. Wasielewski, M.P. Niemczyk, Photoinduced electron transfer in meso-triphenyltriptycenylporphyrin-quinones. Restricting donor-acceptor distances and orientations, J. Am. Chem. Soc. 106 (1984) 5043–5045.
[116] H. Tamiaki, M. Amakawa, Y. Shimono, R. Tanikaga, A.R. Holzwarth, K. Schaffner, Synthetic zinc and magnesium chlorin aggregates as models for

supramolecular antenna complexes in chlorosomes of green photosynthetic bacteria, Photochem. Photobiol. 63 (1996) 92–99.
[117] H. Tamiaki, T. Miyatake, R. Tanikaga, A.R. Holzwarth, K. Schaffner, Self-assembly of an artificial light-harvesting antenna: energy transfer from a zinc chlorin to a bacteriochlorin in a supramolecular aggregate, Angew. Chem., Int. Ed. Engl. 35 (1996) 772–774.
[118] N. Wakao, N. Yokoi, N. Isoyama, A. Hiraishi, K. Shimada, M. Kobayashi, H. Kise, M. Iwaki, S. Itoh, S. Takaichi, Discovery of natural photosynthesis using Zn-containing bacteriochlorophyll in an aerobic bacterium Acidiphilium rubrum, Plant Cell Physiol. 37 (1996) 889–893.
[119] T. Tomi, Y. Shibata, Y. Ikeda, S. Taniguchi, C. Haik, N. Mataga, K. Shimada, S. Itoh, Energy and electron transfer in the photosynthetic reaction center complex of Acidiphilium rubrum containing Zn-bacteriochlorophyll a studied by femtosecond up-conversion spectroscopy, Biochim. Biophys. Acta 1767 (2007) 22–30.
[120] R. Guilard, K.M. Kadish, K.M. Smith, R. Guilard, The Porphyrin Handbook, Academic Press, New York, 2003.
[121] T. Miyatake, H. Tamiaki, A.R. Holzwarth, K. Schaffner, Artificial light-harvesting antennae: Singlet excitation energy transfer from zinc chlorin aggregate to bacteriochlorin in homogeneous hexane solution, Photochem. Photobiol. 69 (1999) 448–456.
[122] H. Tamiaki, Self-aggregates of natural and modified chlorophylls as photosynthetic light-harvesting antenna systems: substituent effect on the B-ring, Photochem. Photobiol. Sci. 4 (2005) 675–680.
[123] H. Tamiaki, K. Nishihara, R. Shibata, Synthesis of self-aggregative zinc chlorophylls possessing polymerizable esters as a atable model compound for main light-harvesting antennas of green photosynthetic bacteria, Int. J. Photoenergy 2006 (2006).
[124] H. Tamiaki, K. Fukai, H. Shimazu, S. Shoji, Synthesis of zinc chlorophyll homo/hetero-dyads and their folded conformers with porphyrin, chlorin, and bacteriochlorin π-systems, Photochem. Photobiol. 90 (2014) 121–128.
[125] G.K. Lahiri, A.M. Stolzenberg, F430 model chemistry. evidence for alkyl-and hydrido-nickel intermediates in the reactions of the nickel (I) octaethylisobacteriochlorin anion, Inorg. Chem. 32 (1993) 4409–4413.
[126] A.M. Stolzenberg, L.J. Schussel, J.S. Summers, B.M. Foxman, J.L. Petersen, Structures of the homologous series of square-planar metallotetrapyrroles palladium (II) octaethylporphyrin, palladium (II) trans-octaethylchlorin, and palladium (II) tct-octaethylisobacteriochlorin, Inorg. Chem. 31 (1992) 1678–1686.
[127] A.M. Stolzenberg, L.J. Schussel, Synthesis, characterization, and electrochemistry of copper (II) and palladium (II) hydroporphyrins: the copper (I) octaethylisobacteriochlorin anion, Inorg. Chem. 30 (1991) 3205–3213.
[128] L. Fiedor, D. Leupold, K. Teuchner, B. Voigt, C.N. Hunter, A. Scherz, H. Scheer, Excitation trap approach to analyze size and pigment−pigment coupling: reconstitution of LH1 antenna of rhodobacter sphaeroides with Ni-substituted bacteriochlorophyll, Biochemistry 40 (2001) 3737–3747.
[129] E. Yang, J.R. Diers, Y.Y. Huang, M.R. Hamblin, J.S. Lindsey, D.F. Bocian, D. Holten, Molecular electronic tuning of photosensitizers to enhance photodynamic therapy: synthetic dicyanobacteriochlorins as a case study, Photochem. Photobiol. 89 (2013) 605–618.
[130] P. Mroz, J. Bhaumik, D.K. Dogutan, Z. Aly, Z. Kamal, L. Khalid, H.L. Kee, D.F. Bocian, D. Holten, J.S. Lindsey, Imidazole metalloporphyrins as photosensitizers for photodynamic therapy: role of molecular charge, central metal and hydroxyl radical production, Cancer Lett. 282 (2009) 63–76.
[131] L.G. Arnaut, Design of porphyrin-based photosensitizers for photodynamic therapy, Adv. Inorg. Chem. Elsevier (2011) 187–233.
[132] P. Mroz, A. Yaroslavsky, G.B. Kharkwal, M.R. Hamblin, Cell death pathways in photodynamic therapy of cancer, Cancers 3 (2011) 2516–2539.
[133] Y. Posen, V. Kalchenko, R. Seger, A. Brandis, A. Scherz, Y. Salomon, Manipulation of redox signaling in mammalian cells enabled by controlled photogeneration of reactive oxygen species, J. Cell Sci. 118 (2005) 1957–1969.
[134] J.W. Springer, K.M. Faries, J.R. Diers, C. Muthiah, O. Mass, H.L. Kee, C. Kirmaier, J.S. Lindsey, D.F. Bocian, D. Holten, Effects of substituents on synthetic analogs of chlorophylls. Part 3: the distinctive impact of auxochromes at the 7-versus 3-positions, Photochem. Photobiol. 88 (2012) 651–674.
[135] H.L. Kee, C. Kirmaier, Q. Tang, J.R. Diers, C. Muthiah, M. Taniguchi, J.K. Laha, M. Ptaszek, J.S. Lindsey, D.F. Bocian, Effects of substituents on synthetic analogs of chlorophylls. Part 1: synthesis, vibrational properties and excited-state decay characteristics, Photochem. Photobiol. 83 (2007) 1110–1124.
[136] H.L. Kee, C. Kirmaier, Q. Tang, J.R. Diers, C. Muthiah, M. Taniguchi, J.K. Laha, M. Ptaszek, J.S. Lindsey, D.F. Bocian, Effects of substituents on synthetic analogs of chlorophylls. Part 2: redox properties, optical spectra and electronic structure, Photochem. Photobiol. 83 (2007) 1125–1143.
[137] O. Mass, M. Taniguchi, M. Ptaszek, J.W. Springer, K.M. Faries, J.R. Diers, D.F. Bocian, D. Holten, J.S. Lindsey, Structural characteristics that make chlorophylls green: interplay of hydrocarbon skeleton and substituents, New J. Chem. 35 (2011) 76–88.
[138] L. Petit, C. Adamo, N. Russo, Absorption spectra of first-row transition metal complexes of bacteriochlorins: a theoretical analysis, J. Phys. Chem. B 109 (2005) 12214–12221.
[139] M.J. Guberman-Pfeffer, J.A. Greco, L.P. Samankumara, M. Zeller, R.R. Birge, J.A. Gascón, C. Brückner, Bacteriochlorins with a twist: discovery of a unique mechanism to red-shift the optical spectra of bacteriochlorins, J. Am. Chem. Soc. 139 (2016) 548–560.
[140] A.V. Simoes, A. Adamowicz, J.M. Dąbrowski, M.J. Calvete, A.R. Abreu, G. Stochel, L.G. Arnaut, M.M. Pereira, Amphiphilic meso (sulfonate ester fluoroaryl) porphyrins: refining the substituents of porphyrin derivatives for phototherapy and diagnostics, Tetrahedron 68 (2012) 8767–8772.
[141] S.M. Pinto, C.A. Henriques, V.A. Tome, C.S. Vinagreiro, M.J. Calvete, J.M. Dąbrowski, M. Pineiro, L.G. Arnaut, M.M. Pereira, Synthesis of meso-substituted porphyrins using sustainable chemical processes, J. Porphyrins Phthalocyanines 20 (2016) 45–60.
[142] M.M. Pereira, C.J. Monteiro, A.V. Simões, S.M. Pinto, L.G. Arnaut, G.F. Sá, E.F. Silva, L.B. Rocha, S. Simões, S.J. Formosinho, Synthesis and photophysical properties of amphiphilic halogenated bacteriochlorins: new opportunities for photodynamic therapy of cancer, J. Porphyrins Phthalocyanines 13 (2009) 567–573.
[143] M.M. Pereira, A.R. Abreu, N.P. Goncalves, M.J. Calvete, A.V. Simões, C.J. Monteiro, L.G. Arnaut, M.E. Eusebio, J. Canotilho, An insight into solvent-free diimide porphyrin reduction: a versatile approach for meso-aryl hydroporphyrin synthesis, Green Chem. 14 (2012) 1666–1672.
[144] J.M. Dąbrowski, M.M. Pereira, L.G. Arnaut, C.J. Monteiro, A.F. Peixoto, A. Karocki, K. Urbańska, G. Stochel, Synthesis, photophysical studies and anticancer activity of a new halogenated water-soluble porphyrin, Photochem. Photobiol. 83 (2007) 897–903.
[145] J.M. Dąbrowski, L.G. Arnaut, M.M. Pereira, C.J. Monteiro, K. Urbańska, S. Simões, G. Stochel, New halogenated water-soluble chlorin and bacteriochlorin as photostable PDT sensitizers: synthesis, spectroscopy, photophysics, and in vitro photosensitizing efficacy, ChemMedChem 5 (2010) 1770–1780.
[146] M. Gouterman, Optical spectra and electronic structure of porphyrins and related rings, The Porphyrins 3 (1978).
[147] M. Gouterman, Study of the effects of substitution on the absorption spectra of porphin, J. Chem. Phys. 30 (1959) 1139–1161.
[148] C. Chang, L. Hanson, P. Richardson, R. Young, J. Fajer, π cation radicals of ferrous and free base isobacteriochlorins: models for siroheme and sirohydrochlorin, Proc. Natl. Acad. Sci. 78 (1981) 2652–2656.
[149] S.L. Murov, I. Carmichael, G.L. Hug, Handbook of Photochemistry, CRC Press, 1993.
[150] A.L. Gryshuk, A. Graham, S.K. Pandey, W.R. Potter, J.R. Missert, A. Oseroff, T.J. Dougherty, R.K. Pandey, A first comparative study of purpurinimide-based fluorinated vs. nonfluorinated photosensitizers for photodynamic therapy, Photochem. Photobiol. 76 (2002) 555–559.
[151] S.K. Pandey, A.L. Gryshuk, A. Graham, K. Ohkubo, S. Fukuzumi, M.P. Dobhal, G. Zheng, Z. Ou, R. Zhan, K.M. Kadish, Fluorinated photosensitizers: synthesis, photophysical, electrochemical, intracellular localization, in vitro photosensitizing efficacy and determination of tumor-uptake by 19F in vivo NMR spectroscopy, Tetrahedron 59 (2003) 10059–10073.
[152] N. Zhao, S. Xuan, B. Byrd, F.R. Fronczek, K.M. Smith, M.G.H. Vicente, Synthesis and regioselective functionalization of perhalogenated BODIPYs, Org. Biomol. Chem. 14 (2016) 6184–6188.
[153] B. Pucelik, I. Gürol, V. Ahsen, F. Dumoulin, J.M. Dąbrowski, Fluorination of phthalocyanine substituents: Improved photoproperties and enhanced photodynamic efficacy after optimal micellar formulations, Eur. J. Med. Chem. 124 (2016) 284–298.
[154] L.B. Rocha, F. Schaberle, J.M. Dąbrowski, S. Simões, L.G. Arnaut, Intravenous single-dose toxicity of redaporfin-based photodynamic therapy in rodents, Int. J. Mol. Sci. 16 (2015) 29236–29249.
[155] A.F. Luz, B. Pucelik, M.M. Pereira, J.M. Dąbrowski, L.G. Arnaut, Translating phototherapeutic indices from in vitro to in vivo photodynamic therapy with bacteriochlorins, Lasers Surg. Med. 50 (2018) 451–459.
[156] B. Pucelik, L.G. Arnaut, J.M. Dąbrowski, Lipophilicity of bacteriochlorin-based photosensitizers as a determinant for PDT optimization through the modulation of the inflammatory mediators, J. Clin. Med. (2019).
[157] B. Pucelik, R. Paczyński, G. Dubin, M.M. Pereira, L.G. Arnaut, J.M. Dąbrowski, Properties of halogenated and sulfonated porphyrins relevant for the selection of photosensitizers in anticancer and antimicrobial therapies, PLoS ONE 12 (2017) e0185984.
[158] J.M. Dąbrowski, L.G. Arnaut, M.M. Pereira, K. Urbańska, G. Stochel, Improved biodistribution, pharmacokinetics and photodynamic efficacy using a new photostable sulfonamide bacteriochlorin, MedChemComm 3 (2012) 502–505.
[159] C. Serpa, J. Schabauer, A.P. Piedade, C.J. Monteiro, M.M. Pereira, P. Douglas, H. D. Burrows, L.G. Arnaut, Photoacoustic measurement of electron injection efficiencies and energies from excited sensitizer dyes into nanocrystalline TiO2 films, J. Am. Chem. Soc. 130 (2008) 8876–8877.
[160] M. Pineiro, A.L. Carvalho, M.M. Pereira, A.D.A.R. Gonsalves, L.G. Arnaut, S.J. Formosinho, Photoacoustic measurements of porphyrin triplet-state quantum yields and singlet-oxygen efficiencies, Chem. Eur. J. 4 (1998) 2299–2307.
[161] G.F. Sá, C. Serpa, L.G. Arnaut, Stratum corneum permeabilization with photoacoustic waves generated by piezophotonic materials, J. Control. Release 167 (2013) 290–300.
[162] F.A. Schaberle, A.R. Abreu, N.P. Gonçalves, G.A.F. Sá, M.M. Pereira, L.G. Arnaut, Ultrafast dynamics of manganese (III), manganese (II), and free-base bacteriochlorin: is there time for photochemistry?, Inorg Chem. 56 (2017) 2677–2689.

[163] A. Franke, A. Scheitler, I. Kenkel, R. Lippert, A. Zahl, D. Balbinot, N. Jux, I. Ivanović-Burmazović, Positive charge on porphyrin ligand and nature of metal center define basic physicochemical properties of cationic manganese and iron porphyrins in aqueous solution, Inorg. Chem. 58 (2019) 9618–9630.
[164] E. Fagadar-Cosma, M.C. Mirica, I. Balcu, C. Bucovicean, C. Cretu, I. Armeanu, G. Fagadar-Cosma, Syntheses, spectroscopic and AFM characterization of some manganese porphyrins and their hybrid silica nanomaterials, Molecules 14 (2009) 1370–1388.
[165] L.V. Wang, S. Hu, Photoacoustic tomography: in vivo imaging from organelles to organs, Science 335 (2012) 1458–1462.
[166] H. Ryeng, A. Ghosh, Do nonplanar distortions of porphyrins bring about strongly red-shifted electronic spectra? Controversy, consensus, new developments, and relevance to chelatases, J. Am. Chem. Soc. 124 (2002) 8099–8103.
[167] L.P. Samankumara, S. Wells, M. Zeller, A.M. Acuña, B. Röder, C. Brückner, Expanded bacteriochlorins, Angew. Chem. Int. Ed. 51 (2012) 5757–5760.
[168] G. Mazzone, M. Alberto, B. De Simone, T. Marino, N. Russo, Can expanded bacteriochlorins act as photosensitizers in photodynamic therapy? Good news from density functional theory computations, Molecules 21 (2016) 288.
[169] Y. Ning, G.-Q. Jin, J.-L. Zhang, Porpholactone chemistry: an emerging approach to bioinspired photosensitizers with tunable near-infrared photophysical properties, Acc. Chem. Res. 52 (2019) 2620–2633.
[170] Y. Ning, X.-S. Ke, J.-Y. Hu, Y.-W. Liu, F. Ma, H.-L. Sun, J.-L. Zhang, Bioinspired orientation of β-substituents on porphyrin antenna ligands switches ytterbium (III) NIR emission with thermosensitivity, Inorg. Chem. 56 (2017) 1897–1905.
[171] Y. Yao, Y. Rao, Y. Liu, L. Jiang, J. Xiong, Y.-J. Fan, Z. Shen, J.L. Sessler, J.-L. Zhang, Aromaticity versus regioisomeric effect of β-substituents in porphyrinoids, PCCP 21 (2019) 10152–10162.
[172] X.-S. Ke, Y. Chang, J.-Z. Chen, J. Tian, J. Mack, X. Cheng, Z. Shen, J.-L. Zhang, Porphodilactones as synthetic chlorophylls: relative orientation of β-substituents on a pyrrolic ring tunes NIR absorption, J. Am. Chem. Soc. 136 (2014) 9598–9607.
[173] X.-S. Ke, H. Zhao, X. Zou, Y. Ning, X. Cheng, H. Su, J.-L. Zhang, Fine-tuning of β-substitution to modulate the lowest triplet excited states: a bioinspired approach to design phosphorescent metalloporphyrinoids, J. Am. Chem. Soc. 137 (2015) 10745–10752.
[174] J.M. Dabrowski, L.G. Arnaut, Photodynamic therapy (PDT) of cancer: from local to systemic treatment, Photochem. Photobiol. Sci. 14 (2015) 1765–1780.
[175] A.P. Castano, T.N. Demidova, M.R. Hamblin, Mechanisms in photodynamic therapy: part three—photosensitizer pharmacokinetics, biodistribution, tumor localization and modes of tumor destruction, Photodiagn. Photodyn. Ther. 2 (2005) 91–106.
[176] M. Korbelik, PDT-associated host response and its role in the therapy outcome, Lasers Surg. Med. 38 (2006) 500–508.
[177] A. Martinez De Pinillos Bayona, P. Mroz, C. Thunshelle, M.R. Hamblin, Design features for optimization of tetrapyrrole macrocycles as antimicrobial and anticancer photosensitizers, Chem. Biol. Drug Des. 89 (2017) 192–206.
[178] L.G. Arnaut, M.M. Pereira, J.M. Dąbrowski, E.F.F. Silva, F.A. Schaberle, A.R. Abreu, L.B. Rocha, M.M. Barsan, K. Urbańska, G. Stochel, C.M.A. Brett, Photodynamic therapy efficacy enhanced by dynamics: The role of charge transfer and photostability in the selection of photosensitizers, Chem. Eur. J. 20 (2014) 5346–5357.
[179] J.M. Dąbrowski, B. Pucelik, M.M. Pereira, L.G. Arnaut, G. Stochel, Towards tuning PDT relevant photosensitizer properties: Comparative study for the free and Zn2+ coordinated meso-tetrakis[2,6-difluoro-5-(N-methylsulfamylo)phenyl]porphyrin, J. Coord. Chem. 68 (2015) 3116–3134.
[180] B. Pucelik, L.G. Arnaut, G.Y. Stochel, J.M. Dabrowski, Design of pluronic-based formulation for enhanced redaporfin-photodynamic therapy against pigmented melanoma, ACS Appl. Mater. Interfaces 8 (2016) 22039–22055.
[181] J.M. Dąbrowski, K. Urbanska, L.G. Arnaut, M.M. Pereira, A.R. Abreu, S. Simões, G. Stochel, Biodistribution and photodynamic efficacy of a water-soluble, stable, halogenated bacteriochlorin against melanoma, ChemMedChem 6 (2011) 465–475.
[182] J.M. Dabrowski, L.G. Arnaut, M.M. Pereira, K. Urbanska, G. Stochel, Improved biodistribution, pharmacokinetics and photodynamic efficacy using a new photostable sulfonamide bacteriochlorin, MedChemComm 3 (2012) 502–505.
[183] J.M. Dąbrowski, M. Krzykawska, L.G. Arnaut, M.M. Pereira, C.J.P. Monteiro, S. Simões, K. Urbańska, G. Stochel, Tissue uptake study and photodynamic therapy of melanoma-bearing mice with a nontoxic, effective chlorin, ChemMedChem 6 (2011) 1715–1726.
[184] R. Saavedra, L.B. Rocha, J.M. Dąbrowski, L.G. Arnaut, Modulation of biodistribution, pharmacokinetics, and photosensitivity with the delivery vehicle of a bacteriochlorin photosensitizer for photodynamic therapy, ChemMedChem 9 (2014) 390–398.
[185] A.P. Castano, T.N. Demidova, M.R. Hamblin, Mechanisms in photodynamic therapy: part two—cellular signaling, cell metabolism and modes of cell death, Photodiagn. Photodyn. Ther. 2 (2005) 1–23.
[186] D. Kessel, Correlation between subcellular localization and photodynamic efficacy, J. Porphyrins Phthalocyanines 8 (2004) 1009–1014.
[187] D. Kessel, Y. Luo, Y. Deng, C. Chang, The role of subcellular localization in initiation of apoptosis by photodynamic therapy, Photochem. Photobiol. 65 (1997) 422–426.
[188] E. Buytaert, M. Dewaele, P. Agostinis, Molecular effectors of multiple cell death pathways initiated by photodynamic therapy, Biochim. Biophys. Acta 1776 (2007) 86–107.
[189] J.W. Snyder, E. Skovsen, J.D. Lambert, P.R. Ogilby, Subcellular, time-resolved studies of singlet oxygen in single cells, J. Am. Chem. Soc. 127 (2005) 14558–14559.
[190] S. Hatz, L. Poulsen, P.R. Ogilby, Time-resolved singlet oxygen phosphorescence measurements from photosensitized experiments in single cells: Effects of oxygen diffusion and oxygen concentration, Photochem. Photobiol. 84 (2008) 1284–1290.
[191] M. Shirmanova, A. Gavrina, N. Aksenova, N. Glagolev, A. Solovieva, B. Shakhov, E. Zagaynova, Comparative study of tissue distribution of chlorin e6 complexes with amphiphilic polymers in mice with cervical carcinoma, J. Anal. Bioanal. Technol. Sci. 1 (2014) 008.
[192] M. Karwicka, B. Pucelik, M. Gonet, M. Elas, J.M. Dąbrowski, Effects of photodynamic therapy with redaporfin on tumor oxygenation and blood flow in a lung cancer mouse model, Sci. Rep. 9 (2019) 1–15.
[193] J. Staron, B. Boron, D. Karcz, M. Szczygiel, L. Fiedor, Recent progress in chemical modifications of chlorophylls and bacteriochlorophylls for the applications in photodynamic therapy, Curr. Med. Chem. 22 (2015) 3054–3074.
[194] V. Rosenbach-Belkin, L. Chen, L. Fiedor, I. Tregub, F. Pavlotsky, V. Brumfeld, Y. Salomon, A. Scherz, Serine conjugates of chlorophyll and bacteriochlorophyll: photocytotoxicity in vitro and tissue distribution in mice bearing melanoma tumors, Photochem. Photobiol. 64 (1996) 174–181.
[195] S. Katz, Phototoxicity of bacteriochlorophyll-serine: photophysical and photochemical basis, Weizmann Institute of Science (1999).
[196] A. Scherz, A. Brandis, M. Greenwald, V. Rosenbach-Belkin, O. Mazor, S. Gross, R. Hammi, Y. Vakrat, G. Simonneaux, H. Scheer, TOOKAD—a novel palladium-bacteriochlorophyll sensitizer for photodynamic therapy: synthesis and characterization, Clin. Basic Appl. Photodyn. Med. (2001) 79.
[197] J. Zilberstein, S. Schreiber, M.C. Bloemers, P. Bendel, M. Neeman, E. Schechtman, F. Kohen, A. Scherz, Y. Salomon, Antivascular treatment of solid melanoma tumors with bacteriochlorophyll–serine-based photodynamic therapy, Photochem. Photobiol. 73 (2001) 257–266.
[198] J. Zilberstein, A. Scherz, A. Bromberg, P. Bendel, M. Neeman, Y. Salomon, Mechanisms involved in chlorophyll based photoinduced cell damage: photodynamic therapy of melanoma, Meeting of the Society of Magnetic Resonance. Nice, France, 1995, pp. 1681.
[199] D. Kelleher, O. Thews, A. Scherz, Y. Salomon, P. Vaupel, Combined hyperthermia and chlorophyll-based photodynamic therapy: tumour growth and metabolic microenvironment, Br. J. Cancer 89 (2003) 2333.
[200] D. Kelleher, O. Thews, J. Rzeznik, A. Scherz, Y. Salomon, P. Vaupel, Hot Topic Water-filtered infrared-A radiation: a novel technique for localized hyperthermia in combination with bacteriochlorophyll-based photodynamic therapy, Int. J. Hyperth. 15 (1999) 467–474.
[201] J. Zilberstein, A. Bromberg, A. Frantz, V. Rosenbach-Belkin, A. Kritzmann, R. Pfefermann, Y. Salomon, A. Scherz, Light-dependent oxygen consumption in bacteriochlorophyll-serine-treated melanoma tumors: on-line determination using a tissue-inserted oxygen microsensor, Photochem. Photobiol. 65 (1997) 1012–1019.
[202] Q. Chen, Z. Huang, D. Luck, J. Beckers, P.H. Brun, B.C. Wilson, A. Scherz, Y. Salomon, F.W. Hetzel, Preclinical studies in normal canine prostate of a novel palladium-bacteriopheophorbide (WST09) photosensitizer for photodynamic therapy of prostate cancer, Photochem. Photobiol. 76 (2002) 438–445.
[203] A. Azzouzi, E. Barret, J. Bennet, C. Moore, S. Taneja, G. Muir, A. Villers, J. Coleman, C. Allen, A. Scherz, TOOKAD® Soluble focal therapy: pooled analysis of three phase II studies assessing the minimally invasive ablation of localized prostate cancer, World J. Urol. 33 (2015) 945–953.
[204] A.-R. Azzouzi, S. Lebdai, F. Benzaghou, C. Stief, Vascular-targeted photodynamic therapy with TOOKAD® Soluble in localized prostate cancer: standardization of the procedure, World J. Urol. 33 (2015) 937–944.
[205] A.-R. Azzouzi, S. Vincendeau, E. Barret, A. Cicco, F. Kleinclauss, H.G. van der Poel, C.G. Stief, J. Rassweiler, G. Salomon, E. Solsona, Padeliporfin vascular-targeted photodynamic therapy versus active surveillance in men with low-risk prostate cancer (CLIN1001 PCM301): an open-label, phase 3, randomised controlled trial, Lancet Oncol. 18 (2017) 181–191.
[206] J.A. Coleman, Clinical trial experience with Tookad soluble vascular targeted photodynamic therapy for genitourinary cancers at Memorial Sloan Ketterin (Conference Presentation), 17th International Photodynamic Association World Congress, International Society for Optics and Photonics, 2019, pp. 1107033.
[207] Z. Huang, Q. Chen, D. Luck, J. Beckers, B.C. Wilson, N. Trncic, S.M. LaRue, D. Blanc, F.W. Hetzel, Studies of a vascular-acting photosensitizer, Pd-bacteriopheophorbide (Tookad), in normal canine prostate and spontaneous canine prostate cancer, Lasers Surg. Med. 36 (2005) 390–397.
[208] J. Trachtenberg, A. Bogaards, R. Weersink, M. Haider, A. Evans, S. McCluskey, A. Scherz, M. Gertner, C. Yue, S. Appu, Vascular targeted photodynamic therapy with palladium-bacteriopheophorbide photosensitizer for recurrent

prostate cancer following definitive radiation therapy: assessment of safety and treatment response, J. Urol. 178 (2007) 1974–1979.
[209] J. Trachtenberg, R.A. Weersink, S.R. Davidson, M.A. Haider, A. Bogaards, M.R. Gertner, A. Evans, A. Scherz, J. Savard, J.L. Chin, Vascular-targeted photodynamic therapy (padoporfin, WST09) for recurrent prostate cancer after failure of external beam radiotherapy: a study of escalating light doses, BJU Int. 102 (2008) 556–562.
[210] R.A. Weersink, J. Forbes, S. Bisland, J. Trachtenberg, M. Elhilali, P.H. Brún, B.C. Wilson, Assessment of cutaneous photosensitivity of TOOKAD (WST09) in preclinical animal models and in patients, Photochem. Photobiol. 81 (2005) 106–113.
[211] M. Gertner, A. Bogaards, R. Weersink, S. McCluskey, M. Haider, C. Yue, J. Savard, S. Simpson, P. Brun, P. Cohen, 839 Initial results of a phase I II trial of WST09-mediated photodynamic therapy (WST09-PDT) for recurrent prostate cancer following failed external beam radiation therapy (EBRT), Eur. Urol. Suppl. 3 (2004) 212.
[212] D. Pendse, C. Moore, N. Arumainayagam, C. Mosse, C. Allen, S. Bown, WST-09 mediated photodynamic therapy for prostate cancer, Abstract (2009).
[213] M.A. Grin, R.I. Reshetnikov, R.I. Yakubovskaya, E.A. Plotnikova, N.B. Morozova, A.A. Tsigankov, A.V. Efremenko, D.E. Ermakova, A.V. Feofanov, A.F. Mironov, Novel bacteriochlorophyll-based photosensitizers and their photodynamic activity, J. Porphyrins Phthalocyanines 18 (2014) 129–138.
[214] O. Mazor, A. Brandis, V. Plaks, E. Neumark, V. Rosenbach-Belkin, Y. Salomon, A. Scherz, WST11, A novel water-soluble bacteriochlorophyll derivative; cellular uptake, pharmacokinetics, biodistribution and vascular-targeted photodynamic activity using melanoma tumors as a model, Photochem. Photobiol. 81 (2005) 342–351.
[215] P.H. Brun, J.L. DeGroot, E.F.G. Dickson, M. Farahani, R.H. Pottier, Determination of the in vivo pharmacokinetics of palladium-bacteriopheophorbide (WST09) in EMT6 tumour-bearing Balb/c mice using graphite furnace atomic absorption spectroscopy, Photochem. Photobiol. Sci. 3 (2004) 1006–1010.
[216] S. Steba Biotech, Study of WST11 in patients with localized prostate cancer, ClinicalTrials. gov [Internet]. National Library of Medicine (US), Bethesda (MD), (2015).
[217] A. Azzouzi, E. Barret, A. Villers, G. Muir, C. Moore, C. Allen, M. Emberton, 86 results of tookad® soluble vasCular targeted PhotodynaMiC theraPy (vtP) for low risk loCalized Prostate CanCer (PCM201/PCM203), Eur. Urol. Suppl. 10 (2011) 54.
[218] N. Arumainayagam, C. Allen, C. Moore, N. Barber, R. Hindley, G. Muir, J. Trachtenberg, L. Cormier, E. Barret, A. Azzouzi, 936 Tookad® Soluble (Padeliporfin) second generation vascular targeted photodynamic therapy (VTP) for prostate cancer: safety and feasibility, Eur. Urol. Suppl. 9 (2010) 294.
[219] S. Quoraishi, C. Moore, C. Allen, L. Abenhaim, M. Emberton, Light density index (LDI) is a predictor of MRI and biopsy outcome for WST-11 (Tookad Soluble™) mediated Vascular Targeted Photodynamic therapy (VTP) in focal treatment of localised prostate cancer, Br. J. Med. Surg. Urol. 3 (2010) 264–265.
[220] C. Eymerit-Morin, M. Zidane, S. Lebdai, S. Triau, A.R. Azzouzi, M.-C. Rousselet, Histopathology of prostate tissue after vascular-targeted photodynamic therapy for localized prostate cancer, Virchows Arch. 463 (2013) 547–552.
[221] I. ClinicalTrials, gov [Internet], Bethesda (MD): US National Library of Medicine. Available from: URL: https://clinicaltrials.gov/ct2/show/NCT03183869.
[222] C.M. Moore, A.R. Azzouzi, E. Barret, A. Villers, G.H. Muir, N.J. Barber, S. Bott, J. Trachtenberg, N. Arumainayagam, B. Gaillac, Determination of optimal drug dose and light dose index to achieve minimally invasive focal ablation of localised prostate cancer using WST 11-vascular-targeted photodynamic (VTP) therapy, BJU Int. 116 (2015) 888–896.
[223] C.M. Moore, C.A. Mosse, C. Allen, H. Payne, M. Emberton, S.G. Bown, Light penetration in the human prostate: a whole prostate clinical study at 763 nm, J. Biomed. Opt. 16 (2011) 015003.
[224] B. Richselsen, M.C. Nielsen, gov [Internet], Bethesda (MD): National Library of Medicine (US), (2000).
[225] A.C. DiSabatino, gov [Internet], National Library of Medicine (US), Bethesda (MD), (2000).
[226] A.M. Bugaj, Vascular targeted photochemotherapy using padoporfin and padeliporfin as a method of the focal treatment of localised prostate cancer-clinician's insight, World J. Methodol. 6 (2016) 65.
[227] A.R. Azzouzi, E. Barret, C.M. Moore, A. Villers, C. Allen, A. Scherz, G. Muir, M. de Wildt, N.J. Barber, S. Lebdai, TOOKAD® S oluble vascular-targeted photodynamic (VTP) therapy: determination of optimal treatment conditions and assessment of effects in patients with localised prostate cancer, BJU Int. 112 (2013) 766–774.
[228] S. Lebdai, A. Villers, E. Barret, C. Nedelcu, P. Bigot, A.-R. Azzouzi, Feasibility, safety, and efficacy of salvage radical prostatectomy after Tookad® Soluble focal treatment for localized prostate cancer, World J. Urol. 33 (2015) 965–971.
[229] https://adisinsight.springer.com/drugs/800030266.
[230] M.J. O'Shaughnessy, K.S. Murray, S.P. La Rosa, S. Budhu, T. Merghoub, A. Somma, S. Monette, K. Kim, R.B. Corradi, A. Scherz, Systemic antitumor immunity by PD-1/PD-L1 inhibition is potentiated by vascular-targeted photodynamic therapy of primary tumors, Clin. Cancer Res. 24 (2018) 592–599.
[231] K. Kim, P.A. Watson, S. Lebdai, S. Jebiwott, A.J. Somma, S. La Rosa, D. Mehta, K. S. Murray, H. Lilja, D. Ulmert, Androgen deprivation therapy potentiates the efficacy of vascular targeted photodynamic therapy of prostate Cancer xenografts, Clin. Cancer Res. 24 (2018) 2408–2416.
[232] O.-J. Norum, P.K. Selbo, A. Weyergang, K.-E. Giercksky, K. Berg, Photochemical internalization (PCI) in cancer therapy: from bench towards bedside medicine, J. Photochem. Photobiol., B 96 (2009) 83–92.
[233] K. Berg, A. Weyergang, L. Prasmickaite, A. Bonsted, A. Høgset, M.-T.R. Strand, E. Wagner, P.K. Selbo, Photochemical Internalization (PCI): A Technology for Drug Delivery, Photodynamic Therapy, Springer, 2010, pp. 133–145.
[234] A.L.F. Dos Santos, D. De Almeida, L.F. Terra, M.C.S. Baptista, L. Labriola, Photodynamic therapy in cancer treatment-an update review, J. Cancer Metastasis Treat 5 (2019) 1–20.
[235] N. Kudinova, T. Berezov, Photodynamic therapy of cancer: Search for ideal photosensitizer, Biochemistry (Moscow) Suppl. Series B: Biomed. Chem. 4 (2010) 95–103.
[236] P. Mroz, Y.-Y. Huang, A. Szokalska, T. Zhiyentayev, S. Janjua, A.-P. Nifli, M.E. Sherwood, C. Ruzié, K.E. Borbas, D. Fan, Stable synthetic bacteriochlorins overcome the resistance of melanoma to photodynamic therapy, FASEB J. 24 (2010) 3160–3170.
[237] Y.-Y. Huang, P. Mroz, T. Zhiyentayev, S.K. Sharma, T. Balasubramanian, C. Ruzié, M. Krayer, D. Fan, K.E. Borbas, E. Yang, In vitro photodynamic therapy and quantitative structure-activity relationship studies with stable synthetic near-infrared-absorbing bacteriochlorin photosensitizers, J. Med. Chem. 53 (2010) 4018–4027.
[238] L. Huang, Y.-Y. Huang, P. Mroz, G.P. Tegos, T. Zhiyentayev, S.K. Sharma, Z. Lu, T. Balasubramanian, M. Krayer, C. Ruzié, Stable synthetic cationic bacteriochlorins as selective antimicrobial photosensitizers, Antimicrob. Agents Chemother. 54 (2010) 3834–3841.
[239] Y.Y. Huang, T. Balasubramanian, E. Yang, D. Luo, J.R. Diers, D.F. Bocian, J.S. Lindsey, D. Holten, M.R. Hamblin, Stable synthetic bacteriochlorins for photodynamic therapy: role of dicyano peripheral groups, central metal substitution (2H, Zn, Pd), and Cremophor EL delivery, ChemMedChem 7 (2012) 2155–2167.
[240] B. Chen, B.W. Pogue, P.J. Hoopes, T. Hasan, Vascular and cellular targeting for photodynamic therapy, Crit. Rev. Eukaryotic Gene Exp. 16 (2006).
[241] N. Solban, I. Rizvi, T. Hasan, Targeted photodynamic therapy, Lasers Surg. Med. 38 (2006) 522–531.
[242] L.B. Rocha, L.C. Gomes-da-Silva, J.M. Dąbrowski, L.G. Arnaut, Elimination of primary tumours and control of metastasis with rationally designed bacteriochlorin photodynamic therapy regimens, Eur. J. Cancer 51 (2015) 1822–1830.
[243] J.M. Dąbrowski, L.G. Arnaut, M.M. Pereira, K. Urbańska, S. Simões, G. Stochel, L. Cortes, Combined effects of singlet oxygen and hydroxyl radical in photodynamic therapy with photostable bacteriochlorins: evidence from intracellular fluorescence and increased photodynamic efficacy in vitro, Free Radic. Biol. Med. 52 (2012) 1188–1200.
[244] D. Kessel, M.G.H. Vicente, J.J. Reiners Jr, Initiation of apoptosis and autophagy by photodynamic therapy, Lasers Surg. Med. 38 (2006) 482–488.
[245] L.C. Gomes-da-Silva, A.J. Jimenez, A. Sauvat, W. Xie, S. Souquere, S. Divoux, M. Storch, B. Sveinbjørnsson, Ø. Rekdal, L.G. Arnaut, Recruitment of LC3 to damaged Golgi apparatus, Cell Death Differ. 26 (2019) 1467–1484.
[246] L.C. Gomes-da-Silva, L. Zhao, L. Bezu, H. Zhou, A. Sauvat, P. Liu, S. Durand, M. Leduc, S. Souquere, F. Loos, Photodynamic therapy with redaporfin targets the endoplasmic reticulum and Golgi apparatus, EMBO J. 37 (2018).
[247] L.C. Gomes-da-Silva, L. Zhao, L.G. Arnaut, G. Kroemer, O. Kepp, Redaporfin induces immunogenic cell death by selective destruction of the endoplasmic reticulum and the Golgi apparatus, Oncotarget 9 (2018) 31169.
[248] L.L. Santos, J. Oliveira, E. Monteiro, J. Santos, C. Sarmento, Treatment of head and neck cancer with photodynamic therapy with redaporfin: a clinical case report, Case Rep. Oncol. 11 (2018) 769–776.
[249] J. Oliveira, E. Monteiro, J. Santos, J.D. Silva, L. Almeida, L.L. Santos, A first in human study using photodynamic therapy with Redaporfin in advanced head and neck cancer, Am. Soc. Clin. Oncol. (2017).
[250] H. Pelicano, D. Carney, P. Huang, ROS stress in cancer cells and therapeutic implications, Drug Resist. Updates 7 (2004) 97–110.
[251] M. Krzykawska-Serda, J.M. Dąbrowski, L.G. Arnaut, M. Szczygieł, K. Urbańska, G. Stochel, M. Elas, The role of strong hypoxia in tumors after treatment in the outcome of bacteriochlorin-based photodynamic therapy, Free Radic. Biol. Med. 73 (2014) 239–251.
[252] M. Korbelik, Induction of tumor immunity by photodynamic therapy, J. Clin. Laser Med. Surg. 14 (1996) 329–334.
[253] A.P. Castano, P. Mroz, M.R. Hamblin, Photodynamic therapy and anti-tumour immunity, Nat. Rev. Cancer 6 (2006) 535.
[254] A.D. Garg, D. Nowis, J. Golab, P. Agostinis, Photodynamic therapy: illuminating the road from cell death towards anti-tumour immunity, Apoptosis 15 (2010) 1050–1071.
[255] D. Nowis, T. Stokłosa, M. Legat, T. Issat, M. Jakóbisiak, J. Gołąb, The influence of photodynamic therapy on the immune response, Photodiagn. Photodyn. Ther. 2 (2005) 283–298.
[256] S.O. Gollnick, C.M. Brackett, Enhancement of anti-tumor immunity by photodynamic therapy, Immunol. Res. 46 (2010) 216–226.
[257] S.O. Gollnick, B. Owczarczak, P. Maier, Photodynamic therapy and anti-tumor immunity, Lasers Surg. Med. 38 (2006) 509–515.

[258] D. Preise, R. Oren, I. Glinert, V. Kalchenko, S. Jung, A. Scherz, Y. Salomon, Systemic antitumor protection by vascular-targeted photodynamic therapy involves cellular and humoral immunity, Cancer Immunol. Immunother. 58 (2009) 71–84.
[259] P. Skupin-Mrugalska, J. Piskorz, T. Goslinski, J. Mielcarek, K. Konopka, N. Düzgüneş, Current status of liposomal porphyrinoid photosensitizers, Drug Discovery Today 18 (2013) 776–784.
[260] J. Piskorz, K. Konopka, N. Düzgüneş, Z. Gdaniec, J. Mielcarek, T. Goslinski, Diazepinoporphyrazines containing peripheral styryl substituents and their promising nanomolar photodynamic activity against oral cancer cells in liposomal formulations, ChemMedChem 9 (2014) 1775–1782.
[261] M. Kryjewski, T. Goslinski, J. Mielcarek, Functionality stored in the structures of cyclodextrin–porphyrinoid systems, Coord. Chem. Rev. 300 (2015) 101–120.
[262] E. Wieczorek, D.T. Mlynarczyk, M. Kucinska, J. Dlugaszewska, J. Piskorz, L. Popenda, W. Szczolko, S. Jurga, M. Murias, J. Mielcarek, Photophysical properties and photocytotoxicity of free and liposome-entrapped diazepinoporphyrazines on LNCaP cells under normoxic and hypoxic conditions, Eur. J. Med. Chem. 150 (2018) 64–73.
[263] R. Allison, H. Mota, V.S. Bagnato, C. Sibata, Bio-nanotechnology and photodynamic therapy—state of the art review, Photodiagn. Photodyn. Ther. 5 (2008) 19–28.
[264] Y.-Y. Huang, S.K. Sharma, T. Dai, H. Chung, A. Yaroslavsky, M. Garcia-Diaz, J. Chang, L.Y. Chiang, M.R. Hamblin, Can nanotechnology potentiate photodynamic therapy?, Nanotechnol. Rev. 1 (2012) 111–146.
[265] G.M.F. Calixto, J. Bernegossi, L.M. De Freitas, C.R. Fontana, M. Chorilli, Nanotechnology-based drug delivery systems for photodynamic therapy of cancer: a review, Molecules 21 (2016) 342.
[266] N. Düzgüneş, J. Piskorz, P. Skupin-Mrugalska, T. Goslinski, J. Mielcarek, K. Konopka, Photodynamic therapy of cancer with liposomal photosensitizers, Therap. Deliv. 9 (2018) 823–832.
[267] R. Misra, S. Acharya, S.K. Sahoo, Cancer nanotechnology: application of nanotechnology in cancer therapy, Drug Discovery Today 15 (2010) 842–850.
[268] V. Monge-Fuentes, L.A. Muehlmann, R.B. de Azevedo, Perspectives on the application of nanotechnology in photodynamic therapy for the treatment of melanoma, Nano Rev. 5 (2014) 24381.
[269] A.G. Hausberger, P.P. DeLuca, Characterization of biodegradable poly (D, L-lactide-co-glycolide) polymers and microspheres, J. Pharm. Biomed. Anal. 13 (1995) 747–760.
[270] K.K. Ng, J.F. Lovell, G. Zheng, Lipoprotein-inspired nanoparticles for cancer theranostics, Acc. Chem. Res. 44 (2011) 1105–1113.
[271] M.K. Bijsterbosch, T.J. van Berkel, Native and modified lipoproteins as drug delivery systems, Adv. Drug Deliv. Rev. 5 (1990) 231–251.
[272] D.E. Marotta, W. Cao, E.P. Wileyto, H. Li, I. Corbin, E. Rickter, J.D. Glickson, B. Chance, G. Zheng, T.M. Busch, Evaluation of bacteriochlorophyll-reconstituted low-density lipoprotein nanoparticles for photodynamic therapy efficacy in vivo, Nanomedicine 6 (2011) 475–487.
[273] J. Conde, G. Doria, P. Baptista, Noble metal nanoparticles applications in cancer, J. Drug Deliv. 2012 (2012).
[274] I. Pantiushenko, P. Rudakovskaya, A. Starovoytova, A. Mikhaylovskaya, M. Abakumov, M. Kaplan, A. Tsygankov, A. Majouga, M. Grin, A. Mironov, Development of bacteriochlorophyll a-based near-infrared photosensitizers conjugated to gold nanoparticles for photodynamic therapy of cancer, Biochemistry (Moscow) 80 (2015) 752–762.
[275] M. Arruebo, R. Fernández-Pacheco, M.R. Ibarra, J. Santamaría, Magnetic nanoparticles for drug delivery, Nano Today 2 (2007) 22–32.
[276] P. Ostroverkhov, A. Semkina, V. Naumenko, E. Plotnikova, P. Melnikov, T. Abakumova, R. Yakubovskaya, A. Mironov, S. Vodopyanov, A. Abakumov, Synthesis and characterization of Bacteriochlorin loaded magnetic nanoparticles (MNP) for personalized MRI guided photosensitizers delivery to tumor, J. Colloid Interface Sci. 537 (2019) 132–141.
[277] E. Plotnikova, M. Grin, P. Ostroverkhov, I. Pantushenko, R. Yakubovskaya, A. Kaprin, Primary screening of photosensitizers of the bacteriochlorin series for photodynamic therapy of malignant neoplasms, Biochemistry (Moscow) Suppl. Series B: Biomed. Chem. 12 (2018) 275–282.
[278] R.C. Huxford, J. Della Rocca, W. Lin, Metal–organic frameworks as potential drug carriers, Curr. Opin. Chem. Biol. 14 (2010) 262–268.
[279] K. Zhang, Z. Yu, X. Meng, W. Zhao, Z. Shi, Z. Yang, H. Dong, X. Zhang, A bacteriochlorin-based metal-organic framework nanosheet superoxide radical generator for photoacoustic imaging-guided highly efficient photodynamic therapy, Adv. Sci. (2019) 1900530.
[280] E.M. Sevick-Muraca, J.P. Houston, M. Gurfinkel, Fluorescence-enhanced, near infrared diagnostic imaging with contrast agents, Curr. Opin. Chem. Biol. 6 (2002) 642–650.
[281] N. Zhao, S. Xuan, Z. Zhou, F.R. Fronczek, K.M. Smith, M.G.A.H. Vicente, Synthesis and spectroscopic and cellular properties of near-IR [a] phenanthrene-fused 4, 4-difluoro-4-bora-3a, 4a-diaza-s-indacenes, J. Org. Chem. 82 (2017) 9744–9750.
[282] L. Jiao, Y. Wu, S. Wang, X. Hu, P. Zhang, C. Yu, K. Cong, Q. Meng, E. Hao, M.G.A. H. Vicente, Accessing near-infrared-absorbing BF2-azadipyrromethenes via a push–pull effect, J. Org. Chem. 79 (2014) 1830–1835.
[283] T. Uppal, N.D.K. Bhupathiraju, M.G.H. Vicente, Synthesis and cellular properties of near-IR BODIPY–PEG and carbohydrate conjugates, Tetrahedron 69 (2013) 4687–4693.
[284] L. Jiao, C. Yu, T. Uppal, M. Liu, Y. Li, Y. Zhou, E. Hao, X. Hu, M.G.H. Vicente, Long wavelength red fluorescent dyes from 3, 5-diiodo-BODIPYs, Org. Biomol. Chem. 8 (2010) 2517–2519.
[285] T. Harada, K. Sano, K. Sato, R. Watanabe, Z. Yu, H. Hanaoka, T. Nakajima, P.L. Choyke, M. Ptaszek, H. Kobayashi, Activatable organic near-infrared fluorescent probes based on a bacteriochlorin platform: synthesis and multicolor in vivo imaging with a single excitation, Bioconjug. Chem. 25 (2014) 362–369.
[286] A. Meares, A. Satraitis, M. Ptaszek, BODIPY–bacteriochlorin energy transfer arrays: toward near-IR emitters with broadly tunable, multiple absorption bands, J. Org. Chem. 82 (2017) 13068–13075.
[287] F. Ogata, T. Nagaya, Y. Maruoka, J. Akhigbe, A. Meares, M.Y. Lucero, A. Satraitis, D. Fujimura, R. Okada, F. Inagaki, Activatable near-infrared fluorescence imaging using PEGylated bacteriochlorin-based chlorin and BODIPY-dyads as probes for detecting cancer, Bioconjug. Chem. 30 (2018) 169–183.
[288] T.W. Liu, J. Chen, L. Burgess, W. Cao, J. Shi, B.C. Wilson, G. Zheng, Multimodal bacteriochlorophyll theranostic agent, Theranostics 1 (2011) 354.
[289] S. Gross, A. Gilead, A. Scherz, M. Neeman, Y. Salomon, Monitoring photodynamic therapy of solid tumors online by BOLD-contrast MRI, Nat. Med. 9 (2003) 1327–1331.
[290] G.-Q. Jin, Y. Ning, J.-X. Geng, Z.-F. Jiang, Y. Wang, J.-L. Zhang, Joining the journey to near infrared (NIR) imaging: the emerging role of lanthanides in the designing of molecular probes, Inorg. Chem. Front. (2020).
[291] D.K. Chatterjee, A.J. Rufaihah, Y. Zhang, Upconversion fluorescence imaging of cells and small animals using lanthanide doped nanocrystals, Biomaterials 29 (2008) 937–943.
[292] C. Wang, L. Cheng, Z. Liu, Upconversion nanoparticles for photodynamic therapy and other cancer therapeutics, Theranostics 3 (2013) 317.
[293] P. Padiyara, H. Inoue, M. Sprenger, Global governance mechanisms to address antimicrobial resistance, Infect. Dis. Res. Treat. 11 (2018).
[294] A. Regiel-Futyra, J.M. Dąbrowski, O. Mazuryk, K. Śpiewak, A. Kyzioł, B. Pucelik, M. Brindell, G. Stochel, Bioinorganic antimicrobial strategies in the resistance era, Coord. Chem. Rev. 351 (2017) 76–117.
[295] A. Kawczyk-Krupka, B. Pucelik, A. Międzybrodzka, A.R. Sieroń, J.M. Dąbrowski, Photodynamic therapy as an alternative to antibiotic therapy for the treatment of infected leg ulcers, Photodiagn. Photodyn. Ther. 23 (2018) 132–143.
[296] N. Kashef, Y.-Y. Huang, M.R. Hamblin, Advances in antimicrobial photodynamic inactivation at the nanoscale, Nanophotonics 6 (2017) 853–879.
[297] D.M.A. Vera, M.H. Haynes, A.R. Ball, T. Dai, C. Astrakas, M.J. Kelso, M.R. Hamblin, G.P. Tegos, Strategies to potentiate antimicrobial photoinactivation by overcoming resistant phenotypes, Photochem. Photobiol. 88 (2012) 499–511.
[298] T. Maisch, J. Baier, B. Franz, M. Maier, M. Landthaler, R.-M. Szeimies, W. Bäumler, The role of singlet oxygen and oxygen concentration in photodynamic inactivation of bacteria, Proc. Natl. Acad. Sci. 104 (2007) 7223–7228.
[299] T. Demidova, M. Hamblin, Photodynamic therapy targeted to pathogens, Int.. J. Immunopathol. Pharmacol. 17 (2004) 245–254.
[300] M.R. Hamblin, T. Hasan, Photodynamic therapy: a new antimicrobial approach to infectious disease?, Photochem. Photobiol. Sci. 3 (2004) 436–450.
[301] M.R. Hamblin, Antimicrobial photodynamic inactivation: a bright new technique to kill resistant microbes, Curr. Opin. Microbiol. 33 (2016) 67–73.
[302] T. Maisch, S. Hackbarth, J. Regensburger, A. Felgenträger, W. Bäumler, M. Landthaler, B. Röder, Photodynamic inactivation of multi-resistant bacteria (PIB)–a new approach to treat superficial infections in the 21st century, J. Deutschen Dermatologischen Gesellschaft 9 (2011) 360–366.
[303] R.T. Aroso, M.J. Calvete, B. Pucelik, G. Dubin, L.G. Arnaut, M.M. Pereira, J.M. Dąbrowski, Photoinactivation of microorganisms with sub-micromolar concentrations of imidazolium metallophthalocyanine salts, Eur. J. Med. Chem. 184 (2019) 111740.
[304] A. Sułek, B. Pucelik, J. Kuncewicz, G. Dubin, J.M. Dąbrowski, Sensitization of TiO2 by halogenated porphyrin derivatives for visible light biomedical and environmental photocatalysis, Catal. Today (2019).
[305] A. Sułek, B. Pucelik, M. Kobielusz, P. Łabuz, G. Dubin, J.M. Dąbrowski, Surface modification of nanocrystalline TiO2 materials with sulfonated porphyrins for visible light antimicrobial therapy, Catalysts 9 (2019) 821.
[306] L. Sobotta, J. Dlugaszewska, P. Kasprzycki, S. Lijewski, A. Teubert, J. Mielcarek, M. Gdaniec, T. Goslinski, P. Fita, E. Tykarska, In vitro photodynamic activity of lipid vesicles with zinc phthalocyanine derivative against Enterococcus faecalis, J. Photochem. Photobiol., B 183 (2018) 111–118.
[307] L. Sobotta, J. Dlugaszewska, D. Ziental, W. Szczolko, T. Koczorowski, T. Goslinski, J. Mielcarek, Optical properties of a series of pyrrolyl-substituted porphyrazines and their photoinactivation potential against Enterococcus faecalis after incorporation into liposomes, J. Photochem. Photobiol., A 368 (2019) 104–109.
[308] L. Sobotta, S. Lijewski, J. Dlugaszewska, J. Nowicka, J. Mielcarek, T. Goslinski, Photodynamic inactivation of Enterococcus faecalis by conjugates of zinc (II) phthalocyanines with thymol and carvacrol loaded into lipid vesicles, Inorg. Chim. Acta 489 (2019) 180–190.
[309] M. Tim, Strategies to optimize photosensitizers for photodynamic inactivation of bacteria, J. Photochem. Photobiol., B 150 (2015) 2–10.

[310] M.R. Hamblin, D.A. O'Donnell, N. Murthy, C.H. Contag, T. Hasan, Rapid control of wound infections by targeted photodynamic therapy monitored by in vivo bioluminescence imaging, Photochem. Photobiol. 75 (2002) 51–57.
[311] L. Huang, M. Krayer, J.G. Roubil, Y.-Y. Huang, D. Holten, J.S. Lindsey, M.R. Hamblin, Stable synthetic mono-substituted cationic bacteriochlorins mediate selective broad-spectrum photoinactivation of drug-resistant pathogens at nanomolar concentrations, J. Photochem. Photobiol., B 141 (2014) 119–127.
[312] K. Sahu, M. Sharma, P. Sharma, Y. Verma, K.D. Rao, H. Bansal, A. Dube, P.K. Gupta, Effect of poly-L-lysine-chlorin p6-mediated antimicrobial photodynamic treatment on collagen restoration in bacteria-infected wounds, Photomed. Laser Surg. 32 (2014) 23–29.
[313] G.P. Tegos, M. Anbe, C. Yang, T.N. Demidova, M. Satti, P. Mroz, S. Janjua, F. Gad, M.R. Hamblin, Protease-stable polycationic photosensitizer conjugates between polyethyleneimine and chlorin (e6) for broad-spectrum antimicrobial photoinactivation, Antimicrob. Agents Chemother. 50 (2006) 1402–1410.
[314] T. Maisch, C. Bosl, R.-M. Szeimies, N. Lehn, C. Abels, Photodynamic effects of novel XF porphyrin derivatives on prokaryotic and eukaryotic cells, Antimicrob. Agents Chemother. 49 (2005) 1542–1552.
[315] G. Meerovich, I. Tiganova, E. Makarova, I. Meerovich, M.R. Ju, E. Tolordova, N. Alekseeva, T. Stepanova, K. Yu, E. Luk'Anets, Photodynamic inactivation of bacteria and biofilms using cationic bacteriochlorins, J. Phys. Conf. Ser. IOP Publishing (2016) 012011.
[316] Y. Kobuke, Artificial light-harvesting systems by use of metal coordination, Eur. J. Inorg. Chem. 2006 (2006) 2333–2351.
[317] G. Stochel, Z. Stasicka, M. Brindell, W. Macyk, K. Szacilowski, Bioinorganic Photochemistry, John Wiley & Sons, 2009.
[318] S. Shoji, Y. Nomura, H. Tamiaki, Heterodimers of zinc and free-base chlorophyll derivatives co-assembled in biomimetic chlorosomal J-aggregates, Photochem. Photobiol. Sci. 18 (2019) 555–562.
[319] Z.-M. Ou, H. Yao, K. Kimura, Preparation and optical properties of organic nanoparticles of porphyrin without self-aggregation, J. Photochem. Photobiol., A 189 (2007) 7–14.
[320] V. Huber, M. Katterle, M. Lysetska, F. Würthner, Reversible self-organization of semisynthetic zinc chlorins into well-defined rod antennae, Angew. Chem. Int. Ed. 44 (2005) 3147–3151.
[321] H.S. Kang, N.N. Esemoto, J.R. Diers, D.M. Niedzwiedzki, J.A. Greco, J. Akhigbe, Z. Yu, C. Pancholi, G. Viswanathan Bhagavathy, J.K. Nguyen, Effects of strong electronic coupling in chlorin and bacteriochlorin dyads, J. Phys. Chem. A 120 (2016) 379–395.
[322] J. Harada, T. Mizoguchi, Y. Tsukatani, M. Noguchi, H. Tamiaki, A seventh bacterial chlorophyll driving a large light-harvesting antenna, Sci. Rep. 2 (2012) 671.
[323] H. Tamiaki, Y. Shimamura, H. Yoshimura, S.K. Pandey, R.K. Pandey, Self-aggregation of synthetic zinc 3-hydroxymethyl-purpurin-18 and N-hexylimide methyl esters in an aqueous solution as models of green photosynthetic bacterial chlorosomes, Chem. Lett. 34 (2005) 1344–1345.
[324] K. Shrestha, J.M. González-Delgado, J.H. Blew, E. Jakubikova, Electronic structure of covalently linked zinc bacteriochlorin molecular arrays: insights into molecular design for NIR light harvesting, J. Phys. Chem. A 118 (2014) 9901–9913.
[325] K. Takano, S.-I. Sasaki, D. Citterio, H. Tamiaki, K. Suzuki, An oxo-bacteriochlorin derivative for long-wavelength fluorescence ratiometric alcohol sensing, Analyst 135 (2010) 2334–2339.
[326] A. Mishra, P. Bäuerle, Small molecule organic semiconductors on the move: promises for future solar energy technology, Angew. Chem. Int. Ed. 51 (2012) 2020–2067.
[327] H. Imahori, S. Kang, H. Hayashi, M. Haruta, H. Kurata, S. Isoda, S.E. Canton, Y. Infahsaeng, A. Kathiravan, T.R. Pascher, Photoinduced charge carrier dynamics of Zn– porphyrin– TiO2 electrodes: the key role of charge recombination for solar cell performance, J. Phys. Chem. A 115 (2010) 3679–3690.
[328] K. Kalyanasundaram, N. Vlachopoulos, V. Krishnan, A. Monnier, M. Graetzel, Sensitization of titanium dioxide in the visible light region using zinc porphyrins, J. Phys. Chem. 91 (1987) 2342–2347.
[329] L. Lu, T. Zheng, Q. Wu, A.M. Schneider, D. Zhao, L. Yu, Recent advances in bulk heterojunction polymer solar cells, Chem. Rev 115 (2015) 12666–12731.
[330] F. Ponsot, L. Bucher, N. Desbois, Y. Rousselin, P. Mondal, C.H. Devillers, A. Romieu, C.P. Gros, R. Singhal, G.D. Sharma, A bacteriochlorin-diketopyrrolopyrrole triad as a donor for solution-processed bulk heterojunction organic solar cells, J. Mater. Chem. C 7 (2019) 9655–9664.